Photosensitive Materials: Optical properties and applications

Julien Lumeau

Aix-Marseille Université
Faculté des Sciences et Techniques de Saint Jérôme

HABILITATION A DIRIGER DES RECHERCHES

Photosensitive Materials: Optical properties and applications

Julien Lumeau

Soutenance le 16 Mars 2012

Discipline : Electronique, Optronique et Systèmes

Ecole Doctorale : Physique et Sciences de la Matière

JURY :
RAPPORTEURS :

M. Alain BARTHELEMY
M. Marc DOUAY
Mme Isabelle SAGNES

EXAMINATEURS :

M. Stefan ENOCH
M. Ludovic ESCOUBAS
M. Michel LEQUIME

ACKNOWLEDGMENTS

First of all I would like to thank Mr. Stefan Enoch, Mr. Ludovic Escoubas and Mr. Michel Lequime for accepting to be committee members of this habilitation, and Mr. Alain Barthelemy, Mr. Marc Douay and Mrs. Isabelle Sagnes for accepting to be the reviewers.

Then I would like to thank Mr. Stefan Enoch and Mr. Hugues Giovannini for accepting to host my HDR defense at the Institut Fresnel. I would also like to address special thanks to Mr. Michel Lequime who has been fully supporting me throughout these academic processes.

I would also thank everybody from Dr Leonid B. Glebov group, starting by himself, who has supported me throughout these years and who has given me so many opportunities. I am also indebted to Mr. Vadim Smirnov with whom I have shared many very tough scientific discussions that helped me revealing many of the mechanisms of PTR glasses. I also want to send my warmest thank you to Prof. Edgar D. Zanotto (LaMaV) who has launched me into the glass science world. Without him, I would not be where I am today. The work which is presented throughout this manuscript is actually the combination of numerous internal and external collaborations. First, within CREOL/UCF and OptiGrate, I would like to acknowledge the glass technology and glass research group members. I would like also to thank all the students I have been working with and especially Dr. Leo Siiman. I would also like to thank the other CREOL and OptiGrate team members: George Venus, Ivan Divliansky, Igor Ciapurin, Eugeniu Rotari, Oleksiy Mokhun…

I would like also to thank all the collaborators, this includes LaMaV people (especially Guilherme Souza), Fresnel people (especially Fabien Lemarchand and Cihan Koc), other Brazilian friends and colleagues (Francisco Serbena, Eduardo Bellini Ferreira, Marcio…), SLAM members (Laurent Sarger, Lionel Canioni…)

Finally I would like to thank my friends and family.

TABLE OF CONTENTS

Chapter 1: Education, professional experiences and background

1.1. General introduction

Before presenting into details any scientific results, it is important to first introduce my education and my professional experiences in order to better understand the logic of the research activities that were carried out over the past 10 years.

For the past decade, I have been working on the applications of photosensitive materials (i.e. materials which local refractive index can be locally modified after exposure to optical radiation). These activities started during my Ph.D. thesis (2001-2004) in the **RCMO** (Recherche en Composants et Materiaux de Couches Minces Optiques) of the **Institut Fresnel**. The title of my thesis was: *Application of photosensitivity for the fabrication of optical interference filters*. During these 3 years I had the opportunity to start developing multidisciplinary research activities that combined both the characterization and the study of photosensitive materials but also how to use these materials in order to fabricate new or optimized optical functions. After defending my Ph.D., I joined in early 2005 the team of Dr Leonid B. Glebov, at **CREOL, University of Central Florida**, in Orlando, FL, USA. I started as a postdoctoral fellow for the first 2 years, before being promoted to a Faculty Research Scientist position. At CREOL, I am today the leader of the Glass Research Group and part of the Holographic Group. In parallel to the research activities I am carrying out at CREOL, I am also a senior research scientist for the **OptiGrate Corp.** which is a small company (~30 employees) that commercializes the products (Volume Bragg Gratings) which were developed at CREOL. Section 1.2 provides general curriculum vitae.

Both at CREOL and OptiGrate, my R&D activities have been dealing with the study of a photosensitive glass: photo-thermo-refractive (PTR) glass which refractive index can be modified after exposure to ionizing radiation followed by a thermal treatment. These glasses are commercially used for the fabrication of holographic optical elements (volume Bragg gratings, VBGs). Despite the common topics and interests, my activities at CREOL and OptiGrate are distinct: while my work at CREOL are more on the research and education sides, the one performed at OptiGrate are more on the development and production side. Finally my main research interest can be enumerated as followed:

- The characterization of the optical properties of photosensitive glasses.
- Understanding the relationship between optical and structural properties and the methods that can be implemented to improve those properties.
- The use of photosensitive materials for the fabrication of new or optimized optical elements.

While a significant part of my activities were directed towards theoretical and experimental research activities performed in the framework of research projects funded by US Government Agencies (DARPA, JTO, DoD, NASA…), I also dedicated large part of my working time to other activities. First of all, I have been actively participating in the writing of proposals in response to the announcement of the Small Business Innovation Research (or SBIR) programs from the Department of Defense (DoD) and NASA in partnership with OptiGrate Corp. For the past 5 years, I have therefore participated in numerous projects as a scientist (Section 5.1), but also for some of them, as a Principal Investigator (PI) for CREOL. The sum of the budgets of all

the projects I have been a PI exceeds $1,000,000. All these projects activities of course also include writing reports and managing schedules and budgets.

The research activities I am participating involve both optics and glass science. Moreover, as it will be described later, those one include a very broad range of topics that required developing a network of collaborations with international Universities and research laboratories. While the team of Dr Glebov has developed a very large number of collaborations, I have been the point of contact for more than half a dozen of them (Section 5.2). It is worth noting that about a dozen of peer-reviewed publication I co-authored have involved some of these collaborators.

Of course, research at the University also involves educating young scientist. From 2001 to 2004, I taught general physics for students at first and second year at the University (Section 5.3.1). Then, for the past 6+ years, I have supervised (or co-supervised) the work of 4 Master and 4 Ph.D. students (one of them defended in 2008 and two are expected to defend within 1.5 years). I have also co-supervised the work of 2 postdoctoral fellows and I am in charge of a research scientist (Section 5.3.2).

Finally, I have published over 30 papers in peer-reviewed journal and been co-author in more than 90 conference papers. I am also co-inventor in 5 filed patent applications (Section 5.4). I am also a reviewer for numerous journals in optics: *Optics Letters, Optics Express, Applied Optics, Applied Physics B, Optics communications, Journal of Applied Physics, Journal of Infrared, Millimeter, and Terahertz Waves*… but also in material science: *Journal of Non Crystalline Solids*, *Journal of the American Ceramic Society, Optical Materials*... Finally, I am a co-chair of the optical coating session of the GOMD2012 (Glass and Optical Materials Division) conference of the American Ceramic Society.

1.2. Curriculum Vitae

Below, you fill find a formal curriculum vitae summarizing my competences and background.

Dr Julien Lumeau
4040 New Broad Circle – Apt. 300
OVIEDO, FL 32765
USA
Cell: 321-948-5115

Citizenship: French
US Permanent Resident
33, Married, 1 Child

Email: jlumeau@creol.ucf.edu

Scientific Experiences/Competences

- OPTICAL METROLOGY
  a. Development of dedicated setups for the measurement of **small absorption coefficient** by laser calorimetry and interferometry. Application to the characterization of holographic optical elements under high power CW radiation (fiber laser and laser diode

bars). Development of a set-up for the measurement of the **angular distribution of scattering**.

b. Development of an interferometric optical set-up based on **interferential spectroscopy** for high resolution mapping of the absolute optical thickness of transparent windows with high precision.

c. Development of a setup for the absolute measurement of **refractive index** in glass substrates.

d. Development of a **low coherence reflectometry/interferometry** setup. Application to the measurement of the residual reflection from anti-reflection coating ($R \sim 10^{-6} - 10^{-5}$).

- LIMEAR AND NON-LINEAR INTERACTION OF ULTRASHORT PULSES WITH GLASS

a. Study of the **nonlinear photosensitivity/photo-ionization** of PTR glasses and the properties of volume Bragg gratings under **high power pulsed laser** (nanosecond (Nd:YAG) and femtoseconde (Ti:Sapphire)): study of supercontinuum generation, multi-photon absorption process and strong-electric-field ionization.

b. Application of linear and non-linear photosensitivity to the recording of **phase plates** (e.g. Fresnel lens).

c. Study of the resonant **third harmonic generation** in transmitting Bragg gratings: sum frequency generation, surface generation, non-linear grating generation.

d. Study of the use of chirped volume Bragg gratings for **stretching and compression of ultra-short pulses** and their temporal shaping.

- OPTICAL FILTERING

a. Application of **volume Bragg gratings** for the fabrication of active and passive narrow bandpass filters: simulations and experimental demonstration of different types of filters: incoherent combination of a **Fabry-Perot filter** and reflecting Bragg grating, coherent combination of two phase shifted volume Bragg gratings, Moiré gratings and coherent combination of a volume Bragg grating and a dielectric mirror.

b. Theoretical study and experimental demonstration of an ultra-narrow bandpass filter joining a **fiber Bragg grating** (or a volume Bragg grating) and a dielectric mirror: development of dedicated calculations programs, deposition of thin films at the end of a fiber tip by electron beam deposition and in-situ laser monitoring using a tunable telecom laser.

c. Study of the methods for the **laser trimming of a narrow bandpass filters** based on a photosensitive spacer (simulations of phase correction, electric field repartition and design of specific filters): application for the creation of ultra-homogeneous filters or staircase variable filters.

- STUDY OF OPTICAL AND CRYSTALLIZATION PROPERTIES OF GLASSES

a. Study and characterization of the **optical properties** of photo-thermo-refractive (PTR) **glass**: losses (spectro-photometric measurements), refractive index change (shearing interferometer, Zygo interferometer) by linear photosensitivity (Argon and He-Cd lasers).

b. Study of the origin of the **losses** in PTR glasses and of the methods to reduce it (optical bleaching, glass purification, new thermal development procedures).

c. Analysis of the structure of **absorption spectra** in UV-Visible-NIR-IR by Gaussian deconvolution. Application to cerium bands, silver containing particles absorption band, water absorption band.

d. Study of the **crystallization properties** of PTR glass: nucleation and growth, homogeneity, relation between crystallization and optical properties: use of differential scanning calorimetry, optical microscopy, X-ray diffraction. Study of induced **stress/relaxation** and its relation to refractive index change. Analysis of warpage effects due to stressed surfaces.

e. Study, characterization and modeling of the refractive index change kinetics of **photosensitive materials**. Investigation of the possible candidates for the fabrication of configurable/programmable filters: polymers and doped silica substrates, silica-germanium-boron-sodium oxide coatings deposited by ion beam sputtering.

Professional Positions

2007 – Present	R&D Scientist at OptiGrate Corp., Florida, USA
2007 – Present	Faculty Research Scientist, Photo-induced Processing Laboratory (PPL), CREOL/University of Central Florida, USA
2005 – 2006	Post-Doctoral Research Scientist, Photo-induced Processing Laboratory (PPL), CREOL/University of Central Florida, USA
2004	Post-Doctoral Research Scientist, Thin Film Research Group (RCMO), Institut Fresnel, Marseille, France
2001 – 2004	Research Assistant, Thin Film Research Group (RCMO), Institut Fresnel, Marseille, France

Education

Ph.D. 2004	Institut Fresnel, Thin Film Research Team, University Paul Cezanne Aix-Marseille III, France Dissertation title: *"Application of photosensitivity for the fabrication of optical interference filters"* Advisor: Prof. Dr. Michel Lequime
M.S. 2001	Institut Fresnel, Thin Film Research Team, University Paul Cezanne Aix-Marseille III, France Thesis title: *"Study, realization and characterization of an optical coherence reflectometry set-up: application to the characterization of anti-reflection coatings"* Advisor: Prof. Dr. Michel Lequime
M.Eng. 2001	*Diplôme d'ingénieur* from the Ecole Nationale Superieure de Physique de Marseille (now Ecole Centrale Marseille), University Paul Cezanne Aix-Marseille III, France

Past and present professional activities

- 120+ communications (including peer-reviewed publications (~30), patent applications (5), conference presentations (~90) and proceedings (~30))
- Proposal writing for DoD and NASA SBIR/STTR program solicitations (in collaboration with the OptiGrate Corp.)
- Report writing for DoD, NASA, JTO, DARPA, MDA… funded projects
- Presentation at kick-off and follow-up meetings in several funded projects
- Principal investigator for CREOL/UCF in several funded projects (total funding: ~$1,000,000)
- In charge of glass research group at CREOL/PPL: supervision of Ph.D. students, Post-Doc and technicians
- In charge of the collaboration with worldwide teams (University of San Carlos (Dr E. Zanotto, Brazil), University of Bordeaux (Dr L. Canioni, France), University of Clausthal (Dr J. Deubener, Germany)…
- Teaching assistant at the University Paul Cezanne Aix-Marseille III (2001 – 2004)
- Reviewer of Elsevier journals: *Journal of Non Crystalline Solids* and *Optics Communications*. Reviewer of the *Journal of the American Ceramic Society*
- Reviewer of the Optical Society of America (OSA) journals: *Optics Letters, Optics Express* and *Applied Optics.* Reviewer of *Applied Physics B* and *Journal of Infrared, Millimeter, and Terahertz Waves*

Additional information

- French: mother tongue
- English: good skills, both oral and written
- German: notions
- Language of programming: Labview

Chapter 2: Photosensitive Materials

2.1. Introduction: Photosensitive materials

The discovery of photosensitivity in 1978 by K.O Hill [1] triggered the development of new optical elements, mainly in fibers and waveguides. The principle of photosensitivity relies on the exposure of a material with energy larger than its bandgap. The linear (or non-linear) interaction generates a change of the material structure that induces a local refractive index change. The mechanisms of the photosensitivity can be multiple. For example, refractive index is associated with a photo-polymerization of photopolymers [2], micro/nano-damage or densification in case of some doped silicate glasses [3,4] or with a local photoionization followed by a nano-crystallization in case of some multicomponent silicate glasses [5,6].
Up to recently, most of the application of photosensitive materials were in guided configuration [7,8], because there were no available materials that combined all the required properties, most of them being either unstable (such as the photopolymers) or having too low refractive index change (like germanium doped silica). Thanks to the development of new glasses as well as the development of reliable ultra-short pulsed lasers, the usage of the photosensitivity in bulk glasses is now possible. Today, there are several categories of photosensitive glasses that allow the fabrication of high quality optical elements: the photopolymers, doped silica or undoped silica excited by short or ultrashort pulses, chalcogenides and the multicomponent silicate glass like photo-thermo-refractive glass. While I studied the first two materials during my Ph.D. thesis, most of the work I have performed while at CREOL, University of Central Florida was on the last category.

2.2. Photo-thermo-refractive glasses

Photo-thermo-induced crystallization in multicomponent silicate glasses doped with Ce, Ag, and F was discovered in 1949 by Stookey [9]. Based on this effect, photo-thermo-induced precipitation of metallic Ag allowed producing black coloration while the precipitation of NaF crystals in UV exposed areas allowed producing white coloration of a glass plate. These two effects paved a way for black-and-white photography in the bulk of silicate glass. However, despite these very promising results, no real applications were found. Thirty years later, it was demonstrated [10] that additional UV exposure and thermal development of a similar glass resulted in a precipitation of metallic Ag particles on the surface of NaF crystals. These particles produced different colors depending on UV dosage. These new results laid the groundwork for full color image recording. But once more, no useful applications were found. It is only after 35 years of study and development of this class of glasses, that refractive index variation due to NaF microcrystals precipitation was revealed but evaluated as insufficient for practical applications [11]. A few years later, this effect was re-investigated and refractive index variation was re-discovered and applied to the recording of the first hologram using the photo-thermo-refractive (PTR) phenomenon [12]. This was the starting point for a large number of improvements in this class of glasses that resulted in the recording of the first holograms in PTR-like glasses with high relative diffraction efficiency [13] and then the first high efficiency volume Bragg grating in PTR glass [14,15]. Today's technology allows the fabrication of holograms in PTR glasses with diffraction efficiency up to 99.9%, absorption in near IR between 1 and 2×10^{-4} cm^{-1}, scattering down to 5×10^{-3} cm^{-1}, aperture up to 50×50 mm^2 which enabled dramatic increase of brightness and power of solid state, fiber and semiconductor lasers [16]. The actual level of PTR glass

technology allows the production of PTR glass with absorption in near IR region of 5×10^{-5} cm^{-1}, refractive index fluctuations 10^{-5}, and apertures up to 100×100 mm^2.

The basic mechanisms of photo-thermo-induced structural transformations in PTR glass (Figure 2.2-1) can be stated as follow: UV-exposure within the absorption band of Ce^{3+} triggers its photoionization of Ce^{3+} into Ce^{3++} and one electron; the latter is trapped by an ionic silver to yield an atomic silver [17]. At this stage of the process, photoionization caused the generation of additional absorption and a refractive index increment of about 10^{-6}. Moreover, exposure of UV-exposed glass to high power visible radiation causes bleaching of pre-nucleation centers [18]. The second stage occurs when heating up to 490°C and consists in the creation of nucleation centers which include Ag and Br [19]. Then, heating up to 520°C results in precipitation of cubic NaF [20]. Cooling of the glass sample down to the room temperature induces stresses caused by difference in coefficients of thermal expansion of NaF and PTR glass which induce refractive index decrement of about 10^{-3} through the photoelastic properties of the glass [21].

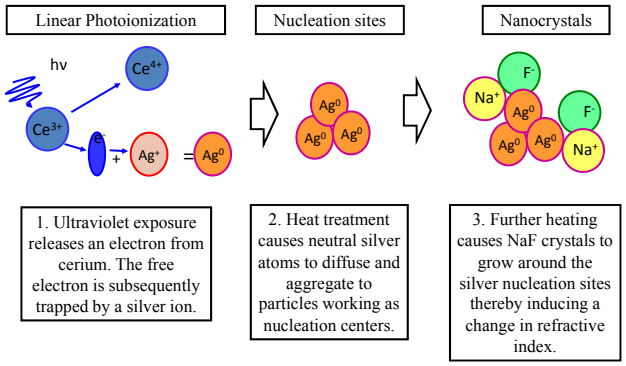

Fig. 2.2-1. Principle of the photo-thermo-refractivity in PTR glasses.

2.3. Application of photosensitive glass and main research directions

The main application of photo-thermo-refractive glasses are for the fabrication of volume Bragg gratings and volume phase masks. Volume Bragg gratings are obtained by holographic recording of a sinusoidal refractive index modulation inside the photosensitive medium. Volume Bragg gratings can be categorized into two main categories: Transmitting and Reflecting (Figure 2.3-1). In case of transmitting Bragg gratings (TBGs), the diffracted beam is on the same side as the transmitted beam, while in case of reflecting Bragg gratings (RBGs), the diffracted beam is on the same side as the reflected beam. The high spectral and angular selectivities of these elements allowed them to be inserted into numerous laser systems in order to improve their properties, mostly selecting a given transverse or longitudinal mode in the cavity [22].

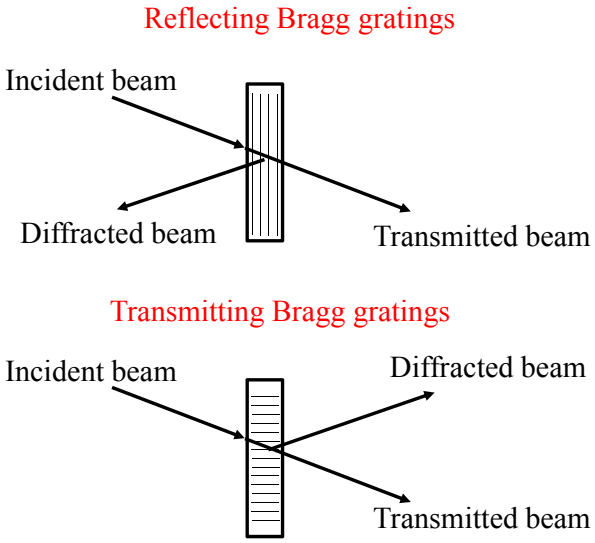

Fig. 2.3-1. Principle of transmitting and reflecting Bragg gratings.

Within my research activities, I have worked in two main topics: The first one consisted in studying the properties of PTR glass, to understand the refractive index kinetics and mechanisms, to understand the source of small losses in PTR glasses and their methods of mitigation… The second topic consisted in designing, fabricating and characterizing new optical elements based on photosensitive materials and including either volume Bragg gratings or dielectric filters in order to fabricate new optical functionalities.

Chapter 3: Optical and structural properties of photosensitive materials

3.1. Study of the refractive index change in photosensitive materials

3.1.1. Study of the photosensitivity of organic materials

During my Ph.D. thesis, I have developed the tools that allowed characterizing the optical properties of photosensitive materials, whether they are thin films or bulk materials. The photosensitivity being associated with the excitation of the materials with a wavelength included in its absorption spectrum and resulting in a local change of the average refractive index of the material, the optical setup I developed allowed detecting the local change of the optical thickness of a plane parallel window (or coating) by measuring the local change of the spectral transmission around 1550 nm.

This technique is based on interferential spectroscopy or more generally on the Fabry-Perot interferometer. Let us consider a plane parallel window. Let us consider an optical flat. When the angle of incidence or the wavelength of a monochromatic plane wave transmitted through this flat is scanned, the beam appears with a modulation of its intensity due to the presence of a Fabry-Perot interferometer resulting from the multiple reflections on each face of the flat. This intrinsic interferometer can be used to measure the local optical thickness (a product of the refractive index and the geometrical thickness) of the flat if coherence length of a light source exceeds difference in optical paths of the beams after multiple reflections [23-24]. If the optical thickness of the flat is varied as a result of some external forcing function (e.g. photosensitivity), the modulation of the intensity of the overall transmitted beam launched at the normal incidence angle will be spectrally shifted. Therefore, the measurement of the spectral dependence of the Airy function as a function of the excitation can be used to extract the refractive index change kinetics. The setup that was developed is presented in Figure 3.1-1 and allowed measuring local change of the optical thickness with a relative precision better than 10^{-6}.

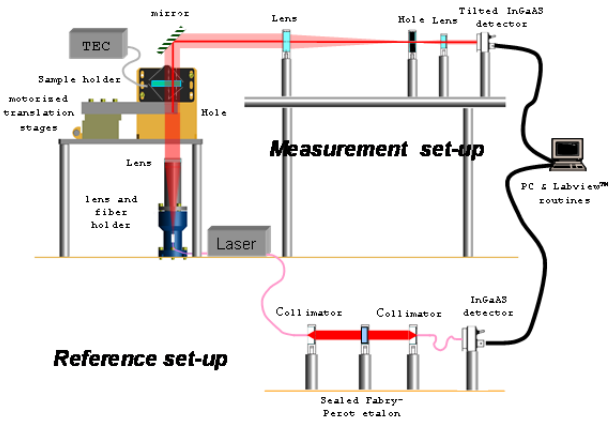

Fig. 3.1-1. Setup based on interferential spectroscopy for the measurement of the refractive index change kinetics of photosensitive glasses.

We used this technique to characterize the photosensitivity of photopolymers [23] (Figure 3.1-2). We showed that while these materials are very attractive in term of price and maximum refractive index change, they cannot be used for the fabrication of optical interference filters because they are not stable and their local optical thickness tends to shift

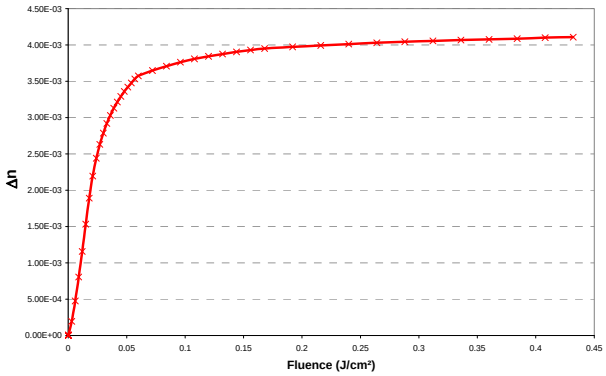

Fig. 3.1-2. Example of the refractive index change kinetics in photopolymers.

with time. Moreover due to their nature, they cannot be easily combined with multi-dielectric stacks. We also studied inorganic materials such as germanium or lead doped silicate glasses. However, despites our efforts, we were not able to identify one material that combines all the required properties to be used in optical interference filters. All these research activities finally allowed showing how attractive the integration of photosensitive materials in optical interference filters is. Moreover we also showed that while doping some of the silicate glasses with elements such as germanium or lead is a necessary condition, it is not enough to produce a photosensitive material.

3.1.2. Refractive index change kinetics in PTR glass: characterization and modeling

As we have discussed previously, the main parameter that allows describing a photosensitive material is its refractive index kinetics, i.e. the evolution of the photo-induced refractive index change as a function of an external excitation. While in most cases, these kinetics only depend on the dosage (the energy density), and the power density (in case of non-linear photosensitivity), in the case of PTR glasses, refractive index change also depends on the thermal treatment temperature and duration. To characterize the kinetics, we developed direct measurements techniques. As shown in the previous section, I developed during my PhD thesis a dedicated setup based on interferential spectroscopy that allowed characterizing numerous types of photosensitive materials [23]. However, this technique being very time consuming I used a different technique to characterize the refractive index change kinetics of PTR glasses. This technique is based on shearing interferometry [25], and allowed fast and directed measurement of the dependence of the refractive index change on dosage. Improvement of this technique allowed reaching an absolute precision of 1 ppm (i.e. 10^{-6}), and we applied this technique to characterize and then model the refractive index change kinetics versus dosage, and thermal treatment temperature and duration (Figure 3.1-3) [26].

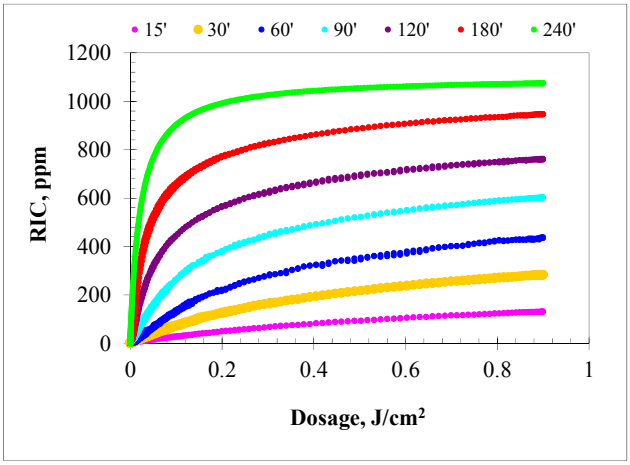

Fig. 3.1-3. Dependence of the refractive index change on dosage of UV-exposure measured in PTR glass after nucleation and thermal treatment at ~515°C for different durations.

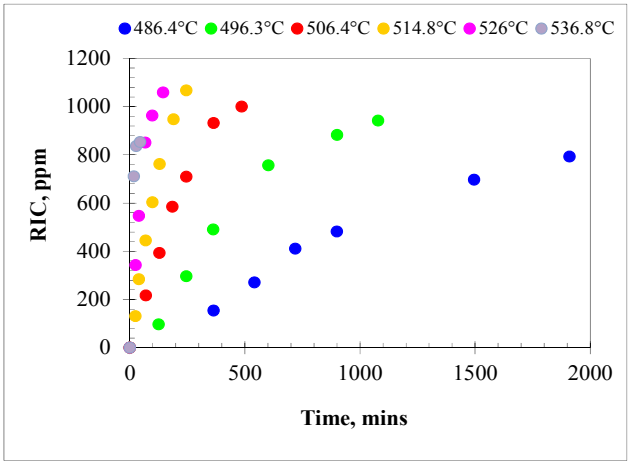

Fig. 3.1-4. Dependence of the refractive index change on thermal treatment duration measured in PTR glass UV-exposed with dosage of 0.9 J/cm^2 and developed at different thermal treatment temperatures.

The first part of our study consisted in analyzing and modeling the isothermal refractive index change versus time at constant dosage of 0.9 J/cm^2 as measured in Figure 3.1-4. Such a modeling is very critical because it can be shown that refractive index change kinetics will change by two orders of magnitude within these 50^{o}C range while most of the holographic optical elements require a precision within 10 ppm on the refractive index change. We applied the Johnson-Mehl-Avrami-Kolmogorov (JMAK) equation [27-29] to model the refractive index change. This model is generally used to model the crystallization kinetics (i.e. the evolution of the volume fraction of crystals versus time and temperature of thermal treatment) of ceramics [30]. As the refractive index change of PTR glass was shown to depend, in first approximation, on the volume fraction of NaF crystals [20,31], this model appeared reasonable. We therefore used the equation (3-1) to model the refractive index change kinetics (*$\Delta n(0.9\ J/cm^2,\ t,T)$*):

$$\Delta n(0.9J/cm^2, t, T) = \Delta n_{max}(0.9J/cm^2, T)\left(1 - exp(-K(T)t^n)\right) \tag{3-1}$$

Where *$\Delta n_{max}(0.9\ J/cm^2,\ T)$* is refractive index at saturation, *K(T)* is a thermodynamic parameter describing the slope at t = 0 versus temperature and *n* is the Avrami coefficient describing the type of crystallization. One common method for extracting each of the three unknown parameters consists in re-writing the equation (3-1) to linearize it:

$$ln\left(-ln\left(1 - \frac{\Delta n(0.9J/cm^2, t, T)}{\Delta n_{max}(0.9J/cm^2, T)}\right)\right) = ln\big(K(T)\big) + nln(t) \tag{3-2}$$

That way, by plotting the left term of the equation (3-2) as a function of *ln(t)*, we could obtain so-called Avrami plots. By fitting each curve with a linear function, we can extract the Avrami coefficient *n* from the slope while the intercept gives *ln(K(t))*. Before performing such data processing, one can see that *$\Delta n_{max}(0.9\ J/cm^2,\ T)$* needs to be pre-determined and is temperature dependent. Based on the curve of Figure 3.1-3, one can estimate an approximate value of *$\Delta n_{max}(0.9\ J/cm^2,\ T)$*. We showed, with good approximation, that the maximum refractive index change appears to be, within our temperature range, almost a linearly dependent function of the thermal treatment temperature and can be described with the equation:

$$\Delta n_{max}(0.9J/cm^2,\ T) = \Delta n(0.9J/cm^2, \infty,\ T) = 5.22(T^oC - 460) + 777 \tag{3-3}$$

As stress is supposed to be one of the main effect causing the refractive index change [21], this linear dependence can be explained by the change of the stress level surrounding the crystal while cooling from thermal treatment temperature down to Tg. Using the equation (3-3), we plotted in Figure 3.1-5 the left term of the equation (3-22) as a function of *ln(t)*. One can see that we obtain parallel linear curves with slope equal to 1.5 ± 0.2, this slope depending also on the extracted *$\Delta n_{max}(0.9\ J/cm^2,\ T)$*. The coefficient *n* is a parameter describing the crystallization mechanisms. When it equals to ~1.5, it can be associated [29,30], from the point of view of a crystallization process, with a diffusion-controlled growth of spherical particles from pre-existing nuclei. NaF crystals are expected to grow isotropically into cubic shape, which is close to the situation predicted by n = 1.5. Finally, we plotted in Figure 3.1-6, the evolution of *ln(K(T))*

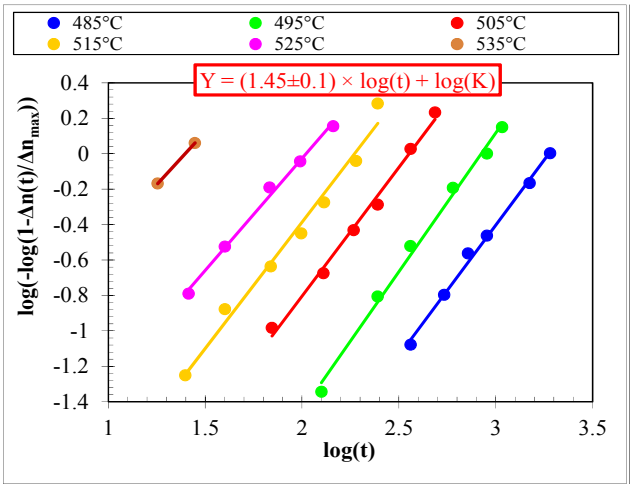

Fig. 3.1-5. Avrami plots calculated from the curves of Fig. 2.1-4.

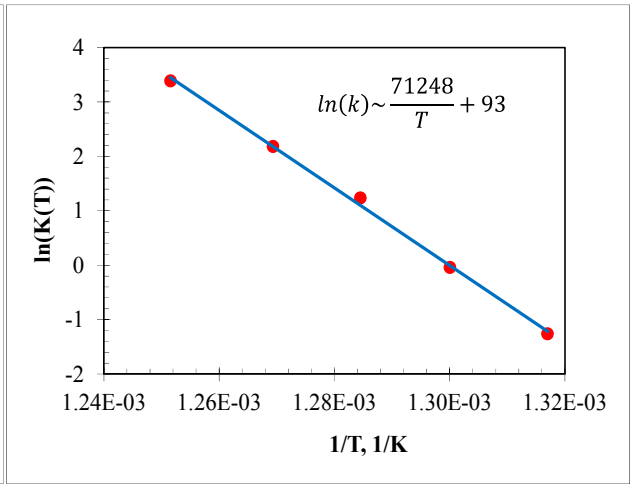

Fig. 3.1-6. Dependence of *ln(K(T))* versus *1/T*.

as a function of *1/T*. A linear dependence can be observed proving that *K(T)* is a thermodynamic parameter that follows a Boltzmann law:

$$K(T) = K_0 \times exp\left(-\frac{E_K}{RT}\right) \tag{3-4}$$

Where E_K is the activation energy and is equal to 592 KJ/mol. In conclusion, we see that combining the equations (3-1), (3-2) and (3-4) allows predicting the refractive index change of this specific melt at constant dosage of 0.9 J/cm^2 and for any thermal treatment temperature and duration.

The second step consisted in modeling the isothermal refractive index change versus dosage. We used the results of Glebov [32], in order to model the refractive index change versus dosage for any thermal treatment duration and temperature as measured in Figure 3.1-3. Glebov showed that by writing balance equations associated with the photochemistry of PTR glass and supposing that trapping of electrons by silver and holes have the same probability, the dependence of the refractive index change (Δn) on dosage (D) follows an hyperbolic function:

$$\Delta n(D) = \frac{n_S D}{D + \varepsilon} \tag{3-5}$$

where n_S is the refractive change at saturation and n_S/ε is the inverse of the slope at $D = 0$. Using the refractive index change at 0.9 J/cm^2 ($\Delta n(0.9\ J/cm^2,\ t,T)$) that can be predicted using JMAK theory (Equation (3-1)), the equation (3-5) becomes:

$$\Delta n(D,t,T) = \frac{\Delta n(0.9J/cm^2,t,T)\big(0.9 + \varepsilon(t,T)\big)D}{0.9\big(D + \varepsilon(t,T)\big)} \tag{3-6}$$

In our case $\varepsilon(t,T)$ is a thermodynamic parameter that needs to be determined for each thermal treatment temperature and duration. Combining the equation (3-1) with the equation (3-6) allows to fit each of the curves of the Figure 3.1-3 with a precision better than 10% (Figure 3.1-7) and to extract the evolution of $ln(1/\varepsilon(t,T))$ as a function of the thermal treatment duration t for each used temperature T (Figure 3.1-8). It is seen that $ln(1/\varepsilon(t,T))$ evolves almost linearly for any of the temperature used in our study. This means that we can define an equation that will accurately predict $1/\varepsilon(t,T)$ as:

$$\frac{1}{\varepsilon(t,T)} = exp(\beta(T)t) \tag{3-7}$$

Where $\beta(T)$ is a temperature dependent parameter. Despite the fact that it is hard to give any physical meaning to this equation, it allows predicting the refractive index versus dosage for any thermal treatment at constant temperature. Finally, we showed that the evolution of $ln(\beta(T))$ as a function of $1/T$ is linear proving that $\beta(T)$ is a thermodynamic parameter that follows a Boltzmann law:

$$\beta(T) = \beta_0 \times exp\left(-\frac{E_\beta}{RT}\right) \tag{3-8}$$

Where E_β is the activation energy and is equal to 393 KJ/mol.

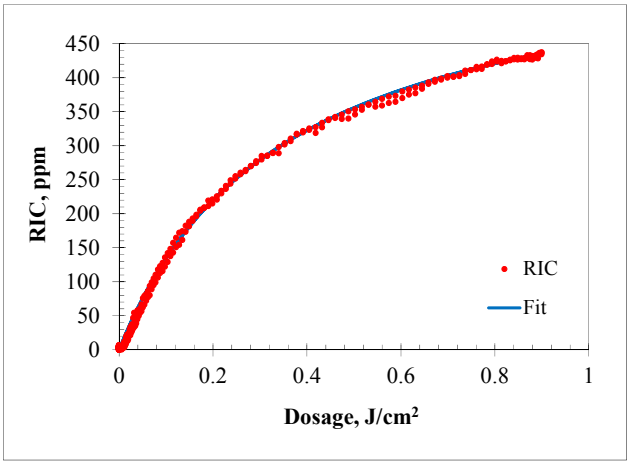

Fig. 3.1-7. Example of a fit of the dependence on the dosage of UV-exposure of the refractive index change measured in PTR glass developed for ~60 minutes at ~515°C.

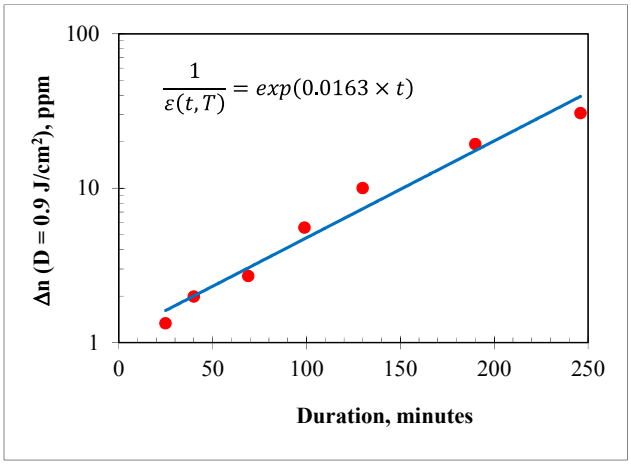

Fig. 3.1-8. Example of a fit of the dependence on the dosage of UV-exposure of the refractive index change measured in PTR glass developed for ~60 minutes at ~515°C.

To conclude this section, we have presented the basic physical models that can be applied for the modeling of the refractive index change in PTR glass. We have shown that three parameters will control the final refractive index change: the dosage of UV-exposure, the thermal treatment duration and the thermal treatment temperature. Regarding the effect of the thermal treatment duration and temperature, we showed that the use of the classical model for crystallization study,

the Johnson-Mehl-Avrami-Kolmogorov (JMAK) theory permits to accurately predict the refractive index for a constant dosage at any of the thermal treatment procedure. We also showed that the Avrami coefficient, describing the type of crystallization process, is equal to 1.5, demonstrating that the refractive index change is based on a diffusion-controlled growth of particles from pre-existing nuclei. Regarding the dosage dependence, the usage of hyperbolic functions as derived from photo-chemistry balance equations, was shown to accurately predict the refractive index for a constant thermal treatment procedure and at any UV-dosage. Finally, we have shown that each of these models uses thermodynamic parameters that follow Boltzmann dependences.

3.1.3. Origin of the refractive index change in PTR glasses

We also studied the origin of refractive index change in PTR glasses. It was shown in ref. [20] that the photosensitivity of PTR glass results from the precipitation of nano-sized sodium fluoride crystals within the glass matrix in the UV-exposed regions after heat treatment. However, it was not clear which particular structural transformations are responsible for the refractive index decrement in such complex multi-component glass. The understanding of the origin of this effect requires a step by step discussion of the mechanisms of photosensitivity in PTR glass. A simplified proposal for photo-thermal crystallization is the following: Before any thermal development of the glass, sodium, fluorine and all other ions are uniformly dissolved in the matrix and the material is totally vitreous. When PTR glass is exposed to long wavelength UV radiation λ>250 nm (e.g. He-Cd laser at 325 nm), Ce^{3+} releases an electron and converts to hole-type Ce^{4+} center. The released electron is then trapped by intrinsic defects of the glass matrix or dopants and impurities in the highest valence state, including silver ions dispersed in the glass matrix. Then silver ions convert to silver atoms. When a UV-exposed glass is nucleated at temperatures between 450 and 500°C, silver atoms agglomerate and form colloidal silver. Another possibility is that silver bromide clusters form [19]. The second part of the crystallization process consists in the heterogeneous precipitation and growth of sodium fluoride crystals on top of the silver (or silver bromide) clusters. NaF growth is then controlled by diffusion of sodium and fluorine from the glass matrix to the crystals, which leave sodium and fluorine depleted regions surrounding each crystal [33]. Thus a simplified model for PTR glass after UV-exposure and heat-treatment supposes that three distinct areas appear (figure 3.1-9):

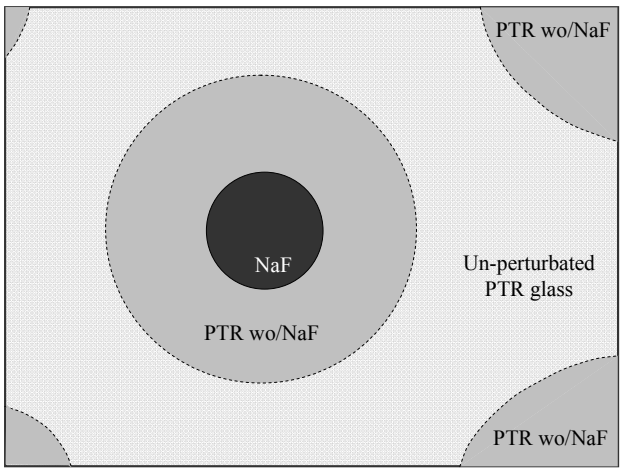

Fig. 3.1-9. Three-phase structure of PTR glass after successive UV-exposure and thermal treatment.

- The first area is a cubic sodium fluoride crystal (shown here as a sphere for simplicity of modeling). For typical conditions of UV-exposure and thermal development used for hologram recording, the average diameter of such crystals is about 20 nm [34] and their

volume fraction is about 0.1% [20]. This means that the average distance between crystals is about 110 nm.

- As sodium and fluorine ions are consumed by the growing crystals, halos with diameter about 3 times larger than the crystal diameter have the same components as virgin PTR glass, but are depleted in sodium and almost exhausted in fluorine.
- The third area, far away from the crystals, is an unperturbed glass region having identical composition as virgin PTR glass.

The precipitation of sodium fluoride crystals correlates with the beginning of the refractive index decrease in the UV-exposed regions of the glass. It must be stressed that a (smaller) change of refractive index also occurs in the unexposed areas [35]. However, as the main application of PTR glass is for recording volume Bragg gratings, the important parameter is the refractive index difference between the UV-exposed area ($n^{UV\text{-}exposed}$) and the unexposed area ($n^{unexposed}$):

$$\Delta n = n^{\mathrm{UV-exposed}} - n^{\mathrm{unexposed}} \tag{3-9}$$

It has been found [12,25] that the overall refractive index change is negative ($\Delta n<0$), therefore, PTR glass is a negative photosensitive medium.

Based on the above description, it is possible to write a phenomenological equation describing possible contributions to the refractive index decrement in both UV-exposed and unexposed areas. For simplification, we supposed that all contributions are additive and we dropped integrals that would take into account an inhomogeneous distribution of each contribution:

$$\begin{aligned}\Delta n^{\exp} &= \left[\Delta n^{\mathrm{Crystalline}} V^{\mathrm{NaF}} + \Delta n^{\mathrm{Vitreous}} V^{\mathrm{PTR\ wo\ NaF}}\right] \\ &+ \left[\Delta n^{\mathrm{V}} V^{\mathrm{PTR\ wo\ NaF}} + \Delta n^{\mathrm{V'}} V^{\mathrm{PTR\ w\ NaF}}\right] \\ &+ \left[\Delta n^{\mathrm{Stress1}} V^{\mathrm{NaF}} + \Delta n^{\mathrm{Stress2}} V^{\mathrm{PTR\ wo\ NaF}} + \Delta n^{\mathrm{Stress3}} V^{\mathrm{PTR\ w\ NaF}}\right]\end{aligned} \tag{3-10}$$

By supposing that there is no significant crystallization in the unexposed areas, the refractive index in those areas would change only due to variations of cooling regimes (which is different from the one used for fine annealing of the glass and results in volumetric changes associated with glass relaxation):

$$\Delta n^{\mathrm{unexp}} = \Delta n^{\mathrm{V'}} \times V^{\mathrm{PTR\ w\ NaF}} \tag{3-11}$$

Each contribution in equations (3-10) and (3-11) is a product (or integration) between the refractive index change (Δn^i) due to each effect and the volume fraction (V^i) of the region contributing to that particular effect. V^{NaF} is the volume fraction of crystals – which is typically between 0.01 and 0.1% – $V^{PTR\ wo\ NaF}$ is the volume fraction of glass that has been depleted in sodium and fluorine, and $V^{PTR\ w\ NaF}$ is the volume fraction of glass that has not been perturbed and, therefore, has the same composition as regular PTR glass.

Let us now describe each one of these contributions. Regarding the refractive index change appearing after thermal treatment in UV-exposed areas, the first term within brackets represents the direct contribution of crystallization to the refractive index change. The appearance of sodium fluoride crystals induces a refractive index change ($\Delta n^{crystalline}$) due to their lower

refractive index (n = 1.32) compared to the refractive index of the original glass matrix (n ~ 1.5). Moreover, one could expect that the atomic refractions of sodium and fluorine are different in the crystalline and vitreous phases. And this effect is accompanied by NaF depletion of the surrounding glass which, in turn, changes the refractive index of the glass matrix ($\Delta n^{Vitreous}$). However, we showed that the molar refraction of Na^+F^- whether it is in vitreous or crystalline phase are equal, such as the contribution from chemical changes are negligible

The terms within the second bracket, Δn^{V} and $\Delta n^{V'}$, refer to changes of refractive index in the NaF depleted and unperturbed PTR glass, respectively, due to the change of specific volume that occurs during cooling of PTR glass (after crystallization treatment) in comparison with the specific volume of the virgin glass, which underwent fine annealing. However, we also showed that the change of specific volume is the same in both perturbed and unperturbed glass.

Finally, the third term represents the stresses that appear in the NaF crystals, surrounding glass and unperturbed glass. Crystallization is typically performed at ~515°C. PTR "glass" is a viscous liquid at this temperature because Tg ~460°C and, therefore, stresses caused by structural transformations quickly relax. But when the material is cooled down from Tg to ~25°C, stresses appear in the elastic medium (glass). It is known that the coefficient of thermal expansion (CTE, α) of silicate glasses increases with an increase of fluorine content [36]. Hence we have:

$$\alpha_{PTR\ wo\ NaF} < \alpha_{PTR\ w\ NaF} < \alpha_{NaF} \qquad (3\text{-}12)$$

The coefficient of thermal expansion (CTE) of regular PTR glass is $\sim 10\times10^{-6}\ K^{-1}$, while that of the cubic NaF crystals is $\sim 36\times10^{-6}\ K^{-1}$, i.e. almost 4 times higher than the glass CTE. Hence, after crystallization and cooling down to room temperature, "hydrostatic" radial and tangential stresses appear within the NaF crystals and induce a refractive index change on them ($\Delta n^{stress1}$) [37], radial and tangential stresses change the refractive index of the surrounding glass ($\Delta n^{stress2}$) [38], and finally there will be some stresses between the depleted and unperturbed glass ($\Delta n^{stress3}$).

Regarding the unexposed (supposedly non-crystallized) parts of the glass, only the change of specific volume during cooling from the crystallization temperature to room temperature could contribute to the refractive index change.

To confirm the role of stress on refractive index change we studied the effect of a change of the sample temperature on crystals (using X-ray diffractometry) and on the refractive index change. First, the effect of an increase of temperature (and residual stress) on the X-ray diffraction spectra of PTR glass was studied (as shown in ref [20], at room temperature the XRD peak of these crystals is

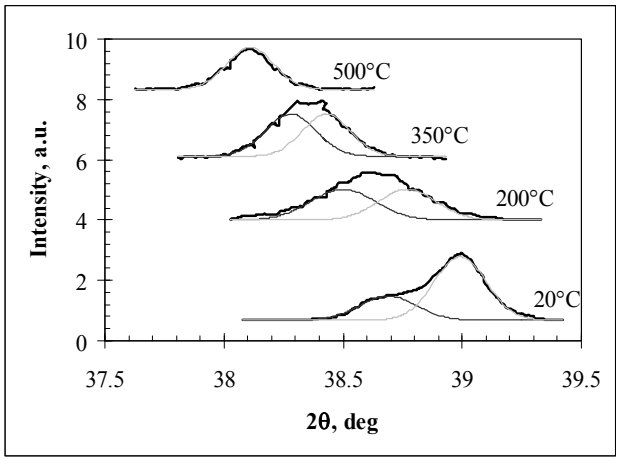

Fig. 3.1-10. XRD spectra measured on UV-exposed and developed PTR glass sample coated with NaF powder at different temperatures. The grey curves represent the decomposition of these spectra with two Gaussian functions that can be ascribed to diffraction peaks of NaF powder and NaF crystals precipitated in the volume of PTR glass.

shifted to smaller angles). A regular PTR glass was UV-exposed and then thermally developed for about 1 hour at 515°C to precipitate NaF nano-crystals. Then this sample was coated with a thin layer of NaF crystal powder. It was found that this sample demonstrates two separated peaks (20°C curve in figure 3.1-10) which could be assigned to NaF crystals in equilibrium (powder) and stretched NaF crystals in glass volume. Then X-ray diffraction spectra were obtained for different temperatures: 200, 350 and 500°C. As can be seen, the two peaks shift to lower angle and tend to become a single one when the temperature reaches 500°C. At this temperature, NaF crystals in bulk and on surface of the glass have identical properties, showing the residual stresses are relieved while heating the glass to temperature above Tg.

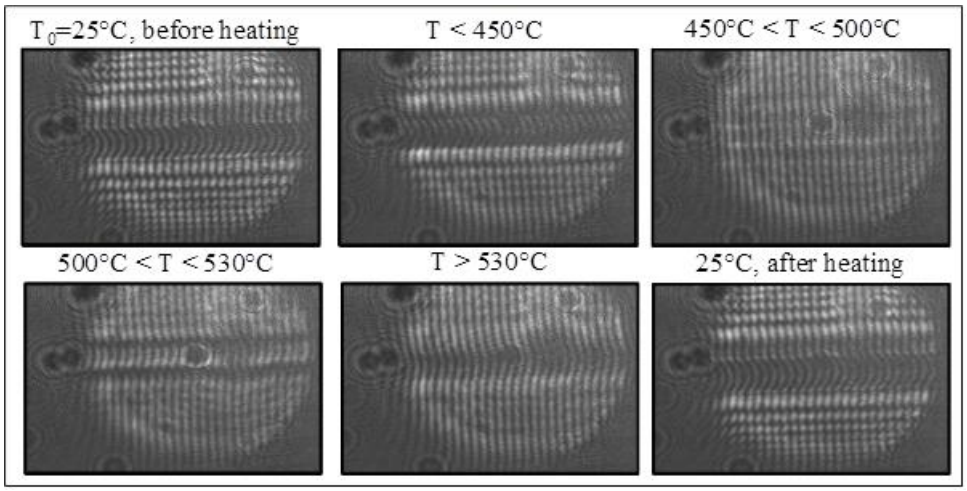

Fig. 3.1-11. Interferograms of a PTR glass sample exposed to a 1 mm Gaussian stripe of radiation at 325 nm and developed for 1 hour at 515°C.

Then the effect of an increase of temperature on the photo-thermo-refractive index change was studied using a custom Michelson interferometer. A PTR glass sample that was previously UV-exposed with a Gaussian stripe and thermally developed for 1 hour at 515°C to induce refractive index change was inserted in the heating cell that was then inserted in one arm of the interferometer. The original refractive index change between exposed and unexposed areas at room temperature was ~450 ppm. Then the cell was heated up to 540°C and the evolution of the interferogram with temperature is shown in Figure 3.1-11. The fringe shift evolved and cancelled at some specific temperature. However, with such an interferometer, only the change of optical thickness is measured and it is not possible to easily decorrelate the refractive index change to the modified physical thickness of the sample [38]. In order to figure out the contribution of glass swelling to the change of optical thickness when a sample is heated, we slightly modified the configuration of the Michelson interferometer. The mirror behind the sample was removed and the back surface of the sample was ground to allow a single reflection from its front face. Then the PTR

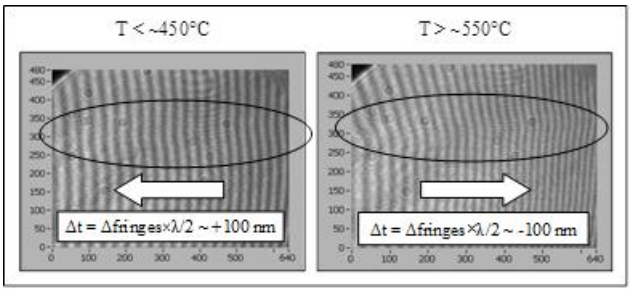

Fig. 3.1-12. Interferograms produced by a reflection from the front surface of PTR glass sample for 2 different temperatures.

glass window was aligned such as this front face reflection interfered on the CCD camera with the reference beam. In that way we measured the distortion of the PTR glass surface at high temperature. Figure 3.1-12 shows the interferograms measured at 450°C and 550°C. One can see that the direction of fringe distortions is different depending on the temperature of measurement demonstrating a change of sign of the glass swelling. Before performing any analysis of the evolution of the interferograms, it must be mentioned that before any heating, the lateral profile of the fringes almost follows the lateral profile of the exciting radiation. It is possible to show that the fringe shift is directly proportional to the change of optical thickness of the PTR glass window. Additionally to an interference pattern, there are horizontal bright lines of diffraction due to the contrast of refractive index between the UV-exposed stripes and the unexposed parts of the glass. When the temperature was increased up to 450°C, no significant change of the interferogram appeared. Then, when the temperature reached about 500°C, the interferogram changed significantly. First, the magnitude of the fringe shift decreased, but the main effect was the disappearance of the diffraction lines. This effect means that even if there are still distortions of the fringes, these distortions are actually no longer due to the refractive index change, but due to a change of physical thickness. Actually, it was shown in Ref. [38] that the refractive index decrease in PTR glass is accompanied by an increase of the glass volume. It was also shown that this increase of volume appears in a broader area than the refractive index change. We therefore measured the change of the physical thickness of PTR glass at different temperatures (figure 3.1-12). At these temperatures the fringes are bended in opposite directions. This means that compared to the unexposed area of the glass, the surface of the exposed stripe is elevated at low temperatures, while it is lowered a higher temperatures. More precisely, a continuous monitoring of the interferogram revealed that below 450°C there is no significant change. Between 450°C and 520°C, the fringe bending decreases, then disappears and finally changes direction. These data are quite relevant for the understanding the evolution of the refractive index change. Below 450°C, there is almost no change in difference between exposed and unexposed areas for both the physical thickness and the refractive index. Then, when the glass is heated to the temperature normally used in the thermal development process, an elimination of the refractive index change occurs simultaneously with a decrease of difference in the physical thickness of between exposed and unexposed areas of the glass sample resulting in a similar shift of the fringes. But since a significant refractive index change no longer exists, diffraction of a probe beam disappears.

To conclude, the main mechanisms of refractive index change in UV-exposed and thermally treated PTR glass were theoretically and experimentally investigated. Transformation of Na and F distributed in PTR glass matrix to crystalline NaF (chemical changes) and structural relaxation process are not the main causes of photo-thermo-induced refractive index changes. Such changes can be minimized or even eliminated by heating up the sample to a temperature exceeding Tg, as those normally used for thermal development of optical holographic elements. Among the variables here considered, the high residual stresses that surround the NaF crystals are the most important cause for photo-thermo-induced refractive index change in PTR glass.

3.2 Study of low losses in PTR glasses

3.2.1 Very low absorption PTR glass and volume Bragg gratings for high power applications

One of the very promising laser applications of holographic optical elements recorded in PTR glass is spectral beam combining by means of volume Bragg gratings (VBGs) [39]. The spectral combining of five 150 W fiber laser beams with an efficiency of 90+% has been recently demonstrated [40]. An analysis of the scalability of this spectral beam combining to the multi-kW level is presented in Ref. [41]. The main effect which lowers the quality of a combined beam is thermal lensing resulted from non-uniform heating of the VBGs by laser radiation. Therefore, one of the key parameters for the success of this application is the level of absorption in PTR glass. However, creation of low absorbing PTR glass and VBGs depends on both development of a high purity technology and reliable measurements. They are challenging because the actual level of absorption in this material corresponds to an attenuation of the laser beam by a tiny fraction of a percent per centimeter and is extremely difficult to detect by conventional photometry. Another challenge comes from the presence of scattering losses with amplitude equal or higher than the absorption losses.

We first analyzed the possible source of absorption in PTR and VBGs. First, it is important to stress that there is no intrinsic absorption of PTR glass in the near IR spectral region [42]. A preliminary study has shown that the main species responsible for absorption in PTR glass could be iron, hydroxyl groups, and silver-containing particles [43] (Figure 3.2-1). The main cause of the increased absorption in the range of 1060 nm is the presence of iron contamination. Iron exists in glasses in two forms: ferrous (Fe^{2+}) and ferric (Fe^{3+}) ions. Ferric ions have absorption in the blue and UV spectral regions. Ferrous ions have absorption bands in the UV region and in the near-IR regions centered at 1075, 2026, and 2985 nm [44]. The band at 1075 nm is the most harmful one for optical components being used in high power beams of Nd and Yb doped lasers as its width extends from 800 to 1400 nm. The absorption produced by silver containing particles and hydroxyl groups is supposed to be a secondary source of absorption in pristine PTR glass in the 1064 nm region [44].

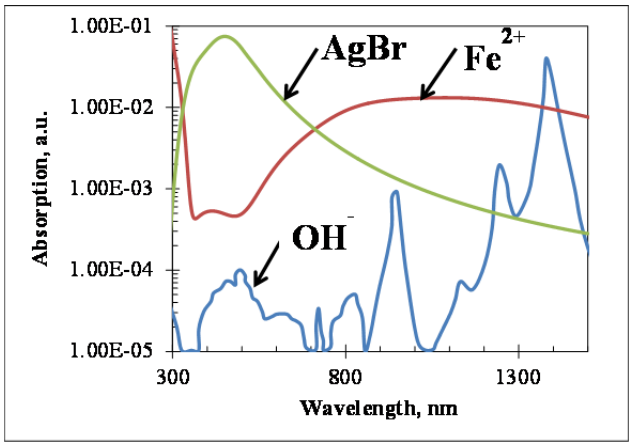

Fig. 3.2-1. Absorption spectra of the main absorbing species in PTR glasses.

Ferrous ions contribute to absorption in PTR glass in two different ways. Usually iron exists in glasses in both forms. Therefore, absorption in the vicinity of 1064 nm is determined by both the total concentration of iron and by the equilibrium ratio of Fe^{2+}/Fe^{3+} in accordance with the redox conditions of the glass melting volume. In conventional optical glasses, there is a way to decrease the IR absorption without requiring a dramatic purification of the glass. Strong oxidizing conditions in melting converts all iron ions to the ferric ones, and ordinary glass can have very low absorption near 1000 nm. However, this method cannot be used for PTR glass as

its photosensitivity is determined by a very strict distribution of valence states of the main photoactive components – silver and cerium. This feature does not allow changing the redox conditions of the PTR glass melt. Therefore, the way to reduce the absorption in pristine PTR glass was by purification of the glass fabrication technology.

Moreover, hologram recording in PTR glass requires exposing the glass to ionizing UV radiation and then thermally developing the glass at a temperature above the glass transition temperature. Photoionization causes the generation of movable electrons that are necessary for the main photochemistry of PTR glass – creation of nucleation centers and nano-crystalline phase growth. However, a fraction of those electrons can produce several side effects that could be a cause of additional absorption. Ferric ions (Fe^{3+}) are one of the best acceptors of electrons in PTR glass. Therefore, trapping of electrons reduces ferric ions to the valence 2^{+}, which has an absorption band at 1075 nm. Since absorption increases during the UV exposure by several times, the final level of absorption then depends on the dosage used - the higher the dosage, the higher the absorption. This result demonstrates that decreasing the amount of Fe^{2+} is a necessary but not sufficient condition for achieving low absorption in PTR glass.

Another consequence of photoionization is the generation of silver bromide-containing particles during thermal treatment. They have an absorption band with a maximum in the 400-500 nm range that is associated with the plasmon resonance of several types of silver bromide-containing particles [43]. While the maximum of this band lies in the blue/green region, its contribution to absorption in the near-IR range is non-negligible due to the presence of a long exponential tail following the Urbach rule [43]. Depending on the UV dosage, the absorption of the processed PTR glass is between 10^{-3} and 10^{-2} cm^{-1} and is therefore one to two orders of magnitude above the desired level of absorption (Figure 3.2-2).

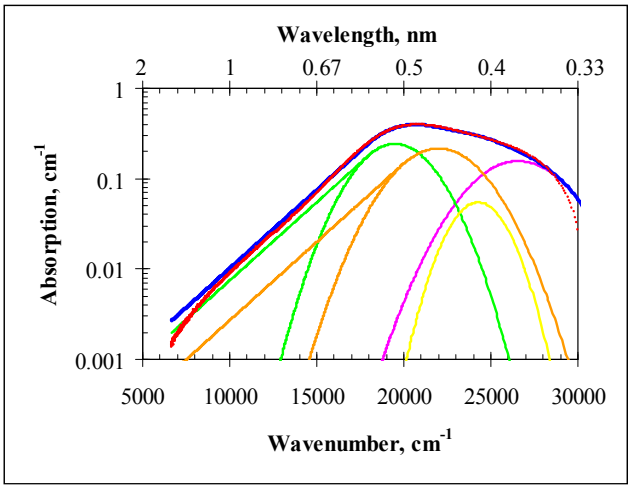

Fig. 3.2-2. Decomposition of the absorption spectra of silver containing particles absorption band using 4 Gaussian bands associated with 2 Urbach exponential tails.

Thus, absorption in PTR glass is determined by both the initial absorption of the original glass and by induced absorption caused by photo-induced reactions. In other words, decreasing absorption required developing methods of mitigation of absorption in both the original glass and in the process of photo-thermal treatment.

The decrease of absorption in the virgin glasses is a chemical process that requires decreasing both the contamination from the raw chemical and the melting process. The development of optimized processes resulted in decreasing the absorption down to 6.5×10^{-5} cm^{-1} at 1085 nm. It is important to note that to provide effective control of small amounts of impurities, we had to develop reliable methods for measuring small absorption. We used spectrophotometric methods to study the spectral dependence of the losses in PTR glass. We combined a commercial Perkin

Elmer Lambda 950 with a precise photometer that allowed measuring the transmission and reflection of radiation at 1085 nm with accuracy of 0.1%. This feature provided an opportunity to calibrate commercial spectrophotometers and to decrease the uncertainty of such measurements by an order of magnitude.

An automated absorption measurement setup was also developed to allow separating absorption losses from scattering losses (Figure 3.2-3). This method measures heating of a sample by laser radiation. It is based on transmission monitoring of the intrinsic Fabry-Perot interferometer produced by the plane-parallel surfaces of the measured sample when it is heated by high power laser radiation. Repeatability of the measurements is better than 10% while the detection limit is below 10^{-5} cm^{-1} at 1.085 μm [45]. A combination of a commercial spectrophotometer, a laser photometer and the laser interferometric calorimeter permitted us to measure small absorption in all samples of pristine and treated PTR glass. We showed that the main source of absorption in processed PTR glass comes from silver bromide containing particles.

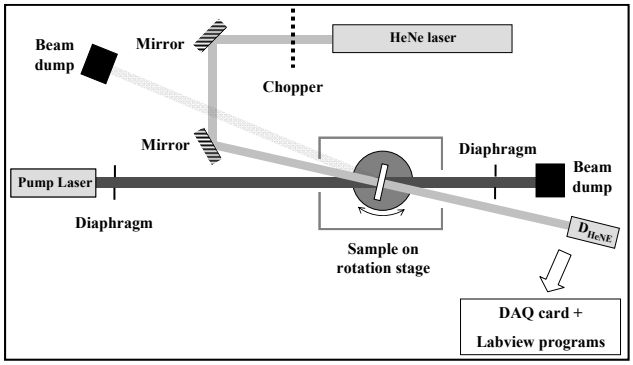

Fig. 3.2-3. Interferometric setup for the measurement of small absorption

Decreasing the absorption in holographic optical elements requires bleaching of the absorption band of these particles that have a maximum at ~465 nm [46]. Bleaching is performed by a frequency-doubled Nd:YAG laser using a non-linear process. However, while this process is now used extensively, its mechanisms are still unclear, causing us to study the evolution of the bleaching efficiency as a function of the energy per pulse. A beam from the frequency-doubled Nd:YAG laser was focused to a spot of one mm in diameter at the level of $1/e^2$. The energy per pulse was varied from 0.36 to 2.15 J/cm^2. Dosages from 100 to 800 J/cm^2 were used. The dependence of the transmitted power at 532 nm as a function of dosage was measured and fitted using hyperbolic functions. The measured data showed that the higher the energy per pulse, the steeper the initial slope (at zero dosage). However, at energy per pulse exceeding 1 J/cm^2, the initial slope tends to saturate and all curves tend to overlap (Figure 3.2-4). In other words, increasing the energy per pulse and approaching the glass damage threshold does not produce faster bleaching. Above 1 J/cm^2, the number of bleached silver particles is then only controlled by the dosage. Additional investigations combined with theoretical calculations have shown that with 1 J/cm^2, the temperature attained is several

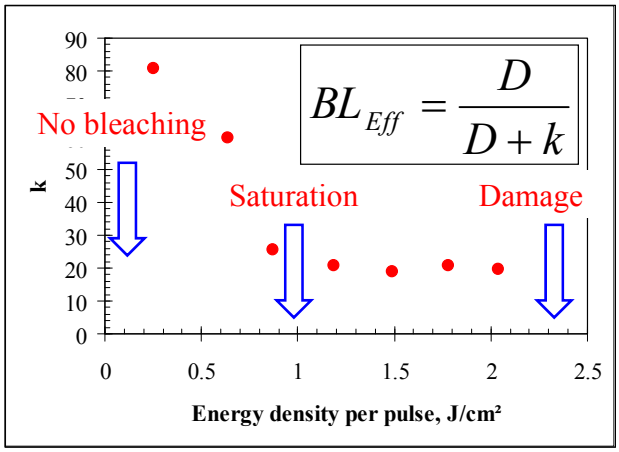

Fig. 3.2-4. Dependence of the initial slope at zero dosage (1/k) of bleaching efficiency on energy density per 10 ns pulse at 532 nm.

times higher than that required for vaporizing any silver containing particles in PTR glass. One must however keep in mind that the huge increase in temperature happens in the particle, but not in the surrounding glass leading to a very large gradient of temperature at the interface between the particle and the glass. Absorption of the pulse occurs within the few nanoseconds of the pulse width followed by very fast cooling of the particle due to the diffusion of the heat into the cold glass matrix. This prevents the particle from being destroyed in one pulse thus requiring a number of pulses to achieve bleaching. It was shown that extensive bleaching by this technique allows almost complete removal, if not total removal, of the absorption by the silver-containing particles. Total bleaching allows returning to a level of absorption comparable to the one achieved before the thermal treatment. Therefore, after bleaching, absorption in volume holographic elements is mostly controlled by the level of the reduced iron impurities in the glass.

Based on the bleaching mechanisms described above, one can see that the destroyed silver particles could not diffuse far from the original particles site. We therefore studied the thermal stability of this optically bleached glass by measuring the evolution of the absorption at 1085 nm versus additional heat-treatment temperature (Figure 3.2-5) One can see that heating up the sample below 200°C does not induce an increase of absorption while heat-treating of the volume holographic element above 200°C induces an increase of absorption, the strength of which depends on the thermal treatment temperature. This observation is extremely important because it defines a maximum allowed laser induced temperature increase of 200°C.

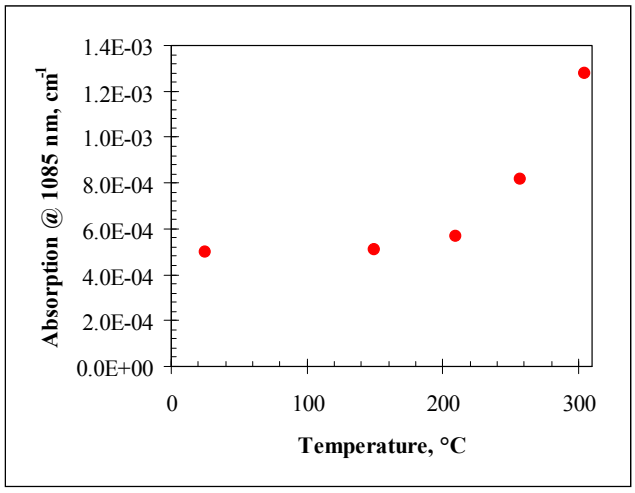

Fig. 3.2-5. Dependence of absorption at 1085 nm of exposed, developed and bleached PTR glass on additional 30 minutes heat-treatment temperature.

One of the main goals of the several projects we ran was to decrease the absorption in a reflecting Bragg grating recorded in PTR glass to the level of 10^{-4} cm^{-1}. The chemical purification that was implemented in the glass fabrication technology enabled decreasing the residual absorption in virgin glasses below 10^{-4} cm^{-1} with record absorption of 6×10^{-5} cm^{-1}. For PTR glass with a quarter of the regular amount of Ce and half of the regular amount of Ag, absorption in pristine glass was equal to ~ 7.5×10^{-5} cm^{-1} at 1085 nm. This glass was then UV-exposed with a dosage of 0.7 J/cm^2 which resulted in an increase in the absorption up to ~ 1×10^{-4} cm^{-1}. This absorption increment is caused by photo-reduction of iron. This smaller increase compared to the regular PTR glass can be explained by the lower number of photons that were absorbed by the Ce^{3+} ions and therefore the lower number of Fe^{2+} ions that were created. The sample was then developed for 60 minutes at 515°C and refractive index change was measured to be ~320 ppm. Such a value is high enough to allow fabricating a high efficiency reflecting Bragg grating. As it was shown previously, the main cause of the absorption is due to silver containing particles which can be bleached using the second harmonic of a Nd:YAG laser. After 30 cycles of such bleaching, this sample was re-polished and edges were re-ground in order to remove all incipient NaF crystallization and Ag precipitation that could result in parasitic

absorption. The absorption of this sample was measured at 1085 nm by laser calorimetry. It was found that its value fluctuated between 0.9 and 1.1×10^{-4} cm^{-1}. At such a low level of absorption, conditioning of the front surfaces and side edges becomes critical to the final measured absorption and most probably explains these fluctuations. Finally, a reflecting Bragg grating for the 1064 nm region was fabricated in the same glass melt by exposure of the glass with a dosage of 0.9 J/cm^2. This sample was then thermally developed to provide 98% diffraction efficiency, and then was extensively bleached and re-polished. Absorption at 1085 nm was measured and demonstrated to be equal to 10^{-4} cm^{-1}.

To provide accurate measurements of the absorption coefficient, periods of laser heating and data acquisition were limited to 30 seconds. It allowed us to minimize temperature changes of the sample and the surrounding environment. However, the time duration of this measurement can be extended until an asymptote or saturation level is reached (i.e. it no longer heats) that is determined by the thermal conductivity in the test sample and the heat exchange with the environment. Using the data obtained after prolonged heating, it is possible to calculate for this experimental configuration the maximum optical thickness change that will occur for this level of heating. Both the absorption coefficient and the change in optical thickness per incident power at 1085 nm at saturation were measured and plotted against each other for PTR glass samples with different absorption coefficients (Figure 3.2-6). The correlation appears linear and the slope of the linear relation has the value of ~5000 nm/W cm^{-1} for ~5 mm thick samples. This means that only linear absorption is responsible for heating of the grating (i.e. there are no nonlinear processes involved in the heating).

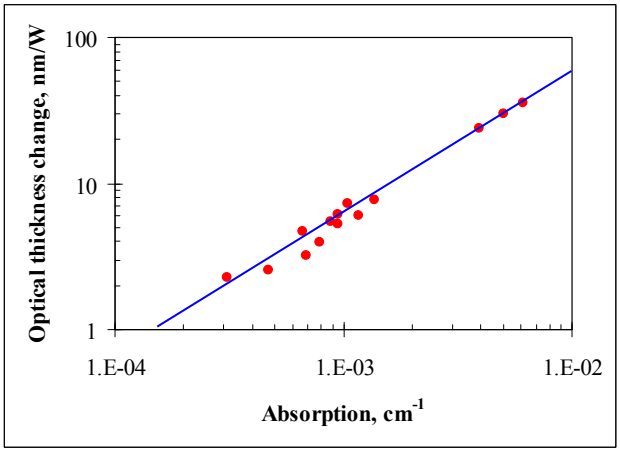

Fig. 3.2-6. Correlation between specific optical thickness change (Δnt/P) and PTR glass absorption coefficient.

Let us consider the effect of high power laser radiation on optical components (volume Bragg gratings) fabricated from PTR glass. The first effect to consider is the possible change of the resonant wavelength. The resonant wavelength of a VBG (let us consider λ_{1064} for specificity) is given by the Bragg formula:

$$\lambda_{1064} = 2n_0\Lambda \tag{2-13}$$

where n_0 is the mean refractive index and Λ the grating period. For simplicity, let us consider uniform heating of the grating by laser radiation. This heating will result in a thermal shift of the central wavelength of the VBG:

$$\frac{1}{\lambda_{1064}}\frac{\partial\lambda_{1064}}{\partial T} = \frac{1}{n_0\Lambda}\frac{\partial n_0\Lambda}{\partial T} = \frac{1}{\Lambda}\frac{\partial\Lambda}{\partial T} + \frac{1}{n_0}\frac{\partial n_0}{\partial T} \tag{3-14}$$

The laser-induced change of the grating period is determined by the laser-induced expansion of the grating material. The geometrical thickness t of such a periodic structure as a VBG can be defined in the following way:

$$t = (N + \varepsilon)\Lambda \tag{3-15}$$

where N is an integer number of periods and ε the fractional number. These two quantities are constant and independent of the temperature of the grating; only Λ changes with heat or stress. Hence, we can write that:

$$\frac{1}{n_0\Lambda}\frac{\partial n_0\Lambda}{\partial T} = \frac{1}{n_0 t}\frac{\partial n_0 t}{\partial T} = \frac{1}{\lambda_{1064}}\frac{\partial \lambda_{1064}}{\partial T} \tag{3-16}$$

In other words, the relative change of the central wavelength of the grating is equal to the relative change of the grating period or to the relative change of the optical thickness of the PTR glass window. Hence, the characterization of the optical thickness change that was described above can be directly used to assess the change of the Bragg wavelength of the volume Bragg grating in PTR glass as a function of the PTR glass absorption coefficient and incident power. Figure 3.2-7 shows this thermal shift of wavelength for natural convective cooling of a glass plate. One can see that if the PTR glass absorption coefficient is equal to 10^{-4} cm^{-1}, 1 kW is expected to shift the central wavelength by ~70 pm while 100 kW will shift it by ~7 nm. The thermal coefficient of the Bragg wavelength in a PTR VBG at 1 μm is equal to ~9 pm/K. It means that for 1 kW and 100 kW of transmitted power with no active cooling, the temperature would reach 8°C and 800°C, respectively. Thus the level of absorption in commercially produced PTR glass and VBGs allows it to be used for spectral beam combining and other types of laser beam control at several kilowatts without active cooling while scaling to tens and hundreds of kilowatts requires decreasing the residual absorption down to 10^{-5} cm^{-1} or/and active cooling of elements.

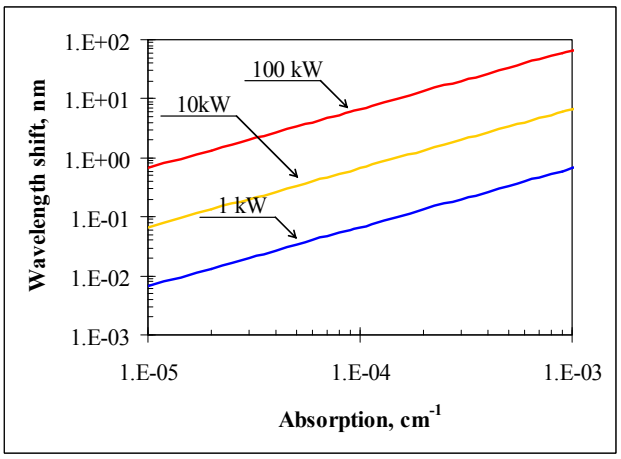

Fig. 3.2-7. Bragg wavelength shift in a conventionally cooled in air PTR glass plate versus the absorption coefficient for different incident power of laser beams.

This very large decrease of absorption in volume Bragg gratings allowed them to be used in high energy laser systems in order to improve their properties. For example, in a *DARPA* project (*Defense Advanced Research Projects Agency*, *SHEDS* project), it was demonstrated that reflecting and transmitting Bragg gratings added in external cavity of diode laser bars allows selecting the longitudinal and transverse modes of the laser (Figure 3.2-8) [39]. Recently, the interest for such diode lasers emitting very narrow lines increased because they allow highly efficient gas pumping using diode lasers. Previously, this was not possible because of the broad

spectrum emission of diode lasers associated with the very narrowband absorption line of gasses (typically a few picometers). Within a project with the *Air Force Research Laboratory*, a 30 W diode bar emitting at 780 nm was locked by a reflecting Bragg gratings, which allowed decreasing the emission spectrum down to 7 GHz and to pump a rubidium gas call with an efficiency of 95% [47] and new projects aim in increasing power of such narrowband diode laser to level of 500 W. It is worth noting that volume Bragg gratings can be used in any laser systems in order to select the longitudinal and transverse mode. As an example in a *NASA*-funded project, volume Bragg gratings associated with Fabry-Perot etalons allowed demonstrating single frequency solid-sate laser 1.5 μm [48].

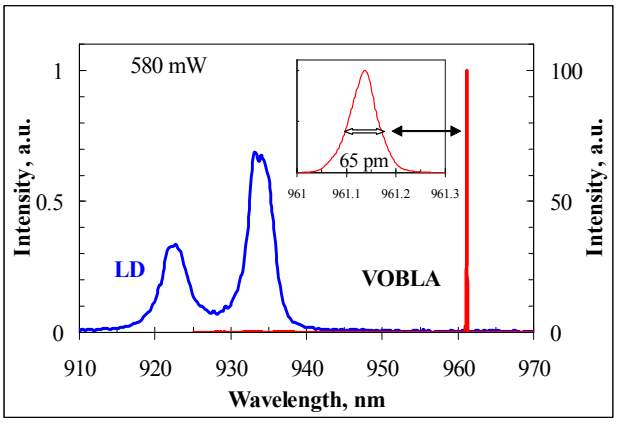

Fig. 3.2-8. Narrowing of the emission spectrum of a diode laser using a reflecting Bragg grating in external cavity.

Another very important application of volume Bragg gratings is spectral beam combining (SBG) (Figure 3.2-9) [49]. The energy of lasers is limited by numerous optical, mechanical and materials parameters. One way to overcome this problem consists in spectrally or coherently combining the beams of high energy lasers in order to form one single high energy laser. One of the methods is based on spectral combination of laser beams with slightly shifted central wavelengths by means of reflecting Bragg gratings. Several project permitted to develop this new technology. One of them, the *ADHELS* project, funded by the *DARPA* allowed to demonstrate the principle and the methods that can be implemented in order to achieve 150 kW of combined CW power. Within this project we demonstrated a decrease of absorption within the 1 μm region by 2 orders of magnitude from typically from 10^{-2} cm^{-1} down to 10^{-4} cm^{-1}. Using these very low absorption gratings, spectral beam combining of 5 beams were demonstrated with a combining efficiency higher than 90%, a combined power of 750 W and a beam quality (M^2) better than 1.6.

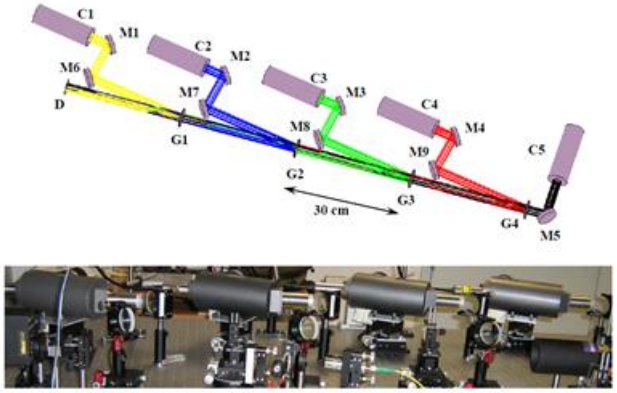

Fig. 3.2-9. Principle of spectral beam combining using reflecting Bragg gratings in PTR glass.

3.2.2. Study of scattering losses in PTR glasses

Scattering in PTR glasses is connected with the precipitation of a crystalline phase in the process of thermal development. The study of crystalline phases in PTR glasses was aided by the use of an X-ray diffractometer. Experimental data in X-ray diffraction were compared with optical data

and a mathematical model was developed to describe the relationships between the parameters of the crystalline phase, refractive index modulation, and scattering.

While X-ray diffractometry is routinely used for measurement of angles of diffraction to determine origin of a crystalline phase, we have developed a methodology of reliable measurement of intensity of a diffracted X-ray beam. This method enabled the measurements of the concentration of the crystalline phase in the bulk of processed PTR glass. Using this method, we achieved a precision of better than 10% for the diffracted intensity and better than 0.05 degrees for the diffracted angle. In order to be able to extract the volume fraction of the crystals in the developed PTR glass, we created a calibration curve obtained by mixing of pristine PTR glass powder with pure NaF crystalline powder with different volume fractions and measuring the resulting diffraction pattern. This approach allowed us to extract the volume fraction of crystals in the glass.

Measurement of the width of the diffraction pattern allowed us to calculate the average crystal diameter using the Sherer formula. It should be noted that the angular width of X-ray diffraction bands are determined by the sizes of monolithic crystals. This is why this formula does not take into account possible clustering of single crystals. It was shown that refractive index change in PTR glass is determined by stresses generated in vicinity of NaF crystals. However, the Sherer formula does not take into account widening of diffraction patterns caused by stresses in a microcrystalline phase. Therefore, we use these calculations as a first approximation for estimation of crystal sizes.

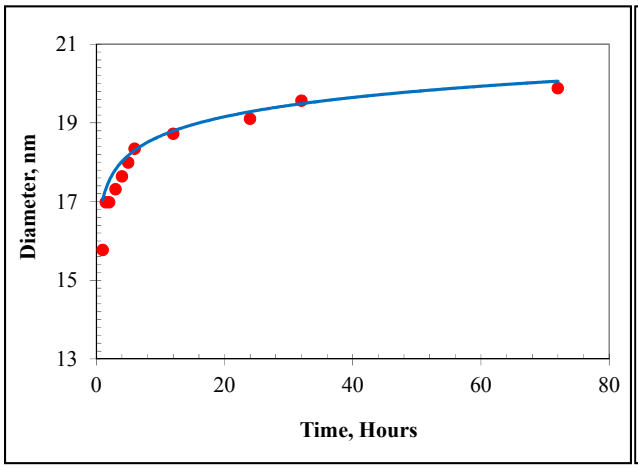

Fig. 3.2-10. Dependence of NaF crystal diameter on duration of thermal development at 515°C.

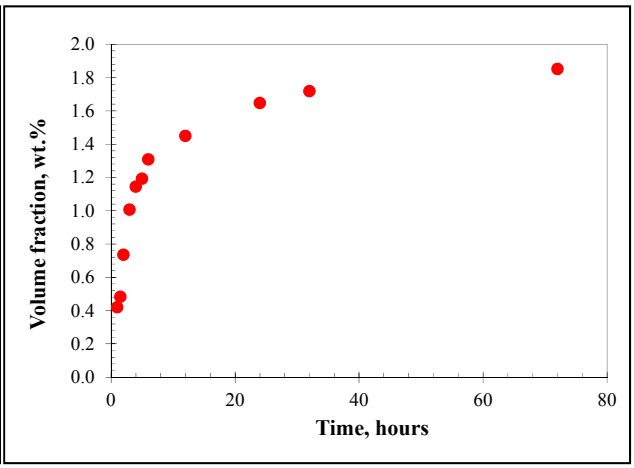

Fig. 3.2-11. Dependence of volume fraction of NaF crystals in PTR glass on duration of thermal development at 515°C.

UV-exposed samples isothermally developed at 515°C for different durations were used for experiments. The refractive index change, the scattering losses and the X-ray diffraction pattern were measured. The 200 diffraction peak of NaF crystals as used for analysis. From the broadening of the diffraction line, the evolution of the average crystal diameter was calculated (Figure 3.2-10). One can see that crystal diameter grows fast and after a few tens of minutes of thermal development, when NaF crystals in UV-exposed PTR glass become detectable in X-ray

diffractometer, their diameter is about 15 nm. At long development time, the growth rate dramatically decreases when the size of crystals approaches ~20 nm. This behavior could be explained by that fact that at long period of thermal treatment all available fluorine is already used and growth is mainly determined by the re-crystallization process which is described by cub-root dependence on period of treatment.

Regarding the volume fraction (Figure 3.2-11), it was found that it changes from ~0.5 up to ~2 vol.%. It was shown that scattering is determined by single crystals and that no clusters of crystals contribute significantly to it. Combining these data using Rayleigh scattering, a model was developed which accurately predicted scattering at any wavelength and for any thermal treatment.

To obtain the effective wave vector and calculate the losses due to scattering, the simple radiative transfer theory, decomposing the field in the material in coherent (not scattered) and incoherent (scattered) components was applied. The effective wave vector in the material is found to be [50]:

$$K^2 = K_{MG}^2 + i\frac{3}{2}k^5 a^3 f\left|\frac{y}{1-fy}\right|^2 \int_0^{\pi}\left(\frac{\sin\theta_s}{2}+\cos^2\theta_s\right)\left(1+(2\pi)^3\eta_0 H\left(\sqrt{k^2\sin^2\theta_s+(k\cos\theta_s-K_r)^2}\right)\right)\sin\theta_s d\theta_s \quad (3\text{-}17)$$

where $y=(\varepsilon_i-\varepsilon_m)/(\varepsilon_i+2\varepsilon_m)$ is the Clausius–Mossotti formula, $\varepsilon_i,\varepsilon_m$ are the dielectric permittivities of the inclusion and surrounding medium, $K_{MG}^2 = k^2(1+2fy)/(1-fy)$ is the Maxwell-Garnett effective wave vector, η_0 is the number of particles / unit volume, θ_s the scattering angle, H is the structure function describing the packing. For low volume fractions of inclusions, the term due to correlated scattering may be neglected. In this case, the losses due to scattering (assuming no absorption) are found to be:

$$\kappa_s = 2\Im(K) = \frac{2k^5a^3f}{K_{MG}}\left|\frac{y}{1-fy}\right|^2(1-8f). \quad (3\text{-}18)$$

A comparison between the experimentally measured and theoretically calculated scattering coefficients is shown in Table 3.2-1. The newly obtained information about inclusion crystal sizes and their concentration resulting from X-ray scattering were used as input parameters for the calculations. Theoretical estimations were performed using radiative transfer theory with uncorrelated inclusion placement (column 3, Table 3.2-1) and the Percus-Yevick pair-correlation function (column 4, Table 3.2-1). Excellent agreement between experimental and theoretical results was obtained. The theory usually produces a slightly larger value for the scattering coefficient than was found from the experiments. The possible reason for that is the presence of a depletion area surrounding the inclusions that can slightly diminish scattering.

Let us now analyze the methods that can be implemented to decrease scattering in PTR glass volume Bragg gratings. The thermal treatment of PTR glass is a 2-step process. First the glass is pre-heat-treated (nucleation) in order to generate silver containing particles (nuclei). The glass is then heat-treated a second time at higher temperatures in order to grow NaF crystals on top of the

silver-containing particles. The refractive index that was achieved is in the first approximation proportional to the volume fraction of crystals. Therefore, it is important to optimize the pre-nucleation heat-treatment procedure in order to generate as many nuclei as possible and thus to minimize the size of the NaF crystals at constant volume fraction. To achieve this, we studied the evolution of the figure of merit of PTR glass (the ratio between the refractive index change in ppm and the losses at 1085 nm in cm^{-1}) as a function of pre-nucleation treatment duration at 485°C followed by a second heat-treatment equal to 60 minutes at 515°C (Figure 3.2-12). One can see that optimization of the nucleation increases the figure of merit by at least a factor of 2.

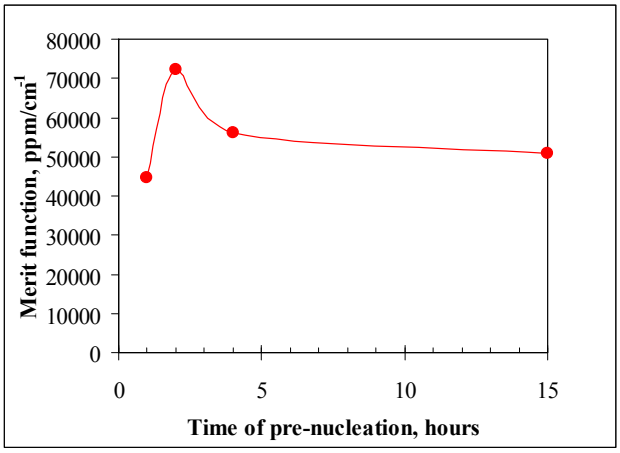

Fig. 3.2-12. Dependence of the merit function of a PTR glass on duration of nucleation.

Table 3.2-1. Experimental and theoretical scattering coefficients at 633 nm of PTR glass after different periods of thermal development.

Thermal treatment duration, hours	Scattering @ 633 nm, cm-1	Scattering (uncorrelated pair-distribution)	Scattering with Percus-Yevick pair-distribution	Volume fraction, vol.%	Crystal diameter, nm
1	0.07857344	0.0765003	0.0794688	0.466933	15.77
1.5	0.11471	0.109258	0.114166	0.537358	16.98
2	0.1542654	0.162249	0.173595	0.816986	16.98
3	0.21152993	0.229507	0.252088	1.119693	17.31
4	0.24816142	0.272207	0.30304	1.271787	17.64
5	0.3187179	0.299464	0.334982	1.325345	17.99
6	0.33078613	0.34423	0.389565	1.454655	18.34
12	0.41105357	0.399808	0.458979	1.611483	18.72
24	0.51288867	0.47295	0.55415	1.831634	19.1
32	0.46750661	0.52582	0.620659	1.910048	19.56
72	0.41246655	0.586539	0.702139	2.057999	19.88

Let us now analyze what are the interrelations between refractive index modulation and scattering. A major goal for all these works was to decrease scattering to the level of 10^{-3} cm^{-1} in PTR glass having a refractive index change high enough to produce a high efficiency reflecting Bragg grating. Typically, a refractive index change between 200 and 300 ppm is enough to provide 99% diffraction efficiency in a few millimeter thick PTR glass plate. We studied the evolution of losses versus refractive index change for different durations and temperatures of the

second heat-treatment. Samples were UV-exposed at 325 nm with a dosage of 0.9 J/cm^2, then nucleated for 100 minutes at 485°C, and then heat-treated for the second time with different regimes, i.e. different durations and temperatures from 485°C up to 525°C. The refractive index changes and losses at 1085 nm were then measured and their interrelation was plotted in Figure 3.2-13. It was found that for a refractive index change above 200 ppm, the scattering losses evolve quasi-linearly with the induced refractive index change, and the parameters of this linear change are not dependent on the thermal treatment temperature. Therefore this first result shows that changing the thermal treatment temperature is not a method that would allow decreasing of scattering for a given refractive index change. This result also shows that for a refractive index change between 200 and 300 ppm, the scattering losses at 1085 nm are between 3 and 4.5 $\times 10^{-4}$ cm^{-1}.

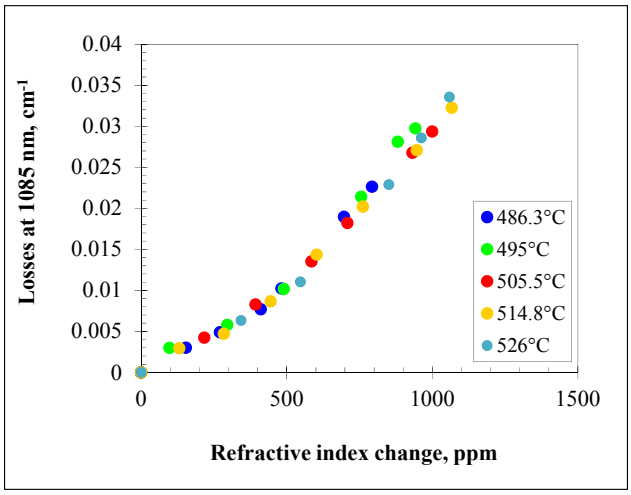

Fig. 3.2-13. Dependence of the losses on refractive index change after thermal development at different temperatures from 485 to 525°C and for different durations.

Up to now, optimization was performed by changing the thermal treatment schedule. However, refractive index change and losses also depend on the dosage of UV-exposure. Therefore we studied the optimization of exposure and thermal processing. The samples were UV-exposed with different dosages from 0.5 to 4 J/cm^2, nucleated for 100 minutes at 485°C and then developed at 515°C for different durations. The refractive index change and losses at 1085 nm were then measured and their interrelation is plotted in Figure 3.2-14. One can see that within the range of refractive index change of interest (200 to 300 ppm), decreasing the dosage will increase the scattering while increasing dosage will have no impact on the scattering and might distort the refractive index modulation. However, increasing dosage might be useful when higher refractive index changes are required. In conclusion, this result means that 0.9 J/cm^2 appears to be an optimal dosage for most of the volume Bragg gratings.

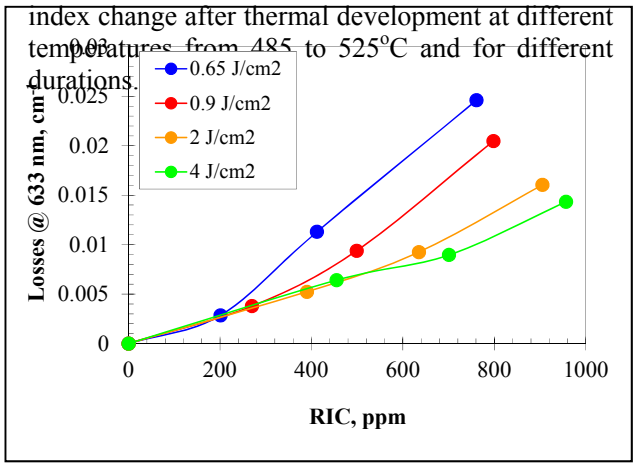

Fig. 3.2-14. Dependence of the losses on refractive index change after UV-exposure with different dosages and thermal development for different durations.

3.3. Study of the linear interaction of an optical radiation with PTR glass and volume Bragg gratings

One of the key point to understand photosensitive materials, and in particular PTR glass, is associated with their interaction with light. Within this section we will limit ourselves to linear

interaction. We will fist present a study of the structure of cerium absorption band and then present a study of the linear diffraction of broadband light source on transmitting Bragg gratings.

3.3.1. Cerium ionization in PTR glass

Cerium in PTR glasses is a key element in PTR glass as it is playing the role of photosensitizer. Cerium presents in glasses two different valence states, namely Ce^{4+} and Ce^{3+}, inducing absorption in the UV-region with respectively a wide ceric peak centered at about 240 nm and a relatively narrow asymmetrical cerous peak with a maximum around 300-320 nm [51]. Meanwhile, spectroscopic study of cerium behavior in glasses has apparent difficulties because of the overlapping of these bands. It was also found that ceric-cerous redox equilibrium in silicate glasses is rather complex and depends on many factors (*i.e.* host-glass composition, temperature, oxygen ion activity and the total amount of cerium present) [52]. However, Ce^{3+} and Ce^{4+} are both present in silicate glasses even under a very strong reducing or oxidizing conditions.

To separate overlapped absorption spectra of Ce^{3+} and Ce^{4+}, a new approach was used. It was recently developed for the study of iron absorption in soda-lime-silica glasses [53]. Similarly to cerium, iron presents two oxidation states (Fe^{2+} and Fe^{3+}) which have overlapped absorption spectra. This approach is based on balance equations for absorption spectra of all studied dopants in glass samples melted under different redox conditions. It allowed separating the overlapped absorption spectra of Fe^{2+}, Fe^{3+} and OH^- ions in UV, visible and NIR regions [53-54]. It is very important to note that this approach used no preliminary assumptions concerning quantity, positions and spectral shape of ferrous, ferric and hydroxyl absorption bands. A reliable algorithm for resolving experimental spectra into characteristic spectra of cerous, ceric and intrinsic glass absorption was developed.

PTR glasses with composition $70SiO_2$-$15Na_2O$-$5ZnO$-$4Al_2O_3$-$5NaF$-$1KBr$ were melted. Cerium-doping of PTR glasses was done using respectively 0.008 mol% of Cerium. To study the spectral shape of Ce^{3+} and Ce^{4+}, PTR glasses were melted under different redox conditions. Standard conditions were obtained by melting in air. Oxidizing conditions were obtained by melting under oxygen atmosphere inside the furnace (flow rate of 10 sccm of O_2). Reducing melting conditions were obtained by adding high purity graphite powder to the initial batch. Therefore, 4 glass samples were prepared, which are undoped glass matrix and Ce-doped glasses melted in air (standard conditions), under oxidizing and reducing atmosphere

The absorption spectra of undoped (PTR_m) and Ce-doped ($PTR_{Ce,s}$) PTR glasses melted in air were measured using a Varian Cary 500 spectrophotometer and are illustrated in **Error! Reference source not found.**. The absorption spectrum of cerium was derived by subtraction of the undoped glass spectrum

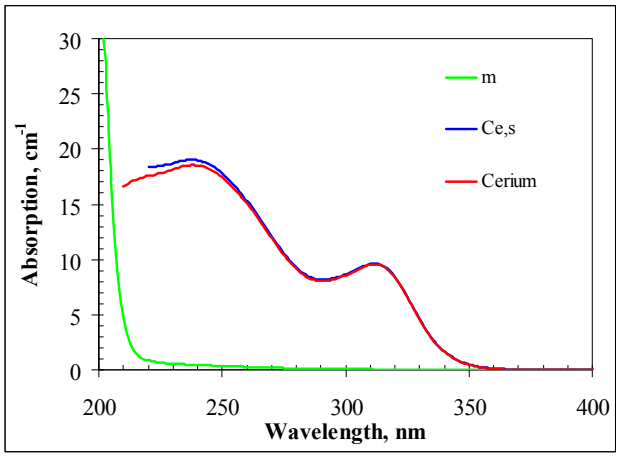

Fig. 3.3-1: Absorption spectra of PTR matrix and Ce-doped PTR glass.

from that of the Ce-doped glass. This absorption spectrum has two maxima; each of them could be associated with one of the oxidation state of cerium. An absorption spectrum of PTR glass matrix in far UV spectral region consists from an exponential tail of glass matrix intrinsic absorption at the short wavelength side and a combination of absorption spectra of impurities of Fe^{3+} and Fe^{2+} at the long wavelength side [53-54]. One can see that absorption of impurities in the range of 220-250 nm for the studied sample was below 1 cm^{-1}. This means that maximum possible effect of impurities on the extracted absorption spectrum of cerium is below 5%.

In the absorption spectrum of cerium, the band with a maximum located near 240 nm is usually ascribed to Ce^{4+} and the band with a maximum around 305 nm - to Ce^{3+}. Similar spectra were measured in PTR glasses melted under different conditions ($PTR_{Ce,\ s}$, $PTR_{Ce,r}$, and $PTR_{Ce,o}$) are presented in Figure 3.3-2. One can see that the ratio between the amplitude of the bands with maximum at 240 and 305 nm depends on the melting conditions due to a change of the ratio between Ce^{3+} and Ce^{4+}. Nevertheless, the positions of these bands are not affected by the glass oxidation or reduction proving that no significant composition change was associated with the redox control. The bands of Ce^{3+} and Ce^{4+} being overlapped, the study the contribution of each oxidation state of cerium requires to separate the contribution to absorption of each type of cerium.

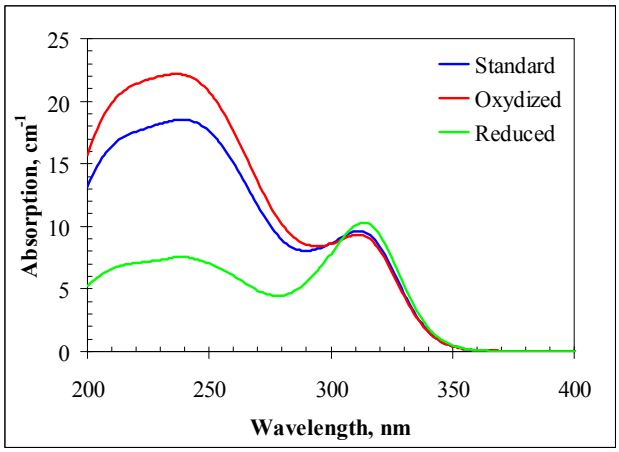

Fig. 3.3-2: Absorption spectra of cerium in PTR glasses melted under different redox conditions.

The absorption spectra of undoped and Ce-doped PTR glasses in the range from 200 to 800 nm come from three main sources: the intrinsic absorption edge of the glass matrix, cerous and ceric ions. Due to the high purity of raw materials used to prepare glasses, we can assume the absence of absorption from any other components. Therefore any experimental absorption spectrum can be described as the sum of the individual absorption bands of each species:

$$A_{\exp,i}(\lambda) = A_G(\lambda) + C_{Ce3,i} \cdot \alpha^{Ce^{3+}}(\lambda) + C_{Ce4,i} \cdot \alpha^{Ce^{4+}}(\lambda), \tag{3-19}$$

$$C_{Ce,i} = C_{Ce3,i} + C_{Ce4,i}\ , \tag{3-20}$$

where $A_{exp,i}$ is the experimental absorption of the sample #i, A_G is the intrinsic absorption of the glass matrix, α^{Ce3+} and α^{Ce4+} are specific absorption spectra of cerous and ceric ions respectively, $C_{Ce3,i}$ and $C_{Ce4,i}$ are the concentration of each type of cerium ions in the glass sample #i.

We solved the system of equations similar to equation (3-19) written for glasses melted under different redox conditions First, we were able to extract the specific absorption spectrum of Ce^{3+} can be extracted as well as the specific absorption of Ce^{3+} (α^{Ce3+}) at λ_{2max} =307 nm is equal to

340 ± 5 cm^{-1}/at. % Ce^{3+}. The absorption spectrum of Ce^{3+} was then modeled using a technique based on its deconvolution into the sum of a number of Gaussian functions:

$$A_{th}(\sigma) = \sum_i A_i^{\circ} \exp\left(\frac{-(\sigma - \sigma_i^{\circ})^2}{W_i^2}\right), \tag{3-21}$$

where $A_{th}(\sigma)$ is the calculated absorption spectrum, $A°_i$, $\sigma°_i$ and W_i are respectively the amplitude, the central wavenumber and the full width at the half maximum of the Gaussian band #i. The principle consists in minimizing the figure of merit (FoM) while using the minimum number of Gaussian functions, with:

$$FoM = \min_{\sigma_i^0, \Delta\sigma_i} \left\{ \int_{\sigma_{min}}^{\sigma_{max}} \left[A_{exp}(\sigma) - A_{th}(\sigma) \right]^2 d\sigma \right\} \tag{3-22}$$

where $A_{exp}(\sigma)$ is the experimental absorption curve and $A_{th}(\sigma)$ is the calculated absorption spectrum. Based on this method, it was found that a minimum of 2 bands are required to model the absorption bands of Ce^{3+} with accuracy corresponding experimental measurements. Parameters of each Gaussian band are presented in Table 3.3-1. Then, we extracted the absorption spectrum of Ce^{4+} ions and modeled using the sum of 2 Gaussian functions which parameters are summarized in Table 3.3-1. Specific absorption of Ce^{4+} at λ_1=240 nm is equal to 1430 ± 10 cm^{-1}/at. % Ce^{4+}. The modeled absorption spectrum of cerium in PTR glass is shown in Figure 3.3-3.

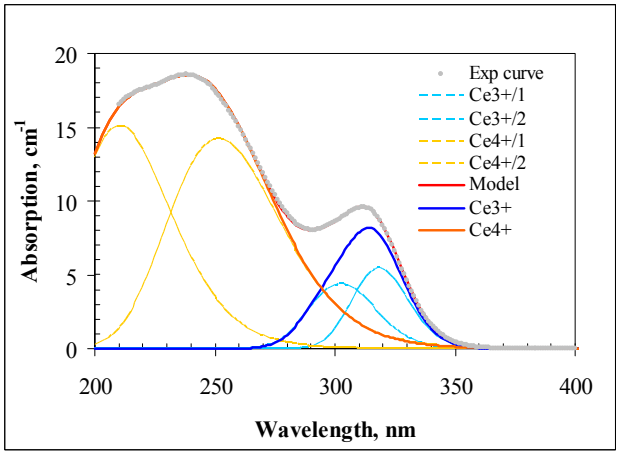

Fig. 3.3-3: Decomposition of the cerium absorption band in PTR glass with Gaussian functions.

Table 3.3-1: Parameters of the Gaussian bands of cerium absorption spectra in a standard SCN glass and PTR glass. A0i is the specific absorption of cerium in the maximum of a Gaussian band, σ_i the central wavenumber, λ_i the central wavelength, and W_i, the full width at half maximum.

Band #	A_i^0 (cm^{-1}/at.%)	σ_i (cm^{-1})	λ_i (nm)	W_i (cm^{-1})
Ce3+/1	126.8	32045 ± 10	312 ± 0.1	1542.4 ± 0.5
Ce3+/2	246.3	33059 ± 10	302 ± 0.1	2072.3 ± 0.5
Ce4+/1	1148.5	40045 ± 10	250 ± 0.1	5278.0 ± 0.5
Ce4+/2	835.5	47488 ± 20	211 ± 0.2	6458 ± 1

As mentioned in the introduction, cerium is used in silicate glasses as photo-sensitizer. In the case of PTR glass the linear photo-thermo-refractive process under near UV excitation exists only because of the presence of cerium in this glass [55]. Therefore, a detailed analysis of the effect of UV-light to the structure of the absorption band of cerium is extremely important. PTR glass matrix doped with cerium ($PTR_{Ce,s}$) was used for this study. The samples were exposed to radiation of a He-Cd laser at 325 nm to dosages of 5 J/cm² (Figure 3.3-4). Absorption spectra were measured after UV-exposure and thermal treatment (one hour at 100°C) to bleach transient color centers. During this UV-exposure, photoionization of Ce^{3+} into $Ce^{4+}$is expected to occur. If this supposition is true, each Ce^{3+} that disappears would be converted into a new Ce^{4+} ion and band of Ce^{4+} would increase accordingly. However, this supposition could not be confirmed when trying to separate the contribution of Ce^{3+} and Ce^{4+} and decomposition into Gaussian functions revealed that UV-exposure did not induce any increase of the Ce^{4+} absorption band but induced a broad band that can be fitted with single Gaussian function with maximum localized for PTR glass at ~242nm The wavelength of this band remains unchanged irrespective of the increased of the dosage while its amplitude increases within increasing the dosage. This induced band is attributed to hole centers (Ce^{3++}) and electrons (e^-) formed during the ionization process:

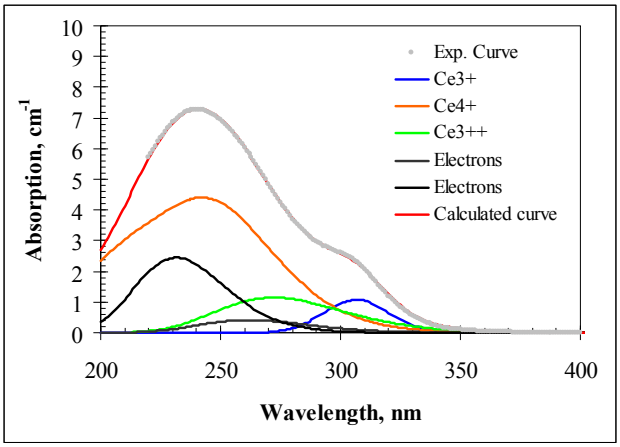

Fig. 3.3-4: Decomposition of cerium absorption spectrum (neutral PTR glass) after UV-exposure with dosage of 5 J/cm2. Decomposition was carried out using Ce3++ and electron bands.

$$Ce^{3+} + h\nu \rightarrow Ce^{3++} + e^- \qquad (3\text{-}23)$$

This result shows that the photochemistry of cerium in silicate glass is rather complex and it justifies our approach of separating contribution of each ion and decomposing them into a sum of Gaussian functions. Actually after UV-exposure, not only two bands will contribute to absorption in UV-range but at least three bands. In other words, without a model for absorption band of cerium, analysis of the evolution of each species is impossible. It is also possible to analyze this broad absorption band of hole and electron centers by decomposing it into several narrower bands (Figure 3.3-4). It is possible to use one band centered at 272 nm that can be associated with Ce^{3++} and 2 bands of electron centers centered at 232 and 262 nm with parameters identical to the one that appear after ionization of multi-component silicate glass matrix [42,56].

3.3.2. Linear diffraction of ultrashort pulses by transmitting Bragg gratings

Recent results with high power continuous-wave (CW) and ultrashort pulsed lasers have demonstrated the usefulness of PTR glass diffractive optical elements for laser beam control [57,58]. The diffraction characteristics of surface gratings for both CW and ultrashort pulses

have been studied for a long time and are well known [59-60]. However the diffraction characteristics of ultrashort laser pulses by volume gratings are not well established. Moreover, volume gratings introduce a new design parameter, angular filtering, that is not available with traditional surface gratings. We therefore investigated ultrashort laser pulse diffraction by transmitting volume Bragg gratings (TBGs) recorded in PTR glass.

The diffraction efficiency of TBGs by plane wave monochromatic illumination is well modeled using Kogelnik's coupled wave analysis [61]. The TBG diffraction efficiency formula given by Kogelnik is

$$\eta(\lambda,\theta) = \frac{\sin^2\left\{\sqrt{\nu(\lambda,\theta)^2 + \xi(\lambda,\theta)^2}\right\}}{1+\xi(\lambda,\theta)^2/\nu(\lambda,\theta)^2}, \tag{3-24}$$

Where

$$\nu(\lambda,\theta) = \frac{\pi n_1 L}{\lambda\cos\theta}, \tag{3-25}$$

$$\xi(\lambda,\theta) = \frac{\pi L}{\cos\theta}\left[\frac{1}{\Lambda}\sin\theta - \frac{\lambda}{2\Lambda^2 n(\lambda)}\right]. \tag{3-26}$$

The parameters in the above equations are as follows: λ is the wavelength of light, θ is the incident angle of light on grating, L is the grating thickness, n_1 is the amplitude of refractive index modulation, $n(\lambda)$ is the refractive index of the grating material as a function of wavelength, and Λ is the grating period. To see how well Equation (3-24) describes ultrashort laser pulse diffraction by TBGs a Ti:sapphire Spectra-Physics Tsunami femtosecond laser system was used to generate femtosecond pulses with the following characteristics: ~150 fs pulse-width, central wavelength tunable from 760 nm to 840 nm, Gaussian spectrum, linear polarization, 80 MHz repetition rate, and energy per pulse on the order of 10 nJ. Several TBGs with different parameters were recorded in PTR glass for this study. Their parameters are summarized in Table 3.3-2.

Table 3.3-2. Parameters of TBGs in PTR glass. †Bragg angle and spectral selectivity calculated for 810 nm central wavelength.

TBG	Λ, μm	L, mm	n_1, ppm	θ_{Br}†, deg	$\Delta\lambda$†, nm
G1	5.97	2.15	200	3.9	33
G2	1	0.74	507	23.9	2.5
G3	5.97	5.11	80	3.9	14

The diffraction efficiency of gratings G1 and G2 was measured using femtosecond pulses with approximately 6.4 nm spectral bandwidth and central wavelength at 810 nm. Figure 3.3-5 compares the experimental measurements with the theoretical monochromatic wave expression given by Equation (3-24). It is seen that experiment and theory agree for grating G1 but not for grating G2. Disagreement with monochromatic theory is expected because an ultrashort laser pulse, according to the Fourier transform relationship between time and frequency, is

polychromatic in nature. However, in the approximation that the spectral selectivity of the grating is greater than the spectral bandwidth of the ultrashort laser pulse, monochromatic wave theory still works. Thus when femtosecond pulses with spectral bandwidth of 6.4 nm were diffracted by the gratings, the efficiency predictions of Equation (3-24) agreed for grating G1 (spectral selectivity equal to 33 nm) but failed for grating G2 (spectral selectivity equal to 2.5 nm). In Ref. [62] it was shown that a convolution between the spectral distribution of a polychromatic source with the monochromatic diffraction efficiency expression gives a new diffraction efficiency formula that correctly predicts experimental measurements. For a Gaussian spectral distribution the new expression is given by

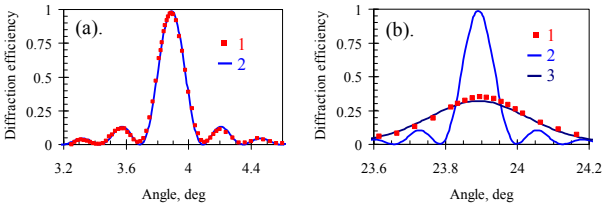

Fig. 3.3-5. Diffraction efficiency of TBGs: (a) grating G1 (b) grating G2. 1 – experiment with 150 fs pulses, 2 – monochromatic wave modeling, 3 – polychromatic wave modeling.

$$\eta(w,\theta) = \sqrt{\frac{2}{\pi}}\frac{1}{w}\int \eta(\lambda,\theta)\exp\left[-2\left(\frac{\lambda-\lambda_0}{w}\right)^2\right]d\lambda \qquad (3\text{-}27)$$

where λ_0 is the central wavelength of the light, w is the $HWe^{-2}M$ spectral bandwidth, and $\eta(\lambda,\theta)$ is given by Equation (3-24). Using Equation (3-27) it is possible to correctly predict the diffraction efficiency of ultrashort laser pulse diffraction by a TBG with spectral selectivity narrower than the pulse bandwidth, Figure 3.3-5(b).

Diffraction of an ultrashort laser pulse by a single TBG leads to spatio-temporal distortion since angular dispersion of the grating causes different wavelength components of the pulse to diffract at different angles, thereby contributing to pulsewidth broadening. Another spatio-temporal distortion, of particular concern when dealing with ultrashort pulses, is pulse front tilt (PFT) [63]. PFT is a time delay across the transverse direction of the pulse due to the fact that the pulse front is no longer perpendicular to the propagation direction after diffraction. The classical formula for PFT is

$$\mathrm{PFT} = 2\tan\theta/c. \qquad (3\text{-}28)$$

where c is the speed of light and θ is the angle of diffraction. To verify that TBGs in PTR glass generate a PFT that obeys Equation (3-28) we employed the technique of spectral interferometry (SI) [64]. When two coherent pulses are combined spatially but not necessarily temporally the result in the spectral domain is an interference pattern. The number of interference fringes corresponds to the relative time delay

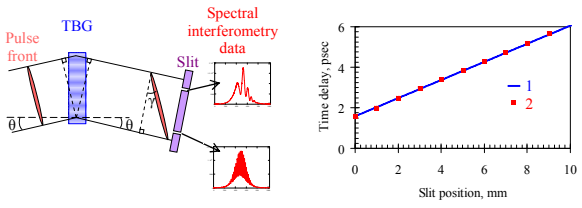

(a). (b).

Fig. 3.3-6. Measuring pulse front tilt of diffracted ultrashort pulses via spectral interferometer: (a) geometrical arrangement (b) pulse time delay calculated from spectral fringe data as a function of slit position, 1 – theory 2 – experiment.

between the two pulses. To implement SI we constructed a Mach-Zehnder interferometer and used one path as a reference while the other path was diffracted by a TBG. After recombination a narrow slit was translated across the beam to collect interferograms from the different transverse parts of recombined beam. Since the reference pulse had a flat pulse front, the change in fringe number (i.e. time delay) is related to the shape of the diffracted pulse front. Figure 3.3-6(a) illustrates how PFT was measured using SI along with a slit to isolate different transverse parts of the diffracted pulse. At each slit position the time delay was measured and a table of time delay versus slit position collected. A linear fit to the data gave a line whose slope was equal to the PFT. The experimentally measured PFT for grating G1 was 0.453 ps/mm. The theoretical value calculated using Equation (3-28) and the Bragg angle for G1 is 0.455 ps/mm. As shown in Figure 3.3-6(b) experiment and theory are in good agreement.

It is important to emphasize that TBGs differ significantly from traditional surface gratings because of their selectivity properties. As seen in Figure 3.3-5(a), grating G1 demonstrated an angular selectivity of about 0.2º FWHM and near 100% diffraction efficiency. The angular filtering properties of TBGs have been used for the selection of a single transverse mode from a laser [66]. A common practice for single transverse mode operation of ultrashort lasers is to insert an aperture inside the cavity to limit the angular spread of the beam. Unfortunately this also has the effect of limiting the spatial area of the laser gain medium used for lasing. By using a TBG pair with the proper angular selectivity characteristics inside an ultrafast laser resonator the laser could be forced to operate with single transverse mode while utilizing the entire area of the laser gain medium. In addition, double pass through the TBG pair would correct for spatial chirp that is inherent with single pass through a grating pair.

3.4. Study of the non-linear interactions in PTR glass and volume Bragg gratings

3.4.1. Study of the non-linear photosensitivity of PTR glasses

Up to now, we have described how to trigger PTR glass photosensitivity via linear excitation of Ce^{3+} (photo-sensitizer in PTR glass) within its spectrum of photosensitivity (280 to 350 nm). Let us now study the methods that can be implemented in order to non-linearly excite PTR glasses. We investigated direct refractive index change in PTR glass by means of direct exposure to high intensity laser pulses: a Ti:sapphire laser for femtosecond pulses and a Nd:YAG laser for nanosecond pulses.

The method for characterizing PTR glass photosensitivity to short laser pulse exposure was the same as in Ref. 25. Glass samples were fixed to a computer controlled translation stage and moved across the excitation laser beam at constant velocity. For scanning along the x-axis this exposure results in a line with a lateral y-axis profile of energy dosage given by:

$$D(y) = \sqrt{\frac{2}{\pi}} \frac{E_p R}{v w} \exp\left(-2\frac{y^2}{w^2}\right) \qquad J/cm^2 \qquad (3\text{-}29)$$

where E_p is the energy per pulse [Joules/pulse], R is the repetition rate of the laser [pulses/sec], v is the scanning velocity [cm/s] and w is the beam waist, $HWe^{-2}M$ [cm]. This equation is only

valid for laser pulses with Gaussian spatial distribution of energy and for scanning conditions that obey v/R < *w*. The intensity I at the center of the incident Gaussian laser pulse is given by

$$I = \frac{2}{\pi}\frac{E_p}{\tau w^2} \qquad W/cm^2 \tag{3-30}$$

where τ is the temporal width, FWHM [s], of the laser pulse. Because both lasers used in our experiments operate at wavelengths outside of the linear photosensitivity region of PTR glass high intensities were required to activate photosensitivity. Long focal length lenses were used to focus the beam to high intensities but still have a large enough focal spot size to make refractive index change measurements. Glass samples were placed after the focus in order to prevent optical damage at the surface. The intensity of laser radiation as given by Equation (3-30) was calculated using this beam waist measurement and it corresponds to the intensity at the front surface of the glass samples. The laser pulse energy was controlled with a rotating polarizer. Femtosecond pulses were generated from a Ti:sapphire regenerative amplifier system operating at $\lambda_0 = 783$ nm, R = 1 kHz, $\tau \approx 120$ fs, and maximum energy per pulse of 1 mJ. Nanosecond pulses were generated from a Nd:YAG laser operating at third harmonic $\lambda_0 = 355$ nm, R = 15 Hz, $\tau \approx 8$ ns, and maximum energy per pulse of 5 mJ. After laser pulse exposure the glass was heat treated for about 2 hours at 515°C to generate the induced refractive index change. The refractive index change was measured using a shearing interferometer setup [25]. Its basic principle is to create an interferogram that relates the index change to a fringe shift. A liquid cell with index matching fluid was used to eliminate glass sample thickness variations from contributing to the fringe shift and therefore the interferometer fringe distortions occured only from refractive index variations.

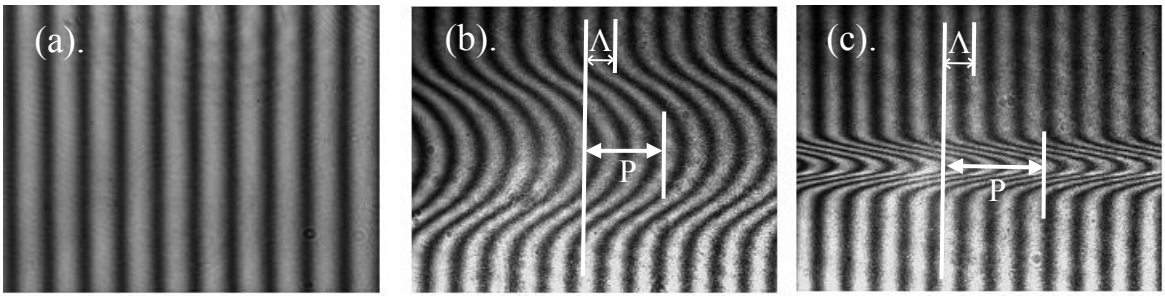

Fig. 3.3-7. Interferograms of thermally developed PTR glass: (a) unexposed region, (b) line exposed by CW He-Cd laser, (c) line exposed by IR femtosecond laser.

Figure 3.3-7 shows typical interferograms of a PTR glass sample after thermal treatment. One can see fringe shift in areas exposed to both low power UV radiation and high power femtosecond pulses of IR radiation. The lateral profile given by Equation (3-29) is evident in the exposed regions. The maximum index change Δn is given by

$$\Delta n = \frac{\lambda_{test}}{2t}\frac{P}{\Lambda} \tag{3-31}$$

where λ_{test} is the wavelength of the laser used in the shearing interferometer setup (here 632.8 nm), t is the thickness of the glass sample (about 2 mm), and (P/Λ) is the fringe shift at maximum distortion. It is important to note that the fringe shift seen in Figure 3.3-7 for IR femtosecond scanning is in the same direction as for He-Cd scanning. This indicates that the refractive index change by femtosecond exposure is negative. Moreover, interferograms taken before thermal treatment show no appreciable fringe shift after laser pulse exposure. The same phenomena were detected after exposure of PTR glass to high power pulsed of third harmonic of Nd:YAG laser at 355 nm. Thus we can reliably attribute the index change in PTR glass induced by IR femtosecond pulses and UV nanosecond pulses as occurring from the photo-thermo-refractive process.

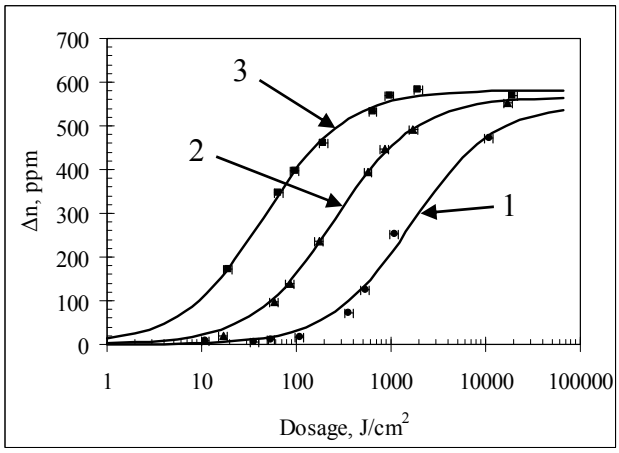

Fig. 3.3-8. Refractive index change as a function of laser pulse dosage for different intensities: (1) 1.9 TW/cm^2 (2) 3.1 TW/cm^2 and (3) 3.5 TW/cm^2. Pulse wavelength 783 nm, pulse duration ~120 fs, spot diameter 200 μm.

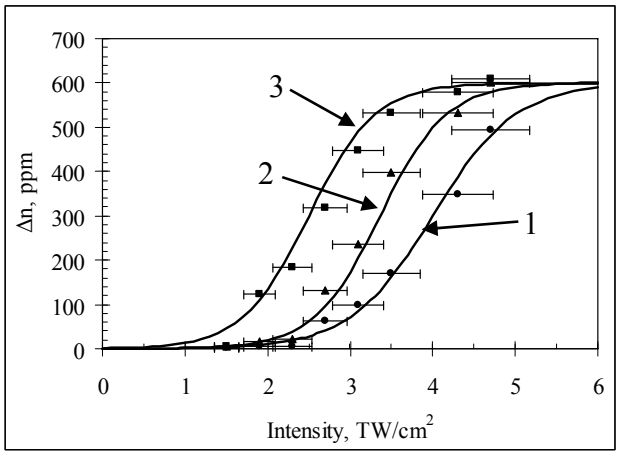

Fig. 3.3-9. Refractive index change as a function of laser pulse intensity for different dosages: (1) 25 J/cm^2 (2) 130 J/cm^2 and (3) 860 J/cm^2. Pulse wavelength 783 nm, pulse duration ~120 fs, spot diameter 200 μm.

The complete photosensitivity curves for PTR glass laser pulse exposure were constructed by scanning lines of different intensities and dosages in the same glass sample. In one square PTR glass sample (25 mm × 25 mm) approximately forty lines could be scanned. After scanning, the glass was thermally developed for 2 hours at 515°C. The refractive index change of each line was measured as described above. Figures 3.3-8 and 3.3-9 show the dependencies of refractive index decrement on dosage and intensity for IR femtosecond exposure. The refractive index change as a function of dosage is plotted on a log scale and extends across a wide range. In contrast, refractive index change as a function of intensity is plotted on a linear scale and shows a sharp onset threshold which quickly reaches saturation. Induced refractive index could not be observed after exposure with intensity below 1 TW/cm^2, while at 5 TW/cm^2 induced refractive index is at saturation. Curves of Δn vs. D could be fitted to hyperbolic curves of the form

$$\Delta n(D) = \frac{n_{\max} D}{k + D} \tag{3-32}$$

where Δn(D) is refractive index change as a function of dosage, n_{max} is the saturation index, and k is a fitting parameter for a specific intensity of irradiation. These hyperbolic curves are solutions to a differential equation describing the process of photosensitivity in PTR glass [34].

Photosensitivity curves for UV nanosecond exposure are shown in Figures 3.3-10 and 3.3-11. Curves of Δn vs. D are again fitted to hyperbolic curves. The Δn vs. I curve for nanosecond exposure shows a more gradual approach to saturation than in the femtosecond exposure case.

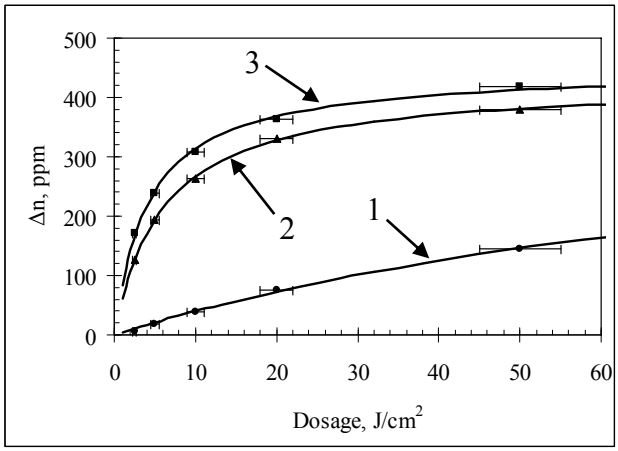

Fig. 3.3-10. Refractive index change as a function of laser pulse dosage for different intensities: (1) 2.5 MW/cm^2 (2) 20 MW/cm^2 and (3) 100 MW/cm^2. Pulse wavelength 355 nm, pulse duration 8 ns, spot diameter 520 μm.

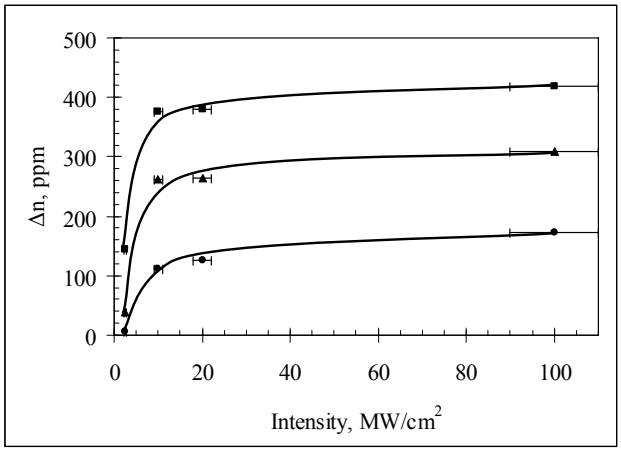

Fig. 3.3-11. Refractive index change as a function of laser pulse intensity for different dosages: (1) 2.5 J/cm^2 (2) 10 J/cm^2 and (3) 50 J/cm^2. Pulse wavelength 355 nm, pulse duration 8 ns, spot diameter 520 μm.

Figures 3.3-8 to 3.3-11 show the evolution of photo-induced refractive index change in PTR glass as a function of dosage and intensity when exposed to high intensity laser pulses. In both femtosecond and nanosecond exposure the Δn vs. I curves depend on the intensity of irradiation. This is in violation to the reciprocity law observed for linear photosensitivity and therefore indicates a nonlinear process. It is well known that linear photosensitivity of PTR glass by He-Cd laser exposure is due to photoionization of cerium and its valence change from Ce^{3+} to Ce^{4+}. The released electrons are trapped by silver and it changes its valency from Ag^{+} to Ag^{0}. The spatial distribution of atomic silver represents a latent image in PTR glass. In the case of photosensitivity by nanosecond pulses the role of cerium is not obvious since the energy of two photons of third harmonic of Nd:YAG laser (7 eV) is significantly higher than the energy which corresponds to a transition within the absorption band of Ce^{3+} (4 eV). To investigate the role of cerium in nonlinear photosensitivity by high intensity laser pulses we prepared a PTR-like glass without the sensitizer cerium. After exposure to high intensity laser pulses and thermal treatment this glass shows a refractive index change with similar dependence on intensity and dosage as in the case of glass with cerium. Moreover, measuring absorption spectra after exposure show that both UV nanosecond and IR femtosecond exposure generate a color center absorption band centered at ~360 nm. This color center band is absent in the case of Ce-doped PTR glass exposure by CW He-Cd laser at 325 nm. However it appears when Ce-doped PTR glass is exposed to the ultraviolet wavelengths of a Xenon lamp or by gamma irradiation and was identified as evidence of glass matrix photoionization [11]. This band is thermally bleached after

thermal treatment for 2 hours at 515°C and an absorption band characteristic of silver containing particles appears centered at about 465 nm. The absence of a color center band at ~360 nm in the case of CW He-Cd laser exposure at 325 nm but its presence in the case of both cerium-doped and cerium-free PTR glass exposed to short laser pulses proves that these pulses produced ionization of glass matrix (not dopants) which results in generation of intrinsic hole color centers with absorption band at ~360 nm and mobile electrons. The fact that cerium free PTR glass exposed to short laser pulses develops a refractive index decrement equal in magnitude with that of cerium-doped PTR glass proves that the rest of structural transformations (reduction of silvers and NaF crystal growth) is similar in Ce-doped and Ce-free glasses.

For glass matrix photoionization in PTR glass to occur, exposure to wavelengths below ~220 nm is necessary [67]. Nanosecond pulses at 355 nm can meet this condition by a two-photon process. This is therefore the most probable phenomenon at the origin of the nonlinear photosensitivity at 355 nm similar to that for sodium-silicate glasses [68]. In the case of PTR glass exposure to femtosecond pulses at 783 nm the mechanism is more complex. It was noticed that the change in refractive index after femtosecond pulse exposure and heat treatment did not begin at the front face of the glass but only after some depth into the glass. This feature was studied in more detail using a long (25 mm) PTR glass sample. Figure 3.3-12 shows the glass sample under high intensity IR femtosecond pulse irradiation. An area of blue luminescence can be seen in the glass bulk. This blue luminescence in silicate glasses results from recombination of intrinsic electron and hole centers produced by glass matrix ionization [69,70]. It was found that the area emitting this luminescence corresponds to the area of refractive index change after heat treatment. The conclusion is that femtosecond pulses at 1.6 eV (780 nm) photoionized the glass matrix of PTR glass which has an absorption edge at 5.8 eV [71], but did not directly modify the refractive index. This implies a 4-photon nonlinear process. These nonlinear photoionization results were generalized by lowering the photon energy of the pulses to 0.9 eV (1430 nm) and using a wider band gap material, fused silica. The band gap of fused silica is about 9.3 eV and therefore to photoionize this glass by 0.9 eV pulses implies an 11-photon nonlinear process. An optical parametric amplifier pumped by femtosecond pulses from a Ti:sapphire laser system was used to generate 0.9 eV pulses with about one picosecond time duration, 1 kHz repetition rate, linear polarization, and energy per pulse about 20 μJ. A 15 mm focal length lens was used for focusing. A fused silica sample 30 mm in length and polished on all sides was tested. When placed inside beam a red filament forms inside fused silica. The filament is red in color because recombination of intrinsic electron and hole centers in fused silica results in a luminescence band at 650 nm [72]. The conclusion is that 0.9 eV ultrashort laser pulses can photoionize a 9.3 eV band gap material. We then investigated theoretically whether the nonlinear photoionization mechanism required for a 4-photon or 11-photon process to occur in silicate glass predicts a laser intensity above the damage threshold for

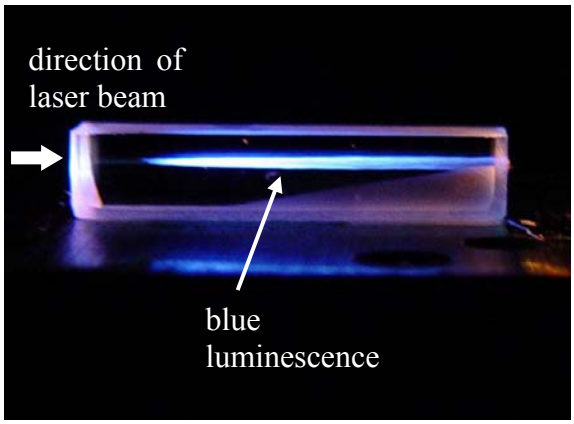

Fig. 3.3-12. Blue luminescence inside PTR glass during femtosecond laser illumination corresponds to the region of photoionization and refractive index change after heat treatment.

glass or if it is possible for a multiphoton process to photoionize silicate glass without causing laser-induced damage.

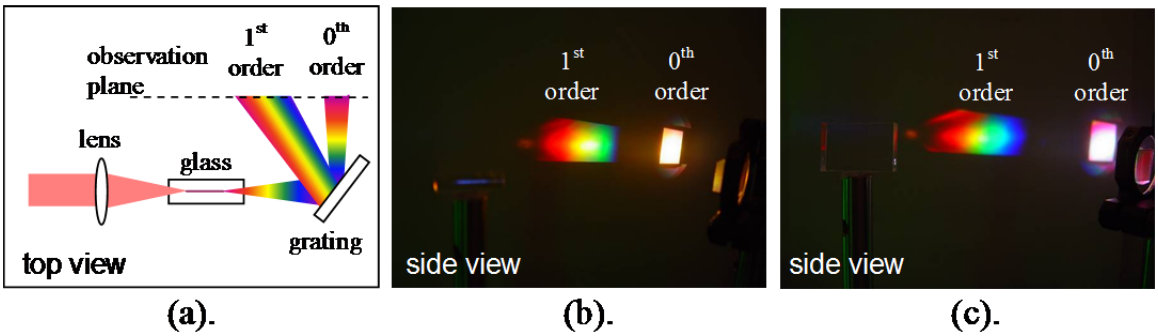

Fig. 3.3-13. Supercontinuum generated in glass by focused femtosecond pulses at 780 nm: (a) experimental setup (b) PTR glass (c) fused silica.

In addition to filament formation there is another interaction that occurs when infrared ultrashort pulses interact with silicate glasses. Spectral broadening of the pulse occurs during pulse propagation in the glass and causes emission of a broad spectrum of wavelengths. This is the phenomenon of supercontinuum generation [73]. Figure 3.3-13(a) shows a setup used to study supercontinuum emission by glass. A diffraction grating is placed at the output of the glass to separate the supercontinuum spectrum into individual wavelength components. The result for PTR glass is that a cutoff for blue wavelength components is observed, Figure 3.3-13(b). PTR glass is transparent down to 350 nm and therefore one expects to see blue wavelengths if they are created by supercontinuum generation. This cutoff is not observed for supercontinuum generation by fused silica as shown in Figure 3.3-13(c). Brodeur and Chin have shown that femtosecond induced supercontinuum in materials extends further into the ultraviolet as the band gap of the material increases [74]. To explain the supercontinuum cutoff in PTR glass we suppose that the intense ultrashort pulses modify the band structure of PTR glass thereby allowing blue wavelengths to absorb via a linear process. This assumption is consistent with the Franz-Keldysh effect which predicts that strong electric fields shift the band edge of a material to lower energies [76,76]. Keldysh derived a theoretical model that gives an analytical expression for the photoionization rate in a solid under the influence of strong sinusoidal varying electric fields [77]. We used this model to predict the limiting intensity inside filaments and compare it to the damage threshold intensity of glass as well as the electron density. The calculations gave a damage threshold intensity of 1×10^{13} W/cm^2 and free electron density of 2×10^{19} cm^{-3}. This value of intensity can be compared to experiments with femtosecond laser pulse damage in transparent dielectrics that reported a damage intensity threshold on the order of 10^{13} W/cm^2 [78]. Our intensity estimate is close to the damage threshold but not necessarily above it. Therefore the experimental case requires further attention. In addition to the intensity estimate we also have a value of 10^{19} cm^{-3} for the free electron density which can be compared to the critical plasma density. A critical plasma absorbs significant amounts of energy and leads to the white light emission. Since this effect was not observed in the ultrashort pulse induced filaments we expect the calculated value of free electron density to be below the critical plasma value. The formula for critical plasma density is given by

$$N_{e,critical} = \frac{m_e \omega^2}{4\pi e^2}. \qquad (3\text{-}33)$$

At the 780 nm wavelength the critical plasma density is 1.8×10^{21} cm^{-3}. This means that our free electron density of 10^{19} cm^{-3} in filaments is at least an order of magnitude below the critical plasma value. Our estimate can also be compared to pump-probe experiments that measured the free electron density in filaments by femtosecond pulses in fused silica and which both report a number on the order of 10^{19} cm^{-3} [78,80]. Overall the estimated values of intensity and free electron density provide reasonable order of magnitude approximations. We conclude by commenting on the nature of the photoionization mechanism responsible for free electron generation. Keldysh showed that it is possible to define a parameter γ that will separate two fundamental processes. In the limit $\gamma >> 1$ photoionization is a multiphoton absorption process whereas when $\gamma << 1$ photoionization is a tunneling process. In our experiments the value of γ is about 1 and therefore photoionization is a mix between multiphoton absorption and tunneling. It is thus not accurate to describe the process observed in in fused silica as 11-photon absorption because the number of photons participating in the act of absorption is reduced due to tunneling effects.

3.4.2. Third harmonic generation

Non-collinear third harmonic generation by a volume transmitting Bragg grating in PTR glass under high-intensity femtosecond pulse irradiation near 800 nm was first observed by Smirnov et al. when a TBG was placed at Bragg angle for the fundamental wavelength [81]. In addition to the expected transmitted and diffracted beams, two THG beams with propagation directions corresponding to the condition of sum-frequency generation were observed. However the phase matching condition for SFG was not satisfied. A possible explanation in terms of self-phase matching via Cherenkov radiation has been proposed [82]. One limitation of this experimental configuration was that the use of femtosecond pulses near 800 nm places THG in the ultraviolet regime and within the absorption region of PTR glass. This configuration prevented propagation of surface or bulk third harmonic inside the PTR glass and therefore did not allow for a complete study of the THG phenomena. Investigation of THG by a TBG in PTR glass at third harmonics within the transparency range of PTR glass requires fundamental pulses longer than 1000 nm. Therefore, we studied THG by a TBG in PTR glass using femtosecond pulses at 1300 nm and 1588 nm. For this case third harmonics are centered at 433 nm and 529 nm and two new angular orientations of the TBG were shown to produce non-collinear third harmonic generation.

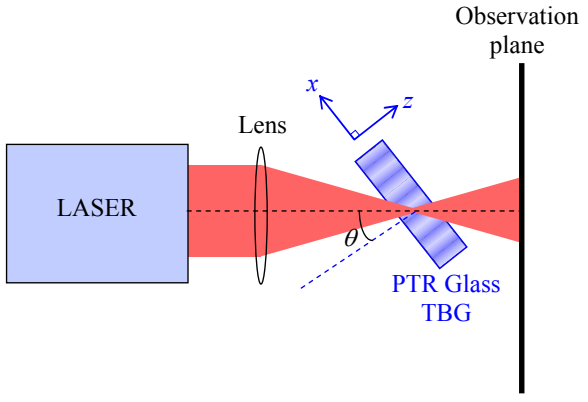

Fig. 3.3-14. Experimental arrangement for investigating third harmonic generation and diffraction by transmitting Bragg gratings in PTR glass.

We first used a Ti:sapphire regenerative amplifier laser system generating femtosecond pulses with the following parameters: pulsewidth ~120 fsec, repetition rate 1 kHz, central wavelength at 780 nm and pulse energies up to 1 mJ. The beam was focused by a lens with focal length equal to 1 m. An unslanted TBG with spatial period 4 μm, thickness 0.85 mm, and amplitude of refractive index modulation 467 ppm, was placed near the focal plane. Figure 3.3-14 shows the experimental arrangement.

The angle θ of the TBG was set to Bragg angle for 780 nm and calculated according to Bragg's law

$$\sin\theta = \frac{\lambda}{2n(\lambda)\Lambda}, \tag{3-34}$$

where $n(\lambda)$ is the refractive index of PTR glass at wavelength λ. Figure 3.3-15 shows that after propagation through the TBG, two THG beams ($3\omega^{(i)}$ and $3\omega^{(ii)}$) appeared between the diffracted (ω_D)and transmitted (ω_T) beams. We call this configuration two-beam THG and distinguish the beams by labeling THG closest to the transmitted beam as $3\omega^{(i)}$ and THG closest to the diffracted beam as $3\omega^{(ii)}$. A spectrometer confirmed that the beams were at 266 nm. Figure 3.3-15(b) shows that the direction of the two THG beams is determined by assuming a SFG interaction between transmitted and diffracted photons, i.e. two transmitted photons plus one diffracted photon or vice versa. For this grating spatial period (4 μm) and wavelength of irradiation (780 nm) no other angles were observed to generate non-collinear THG.

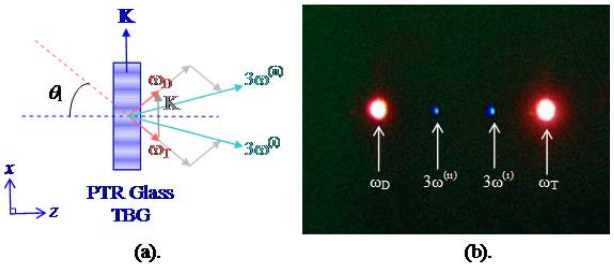

Fig. 3.3-15. Two-beam THG by a PTR glass TBG irradiated with IR femtosecond pulses: (a) wave vector additions of transmitted and diffracted photons to produce third harmonic (b) photograph from experiment. Λ – grating vector, ω_T – transmitted photon, ω_D –diffracted photon. Phase-matching is not satisfied.

The wavelength dependence of THG was tested with an optical parametric amplifier (OPA) laser system (pulsewidth <200 fsec, pulse energies up to 0.1 mJ, and repetition rate at 1 kHz) that generated femtosecond pulses at 1300 nm and 1588 nm. Long focal lenses focused the femtosecond beam in order to achieve intensity at the focal point of about 10^{12} W/cm^2. A TBG in PTR glass with 4 μm spatial period, 0.97 mm thickness, and amplitude of refractive index modulation of 607 ppm was placed near the focal plane. At the wavelengths 1300 nm and 1588 nm it was again observed that for the TBG oriented at Bragg angle for fundamental, two THG beams appeared between the transmitted and diffracted beams. We will designate the Bragg angle for

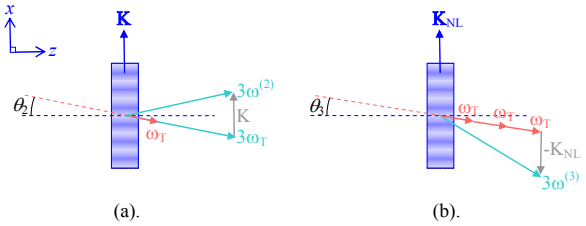

Fig. 3.3-16. Wave vector conditions for non-collinear THG by a PTR glass TBG: (a) front surface diffracted THG (b) nonlinear grating THG. Λ_{NL} – nonlinear grating vector.

fundamental as θ_1. In addition to THG at θ_1 two other angles also resulted in non-collinear generation of third harmonic. These two interactions are illustrated in Figure 3.3-16 along with the assumed wavevector conditions responsible for their generation. At angle θ_2, THG is attributed to Bragg diffraction for incident light at wavelength λ/3. This interaction is likely due to generation of third harmonic at the front interface of the glass grating and subsequent diffraction. This phenomenon could not be seen with fundamental pulses at 780 nm because of absorption of 266 nm light in the bulk of PTR glass after generation by the front surface. We designate THG at angle θ_2 as surface diffracted THG. The appearance of THG at angle θ_3 represents a non-Bragg resonance condition where three fundamental photons interact with a grating vector to generate the third harmonic. We label the THG process at angle θ_3 as generation and diffraction by a nonlinear grating. By imposing phase-matching on the three assumed wavevector interactions we were then able to derive theoretical values for the angles at which THG is expected.

Let us now analyze into more details that three interactions with a TBG in PTR glass that exhibit non-collinear THG under high-intensity femtosecond irradiation. For the two-beam THG interaction shown in Figure 3.3-15(b) the assumed SFG wavevector equations can be written as

$$\mathbf{k}_{3\omega^{(i)}} = 2\mathbf{k}_{\mathrm{T}}(\lambda,\theta) + \mathbf{k}_{\mathrm{D}}(\lambda,\theta), \tag{3-35}$$

$$\mathbf{k}_{3\omega^{(ii)}} = \mathbf{k}_{\mathrm{T}}(\lambda,\theta) + 2\mathbf{k}_{\mathrm{D}}(\lambda,\theta), \tag{3-36}$$

where the transmitted wavevector $\mathbf{k}_{\mathrm{T}}(\lambda,\theta)$and the diffracted wavevector $\mathbf{k}_{\mathrm{D}}(\lambda,\theta)$ are given by

$$\mathbf{k}_{\mathrm{T}}(\lambda,\theta) = \mathbf{k}(\lambda,\theta), \tag{3-37}$$

$$\mathbf{k}_{\mathrm{D}}(\lambda,\theta) = \mathbf{k}(\lambda,\theta) + \mathbf{K}, \tag{3-38}$$

and the incident wavevector $\mathbf{k}(\lambda,\theta)$ and grating vector $\mathbf{K}$ are

$$\mathbf{k}(\lambda,\theta) = \frac{2\pi}{\lambda} n(\lambda)\left[\sin\theta\,\hat{\mathbf{x}} + \cos\theta\,\hat{\mathbf{z}}\right], \tag{3-39}$$

$$\mathbf{K} = \frac{2\pi}{\Lambda}\hat{\mathbf{x}}. \tag{3-40}$$

It is also important to take into account the refractive index dispersion. In order for the wavevectors given by Equations (3-35) & (3-36) to be phase-matched their magnitude must equal the magnitude of a third harmonic wavevector, i.e.

$$k_{3\omega} = k(\lambda/3,\theta) = 3\left(\frac{2\pi}{\lambda}\right) n(\lambda). \tag{3-41}$$

However, when the laser and grating parameters used to generate the THG beams seen in Figure 3.3-15(b) are substituted into Equation (3-41) we have a mismatch. In general there will

always be a mismatch. This suggests that the SFG assumption which Equations (3-35) & (3-36) represent is wrong. Nevertheless the SFG assumption proves useful for studying the intensity dependence of the two THG beams as a function of angle as will be shown in the next section. For now let us continue to analyze the phase-matching conditions and look at the other two cases where THG was observed. To check phase-matching for the wavevector interactions at angle θ_2 and θ_3 we write

$$\mathbf{k}_{3\omega^{(2)}} = \mathbf{k}(\lambda/3, \theta) + \mathbf{K}, \tag{3-42}$$

$$\mathbf{k}_{3\omega^{(3)}} = 3\mathbf{k}(\lambda, \theta) + \mathbf{K}_{\mathrm{NL}}. \tag{3-43}$$

Equation (3-42) relates to the case seen in Figure 3.3-16**Error! Reference source not found.**(a) and Equation (3-43) relates to the case seen in Figure 3.3-16(b). The angle θ in each of the above wavevector equations is solved for by imposing the phase-matching condition given by Equation (3-41). The grating vectors $\mathbf{K}$ and $\mathbf{K}_{\mathrm{NL}}$ are both evaluated using Equation (3-40). We label the angles that satisfy Equation (3-42) & (3-43) as θ_2 and θ_3 respectively. The resulting solutions are for angles inside a medium of refractive index n and are converted to angles in air by Snell's law

$$\theta = \sin^{-1}\left[n \sin\theta_{\mathrm{media}}\right]. \tag{3-44}$$

Table 3.3-1-3 shows that the theoretical angles agree with the experimentally measured values. Also, the theory is able to account for the large change in angle θ_3 as the wavelength changed from 1300 nm to 1588 nm. Hence we have justified the assumed wavevector equations given by Equation (3-42) & (3-43).

Table 3.3-1. Theoretically derived and experimentally measured angles of grating orientation to obtain non-collinear THG for a PTR glass TBG (Λ = 4 μm, L = 0.97 mm, n_1 = 607 ppm).

Angle	λ = 1300 nm		λ = 1588 nm	
	experiment	*theory*	*experiment*	*theory*
θ_1	9.8°	9.36°	11.5°	11.45°
θ_2	3.5°	3.1°	3.4°	3.8°
θ_3	14.8°	14.4°	7.7°	8.2°
$-\theta_3$	-14.3°	-14.4°	-8.3°	-8.2°
$-\theta_2$	-2.9°	-3.1°	-3.9°	-3.8°
$-\theta_1$	-9.6°	-9.36°	-11.8°	-11.45°

It was seen in the previous section that phase-matching assuming SFG is not satisfied for the two-beam THG condition at angle θ_1. To see if we can support a SFG interaction we measured the angular selectivity of the two THG beams using a Ti:sapphire regenerative amplifier laser system operating at 780 nm and a 4 μm period TBG. Figure 3.3-17 shows the experimentally obtained angular selectivity profiles for the two THG beams. It is evident that the $3\omega^{(i)}$ and $3\omega^{(ii)}$ beams shows different angular dependencies. To model the angular selectivity of third harmonic

generation for the two-beam THG case let us assume SFG interactions. We can then write the intensity of THG for each of the beams as:

$$I_{3\omega^{(i)}} = \kappa I_{\omega_T} I_{\omega_T} I_{\omega_D}, \tag{3-45}$$

$$I_{3\omega^{(ii)}} = \kappa I_{\omega_D} I_{\omega_D} I_{\omega_T}, \tag{3-46}$$

where κ is a constant, $I\omega_T$ is the intensity of the transmitted beam and $I\omega_D$ is the intensity of the diffracted beam. Assuming that the spectral selectivity of the TBG is larger than the bandwidth of the laser it is possible to neglect the integration between the spectral profile of the beam and the diffraction efficiency of the TBG.

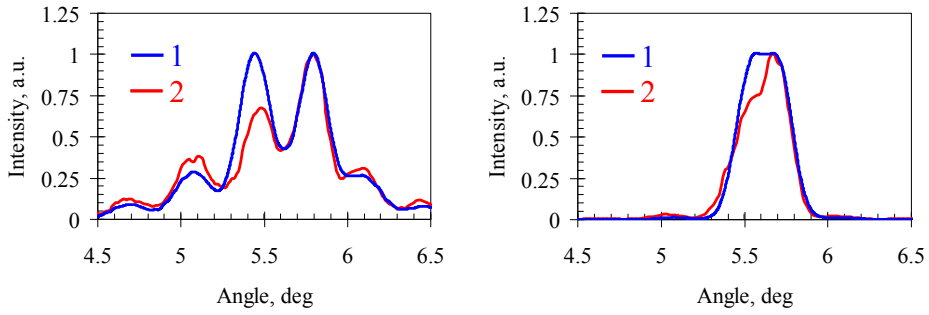

(a). (b).

Fig. 3.3-17. Dependence of third harmonic intensity on incident angle for the two-beam THG case: (a) 3ω(i) beam (b) 3ω(ii) beam. 1 – theory 2 – experiment.

When the grating selectivity is greater than the laser spectral bandwidth the intensity of the diffracted and transmitted beams can be written as

$$I_{\omega_D} = I_0 \eta(\theta), \tag{3-47}$$

$$I_{\omega_T} = 1 - I_{\omega_D}, \tag{3-48}$$

where I_0 is the incident intensity and $\eta(\theta)$ is the diffraction efficiency of the TBG as a function of incident angle θ that can be easily modeled using Kogelnik coupled wave theory of diffraction [61]. Figure 3.3-17 shows how the theoretical solutions compare to the experimentally measured THG intensities. It is seen that the theoretical model produces angular profiles for $3\omega^{(i)}$ and $3\omega^{(ii)}$ that account for the main intensity fluctuations seen in the experimental measurements. Lobe maxima and minima are in agreement for both experiment and theory. The model however does not predict the asymmetry seen in the experimental measurements. This asymmetry is likely a consequence of the asymmetry of the fundamental pulse spectrum.

In conclusion we have shown new conditions for THG from a TBG in PTR glass illuminated by high intensity infrared femtosecond pulses. The two new interactions correspond to Bragg

diffraction at 3ω and a three photon interaction with the modulated nonlinear refractive index of PTR glass. We measured the angular selectivity of THG for the two-beam THG condition. A simple theoretical model assuming SFG was used to explain the measured angular profiles.

Chapter 4: Application of Photosensitive Materials

4.1. Optical interference filters based on photosensitive materials

In this section we will first introduce how photosensitivity can be beneficial towards the optimization of optical interference filters [83]. We considered Fabry-Perot filters, i.e. filter consisting in a half wave spacer surrounded by two dielectric mirror made by alternating high and low refractive index quarter wave layers. However, it is obvious that the described approach can be applied to any thin film filters. The spectral response of such Fabry filter is composed with a narrowband resonance at the central wavelength of the layers and around this resonance which corresponds to a high transmission, the filter is rejecting all the light. It can be shown that if the optical thickness of the spacer is modified, the center wavelength of the filter is then shifted to a different wavelength. It becomes obvious that if the spacer is made of a photosensitive material, it becomes possible to locally change the refractive index of the spacer and consequently to locally adjust the central wavelength of the filter. During my Ph.D. thesis, we theoretically studied the methods for correcting the local refractive index of the spacer of a Fabry-Perot filter and we showed that the only effect that can be seen is a displacement of the central wavelength of the filter while no deformation of the spectral shape of the filter could be observed. We also studied into details the effects that occur during this correction as well as proposed methods that allow achieving relative change of the central wavelength of the filter much larger than the one of the refractive index of the spacer. For example, we showed that the usage of *Solid Spaced Etalon* which are composed with a thick spacer made out of typically 100 µm high quality fused silica windows, which both faces have been coated with dielectric mirror is a very promising method for adjusting the central wavelength of a filter over a broad spectral range. Typically 30 nm shift of the central wavelength of a filter can be achieved using refractive index change below 10^{-2} (which should be limited to 1 nm or less). This new approach allows designing filters that would either have an ultra-homogeneous central wavelength, or in contrary a discrete evolution of the central wavelength over the aperture of the filter (Figure 4.1-1).

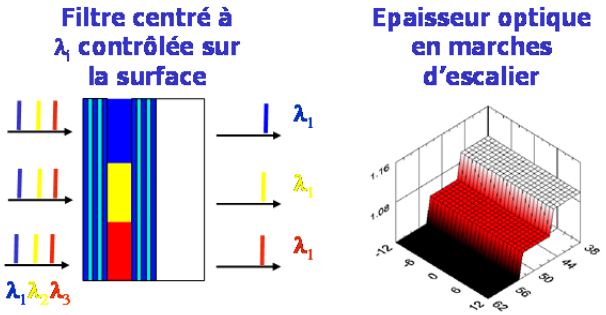

Fig. 4.1-1. Principle of the local correction of the optical thickness of a Fabry-Perot filter for the fabrication of narrowband filters with discrete varying central wavelength.

4.2. New filters based on volume Bragg gratings

4.2.1. Reflecting Bragg gratings and Braggrate™ Notch Filter

High efficiency reflecting Bragg gratings (RBGs) can be holographically recorded inside PTR glass using beams from a He-Cd laser. They are obtained by writing inside the photosensitive medium a sinusoidal refractive index modulation. Typical spectral dependence of the diffraction efficiency on incident wavelength is shown in Figure 4.2-1. RBG are very narrowband reflecting filters. Diffraction efficiency can exceed 99.7%, bandwidths range from 30 to several hundreds of nanometers while angular acceptance is between 1 and 100 mrad and aperture of 35×35 mm^2

or more with very low wavefront distortions (λ/2) are within today's technological capabilities. Finally the technology of High Efficiency Volume Diffractive Elements in Photo-Thermo-Refractive Glass is protected by two issued patents [15,84]. High efficiency RBGs can be deployed as ultra-narrow bandpass and notch filters. They can be used for a variety of spectroscopic applications, for example, advanced Raman spectroscopy. Bandpass filters are formed from RBGs with diffraction efficiencies of about 95% and linewidths of 2-5 cm^{-1} at FWHM (i.e. between 80 and 200 pm at 633 nm). Since the filter is reflecting, it should be placed in a system accordingly, so that the reflected beam is directed to the sample under study and the "filtered out" signals are passed through and guided out of the critical areas. The available wavelength range of bandpass filters is 400-2500 nm, however, they are most frequently used for Raman applications: 1) ASE filtering of semiconductor laser diodes at 785 nm; 2) Cleaning of plasma lines of red HeNe lasers at 632.8 nm. Figure 4.2-2 demonstrates the performance of a 785 nm ASE filter. The "original" spectrum is from a multimode laser diode with spectral contrast of ~40 dB. After ASE filtering with an RBG bandpass filter, the spectral contrast is improved by more than 30 dB at 1 nm from the center of the laser line. The filter can be easily angle-tuned to the resonant wavelength in a several nanometers range without any performance degradation. It should be pointed out the line width of the cleaned laser is almost unaltered as compared to the original LD linewidth as the bandpass RBG band is as narrow as the one of the laser. Thus, VBG based bandpass filters enable laser beam cleaning as close as 2-5 cm^{-1} (i.e. between 120 and 300 pm at 785 nm) to the laserline center. Losses of such bandpass filters are mostly determined by the diffraction efficiency of the gratings and, therefore, are about 5%.

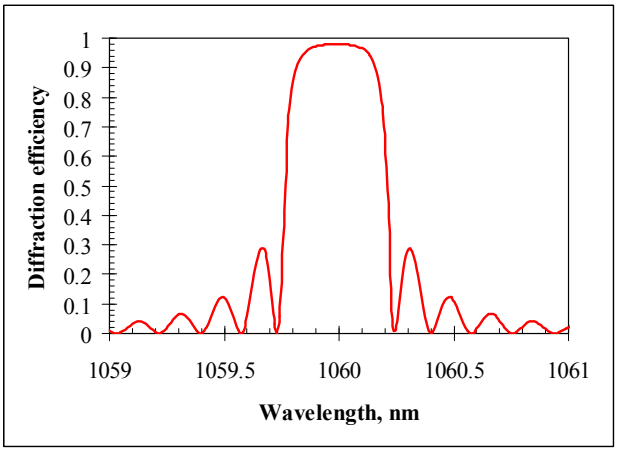

Fig. 4.2-1. Typical spectral dependence of the diffraction efficiency on incident wavelength of a RBG.

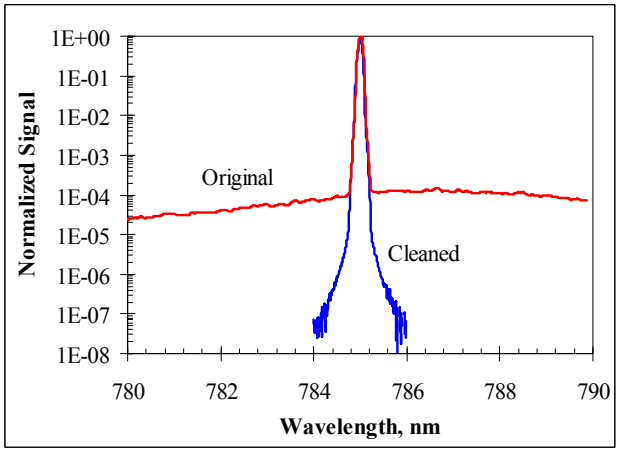

Fig. 4.2-2. Performance of a narrow 785 nm bandpass filter from a standard RBG with 95% diffraction efficiency and bandwidth of about 3 cm^{-1}. The original spectrum is from a multimode 785 nm laser with the linewidth of about 150 pm.

High diffraction efficiency RBGs can also be used as BragGrate™ Notch Filters (BNFs) for Rayleigh light rejection in Raman spectroscopy. In this case, RBG efficiencies are maximized for most effective Rayleigh light suppression. Specially developed technology of high efficiency VBGs allows fabrication of 3-4 mm thick notch filters with optical densities OD>5 and line widths of 5-10 cm^{-1} at FWHM (i.e. between 300 and 600 pm at 785 nm). Typical commercially

available single BNFs have OD3-4 and transmission of about 80-85% at 633 nm wavelength, and OD4-5 with transmission of about 90-95% at 785 nm. The filters are typically coated with broadband anti-reflective coating enabling low Fresnel reflectivities in the range from 400-1100 nm, therefore, providing good optical performance at Raman frequencies up to 5000 cm^{-1}. Figure 4.2-3 shows the suppression of 785 nm light from a multimode LD Raman light source. The laser beam is collimated with about 1 mm diameter and goes sequentially through a set of 2 notch filters. The first BNF rejects about 55 dB of the original light, while the second filter removes completely the residual signal around 785 nm. It is clearly seen that the line width of both BNFs is as narrow as that of the original laser.

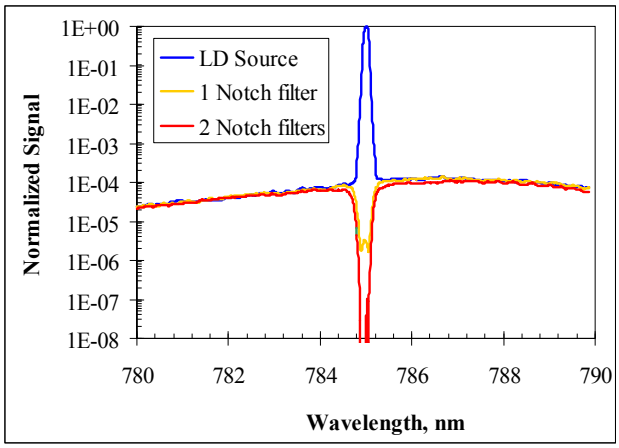

Fig. 4.3-3. Suppression of 785 nm laser line with a set of 2 BragGrate™ Notch Filters (BNFs). Each filter has optical density higher than OD and the linewidth less than 10 cm^{-1}.

Such narrow band notch filters enable unique applications in ultra-low wavenumber Raman spectroscopy. Typically, Stokes and anti-Stokes Raman excitation of 5-10 cm^{-1} are accessible only with triple monochromator stage systems, which are very bulky, expensive, and have rather low optical throughput. Recently we demonstrated with our partners that symmetrical Stokes and anti-Stokes Raman bands with frequencies less than 10 cm^{-1} can be measured simultaneously with only one stage monochromator Raman systems, thus, dramatically reduce the equipment size and cost as well as significantly boost the system optical throughput.

4.2.2. Fabry-Perot-Bragg Filter

Fabry-Perot-Bragg (FPB) filters [85,86] are the first evolution of RBG/BNF that allows significant decrease of the bandwidth of the filter. FPBs are ultra-narrow bandpass filters. They consist of the incoherent combination of two optical components: a Fabry-Perot etalon (FPE) and a high-efficiency volume Bragg grating (VBG) recorded in photo-thermo-refractive (PTR) glass (Figures 4.2-4-a and b). In these FPB filters, the FPE is used to define a comb of discrete narrow bands with desirable shape and bandwidth, while the volume Bragg grating which has a high spectral and angular selectivity is used to select only one of these bands. Due to the angular dependence of the central wavelength of a volume Bragg grating, it is possible to change its inclination and change the selected FPE resonance. Using this technique, the filter can be discretely tuned from one resonance to another. Properties of such filter are very robust, whatever the tuned wavelength due to the fact that maximum transmission, spectral width and rejection are mainly defined by the FPE and are constant over a broad range of wavelength. It is also possible to make FPB filters continuously tunable by tilting the FPE by a few degrees and shifting the central wavelength of the comb by one free spectral range. To achieve the desired spectral properties, several types of elements can be combined. Regarding the etalon, high finesse single cavity FPE can be used in order to achieve ultra-narrow bandpass and double cavity FPE can be used to achieve square profile and better rejection. Regarding the volume

Bragg gratings they can be either a reflecting Bragg gratings (RBG) and in this case, the diffracted beam is on the same side than the incident beam, or a transmitting Bragg gratings (TBG) and in this case the diffracted beam is on the same side than the transmitted beam. To illustrate the typical properties of such filters, we present below two examples of such combination. The first case combines an ultra-narrowband single cavity FPE and a RBG while the second case combines a double cavity FPE and a RBG.

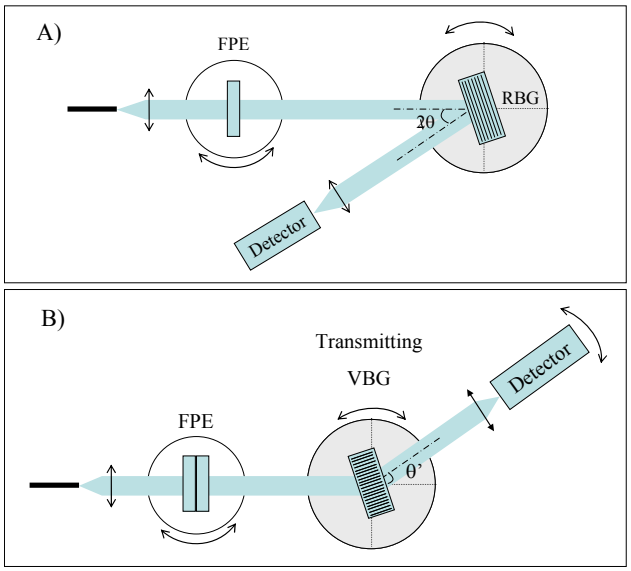

Fig. 4.2-4. Fabry-Perot-Bragg filter geometry. A) is the case of the combination of a simple cavity FPE and a RBG. B) is the case of the combination of a double cavity FPE and a TBG.

A 25 pm bandwidth single cavity FPE with free-spectral range of 0.8 nm was combined with a RBG in order to obtain a reflecting ultra-narrowband Fabry-Perot-Bragg (FPB) filter. Throughput of the filter was measured for low inclination of the grating. In this case the filter is centered at 1064.9 nm. The spectral selectivity of the proposed narrow band filter resulting from the incoherent association of this RBG and the FPE is presented in Figure 4.2-5. Only one resonance appears in a wide spectrum. This unique narrow band resonance has a 25 pm bandwidth at FWHM. It can be seen that two small resonances (T < 1%) are still visible close to the main resonance peak. To investigate in details the origin of these peaks, the inclination of the filter was changed in order to obtain a new coincidence between the FPE and the RBG at a different wavelength (~1055 nm). Then diffraction efficiency of the RBG and throughput of the FPB filter were recorded for the same RBG inclination. Measurements are represented in Figure 4.2-6.

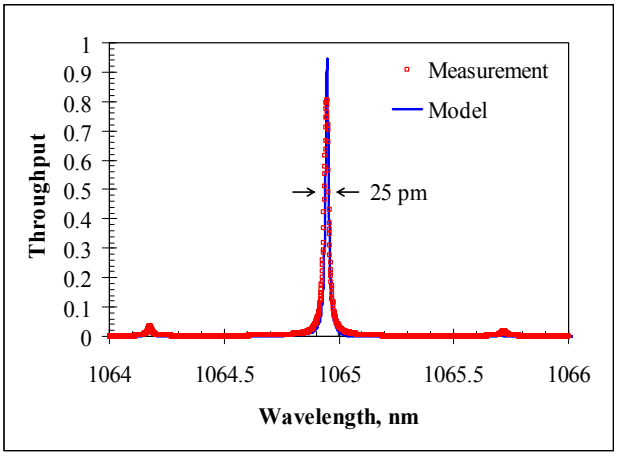

Fig. 4.2-5. Throughput of the FPB filter for 1064 nm region, for low inclination of the RBG

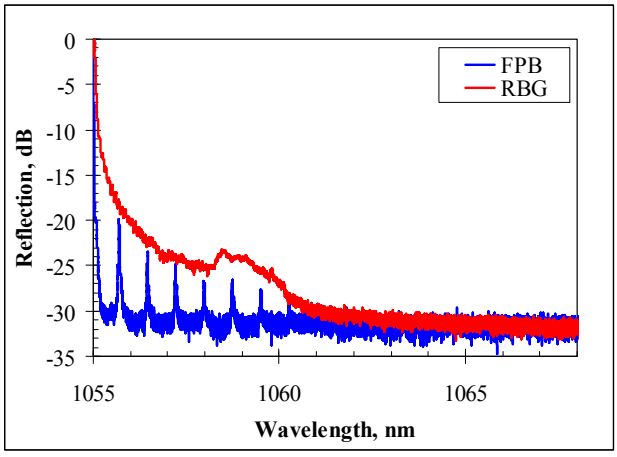

Fig. 4.2-6. Throughput of the FPB filter for 1064 nm region, for larger inclination of the RBG. In blue, throughput of the FPB filter and in red the diffraction efficiency of the RBG.

This graph demonstrates that rejection of the RBG is very efficient only about 6 nm away from the resonant wavelength. Outside this band, rejection is higher than 30 dB (detection limit of our measurement setup). Inside this 6-nm band, rejection is better than 30 dB except for 25 pm width narrow lines, equally separated by 0.8 nm and coinciding with the FPE resonances. At these resonant wavelengths, rejection is however better than 20 dB. Rejection close to the main peak can be severely improved by manufacturing a RBG with narrower line (such as 0.2 nm) and apodizing it. Moreover, according to the very low level of losses of the RBG, rejection can be severely improved by cascading two or more RBGs. Such solution would also have as consequence to avoid any rotation of the output beam when the RBG is rotated.

As it was already introduced, the designed and manufactured FPB filters can be tuned by several tens of nanometers. RBG was originally centered at 1065.5 nm. However, the central wavelength of the RBG can be tuned to lower wavelengths by rotating it. Therefore, it is possible to select any resonant wavelength of the FPE by changing the inclination (rotating) of the RBG. Moreover, since the spectral response of the final filter is determined by the FPE, no distortion of this spectral response appears during tuning. Figure 4.2-7 shows the throughput of the filter measured for three different angles (~2.8°, ~7.9°, ~11.2°). Filter is shown to be tunable by 10+ nm without any spectral shape distortion and constant bandwidth equal to 25 pm. Moreover, even if only discrete tunability of our filter is shown here, continuous and fine tunability can be obtained if the inclination of the FPE is also adjusted to the desirable wavelength. According to the free spectral range of FPE which is limited to several tenths of nanometer, inclinations of the FPE of a few degrees would be enough to shift the whole comb by one free spectral range (FSR) and therefore tune to all the addressable wavelengths.

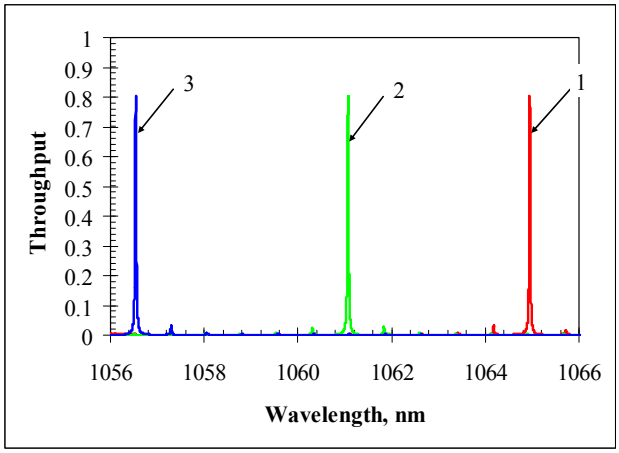

Fig. 4.2-7. Throughput of the FPB filter for 1064 nm region, for different inclination (α) of the reflecting VBG: curve 1: α ~ 2.8°, curve 2: α ~ 7.9°, curve 3: α ~ 11.2°)

The second configuration of FPB filters consists in the combination of a double cavity FPE and a TBG. Throughput of the filter measured for one inclination of the TBG corresponding to a coincidence with a resonance of the FPE is shown in Figure 4.2-8. TBG demonstrates a larger spectral selectivity than the RBG. Hence this justifies the use of FPE with large FSR in order to allow the TBG to select only one resonance of

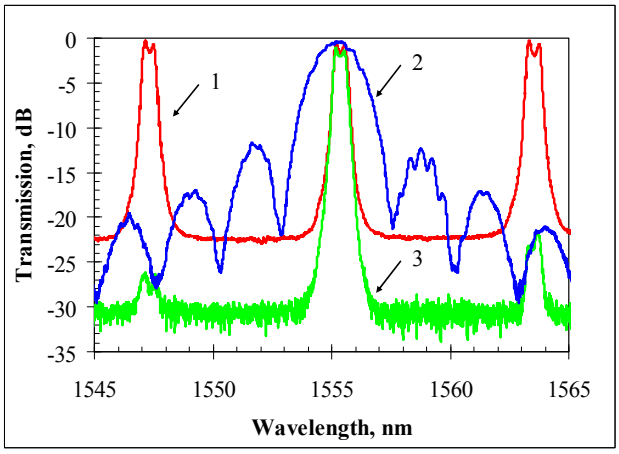

Fig. 4.2-8. Throughput of the double cavity FPE (curve 1), the TBG (curve 2) and of the FPB filter (curve 3) for one inclination of the TBG.

the FPE. The fabricated filter presents only one resonance which shape given by the FPE and throughput higher than 80%. Outside the resonance, the rejection is given by the product of the diffraction efficiency of the TBG and the transmission of the FPE. All remarks regarding improvement of the rejection (apodization, combining of two RBGs or TBGs) can be applied to this configuration too. Moreover, it is important to note that the fabricated FPB filter combines high spectral selectivity of a few tens or hundreds of picometers as defined by the FPE and high angular selectivity as defined by the TBG. FPB therefore capture the best of each element (FPE and VBG) and combines them into one unique filter. Finally, the filter can be tuned by several nanometers or tens of nanometers by changing the inclination of the TBG (Figure 4.2-9).

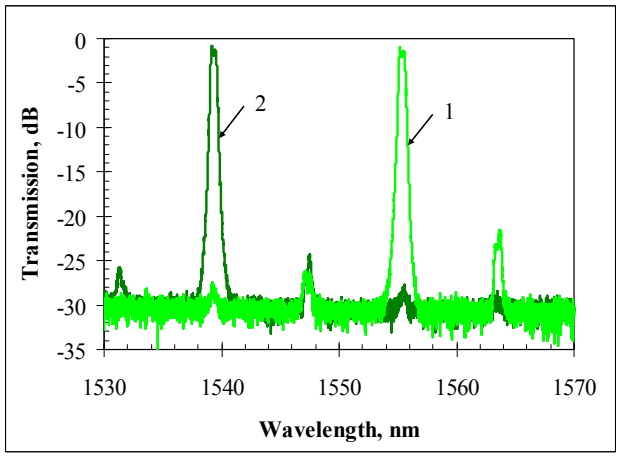

Fig. 4.2-9. Throughput of the FPB filter for 1550 nm region, for 2 different inclinations of the TBG (curves 1 and 2).

4.2.3. Moiré-Bragg Filter

FPB filters have shown to allow producing filters with very narrow bandwidth and broad range tunability. However, one of the main drawbacks of such configuration is that it is composed of two distinct elements and the fabrication of ultra-narrowband Fabry-Perot etalons is very expensive. Another alternative solution was recently proposed. It consisted in replacing both mirrors of the Fabry-Perot etalon with reflecting Bragg gratings and forming the equivalent of a π-shifted volume Bragg gratings [87]. Filter with bandwidth of 25 pm at 1064 nm was demonstrated. However, this combining was performed in air and therefore did not allow robust applications as required for laser systems. Last year, it was thus proposed to modify the structure of the filter and replace the physical π phase shift with a cancelation of the refractive index modulation in the middle of the filter, as obtained when generating a moiré pattern. A moiré pattern is an interference pattern created by two grids having slightly different periods. The phenomenon of Moiré pattern is illustrated by a well-known formula of trigonometry:

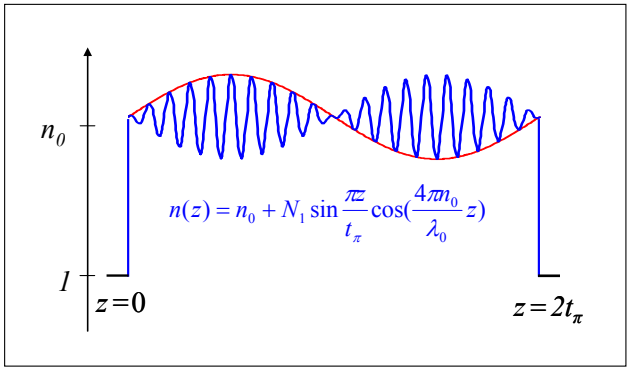

Fig. 4.2-10. Spatial profile of refractive index modulation in a MBG with one Moiré period, i.e. two semi-periods t_π with π phase shift between them.

$$\cos(\alpha)+\cos(\beta)=2\cos\left(\frac{\alpha+\beta}{2}\right)\cos\left(\frac{\alpha-\beta}{2}\right) \qquad (4\text{-}1)$$

Formula (1) shows that a combination of two elementary periodic functions with different periods results in a complex pattern which has a high frequency component with a period that is average between elementary periods and low frequency envelope with a period determined by the difference between elementary periods. When each grid is produced by the interference of two beams, we obtain the superposition of two shifted Bragg gratings and the recording of so-called moiré Bragg gratings (MBG) (Figure 4.2-10). It is worth mentioning that the zero of the refractive index modulation is equivalent of a π-phase shift of the refractive index modulation. Such structure was widely investigated in the past in fibers [88]. However, due to the unavailability of bulk photosensitive materials with high optical homogeneity, no experimental demonstration of MBGs was performed. PTR glass allows recording of high efficiency reflecting Bragg gratings (RBGs) in a several millimeters thick glass sample and losses can be kept low below 1%. Hence, PTR glass makes an ideal candidate for the recording of a MBG with very high transmission at resonance [89]. For the recording, the beam from a single transverse mode He-Cd laser at 325 nm is expanded from 1 mm to 25 mm using 2 beam expanders. This beam is split into two beams with equal intensity. Both beams are reflected by two high quality mirrors and overlapped in the plane of recording (Figure 4.2-11). Two gratings were recorded sequentially by changing of the incident angles of pairs of beams from 1-2 to 1'-2'. The period of each of the gratings (Λ_1, Λ_2) is determined by the angle between the two interfering beams inside of the photosensitive plate:

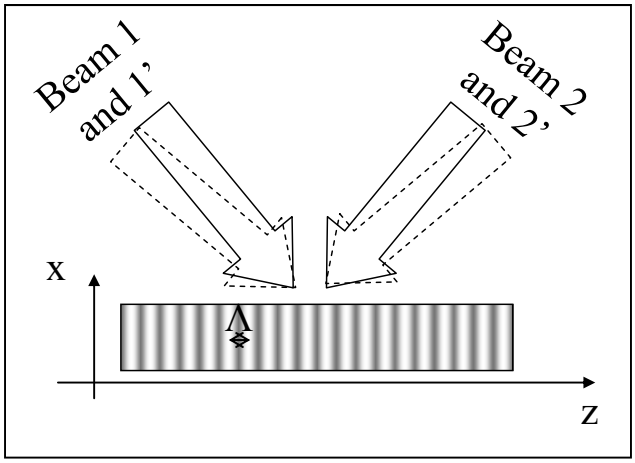

Fig. 4.2-11. Sequential recording of a Moiré grating by two pairs of beams: 1-2 and 1'-2'.

$$2n_0\Lambda_{1,2} = \frac{\lambda_R}{\sin(\theta_{1,2})} = \lambda_B \tag{4-2}$$

where n_0 is the refractive index of a recording medium, λ_R the wavelength of recording, θ the angle between the two beams inside the recording medium and λ_B the wavelength diffracted by the recorded grating at normal incidence along Z-axis in Figure 4.2-11. It is therefore possible to change the period of the grating by changing the angle between the two beams. With high precision rotary stages, angle between the two beams can be controlled with precision better than 0.001°. The change of Bragg wavelength corresponding to such a change of angle is given by:

$$\Delta\lambda_B = \frac{\lambda_B}{\tan(\theta)}\Delta\theta \tag{4-3}$$

With such resolution, the shift of Bragg wavelength can be controlled with a precision better than 50 pm at 1 μm. As it will be shown later, such shift allows obtaining filter with bandwidth in the range of a few picometers in a few millimeters PTR glass substrates. By means of sequential two-beam recording with the same bisectors, the vector of a MBG can be perpendicular to the normal of the photosensitive plate surface, i.e. along the z axis in Figure 4.2-11. A part of the

recorded doubled grating with t_π thickness along Z-axis in Figure 4.2-11 can be cut from the photosensitive plate to keep only one low-frequency period of the refractive index modulation for obtaining an ultra-narrowband transmitting filter.

To confirm these theoretical modeling, a MBG was experimentally demonstrated. The Moiré grating was recorded in a PTR glass wafer using the two-beam sequential technique described above. The two recorded RBGs had central wavelengths of 1547.2 and 1547.4 nm. The sample was thermally developed and then positions of zeros at the refractive index modulation profile were determined by scanning of a He-Ne laser beam with diameter of 1 mm along Z axis in Figure 4.2-11. This sample was cut in the vicinity of the zeros of the refractive index modulation profile to thickness equal to 6 mm i.e. one low frequency period ($2t_\pi$) and then ground, polished and AR coated. Overall refractive index modulation was estimated in the range of ~120 ppm. Spectral selectivity of this Moiré grating was characterized. Typical spectral transmission measured at the throughput of the filter is shown in Figure 4.2-12. This filter shows transmission higher than 95%. Bandwidth is equal to ~50 pm at FWHM and rejection bandwidth to 200 pm. Rejection outside the resonance is in the range of 10 dB. Parameters of such a filter can be improved by optimization of a fabrication process and combining it with an additional RBG or by using a VBG with higher diffraction efficiencies in Ref. [85].

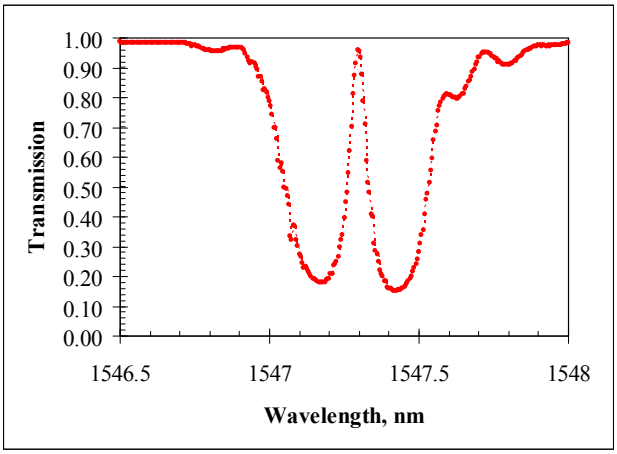

Fig. 4.2-12. Experimental spectral selectivity of a Moiré grating recorded in PTR glass. Separation between resonant wavelengths of elementary RBGs – 200 pm. Thickness – 6 mm. Refractive index modulation – 120 ppm.

4.2.4. Hybrid Bragg-dielectric filters

We also studied an alternative solution to moiré Bragg gratings. This new approach is based on a monolithic Fabry-Perot cavity which consists in a RBG with a multilayer dielectric mirror (MDM) deposited on its surface (RBG/MDM filter), Figure 4.2-13. Such a filter was demonstrated in guided configuration using fiber Bragg gratings [90] but no experimental demonstration in free space could be done with the unavailability of materials for recording high quality volume Bragg gratings. Spectral response of the Bragg-dielectric filter resulting from the coherent combination of a RBG (Bragg

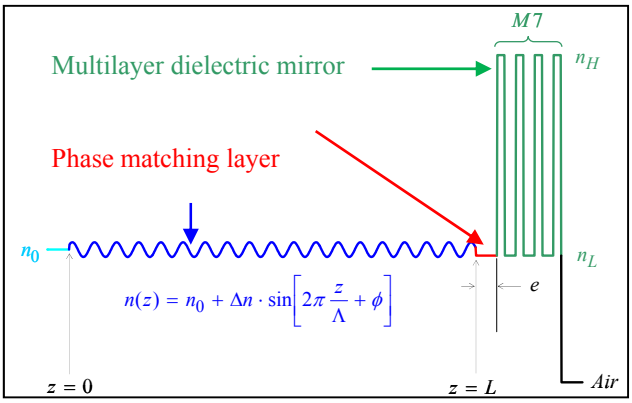

Fig. 4.2-13. Spatial profile of refractive index in a RBG/MDM filter formed a reflecting Bragg grating and multilayer dielectric mirror with a phase matching layer

wavelength: 852 nm, thickness: 2.84 mm, refractive index modulation: 170 ppm (1.7×10^{-4}) and a MDM (with 9 quarter-wave alternated high/low refractive index layers) was modeled by decomposing the RBG into elementary homogeneous thin layers and applying the admittance theory for thin films on the whole RBG/MDM assembly [91]. A typical spectral shape for the RBG/MDM filter calculated with the mentioned model is shown in Figure 4.2-14. This filter is a Fabry-Perot resonator formed by two mirrors. This filter reflects a broadband corresponding to the reflection band of the MDM. But the main feature of this filter is that an ultra-narrow band resonance appears at the Bragg wavelength of RBG. This resonance corresponds to a high transmission line of the filter. It is important that the resonance can be observed, even if the gap between the RBG and the MDM is equal to zero. This is due to the fact that the RBG is a resonant cavity itself [92] as it acts as a virtual plane mirror situated at a certain distance from its front surface. This distance depends on the thickness and diffraction efficiency of the RBG [87]. Theoretically this transmission at resonance is equal to 100% if the RBG and the MDM have identical reflection coefficients at the Bragg wavelength. One can see that very close to the resonance (in the range where diffraction efficiency of the RBG is not zero) rejection will be high (generally much better than 15/20 dB) due to the coherent nature of the combination between both types of mirrors. Then, in a broader range, rejection is given by the reflection coefficient of the DM and therefore is limited to 10 dB for 90% reflection MDM but can be increased by increasing the MDM's reflection coefficient.

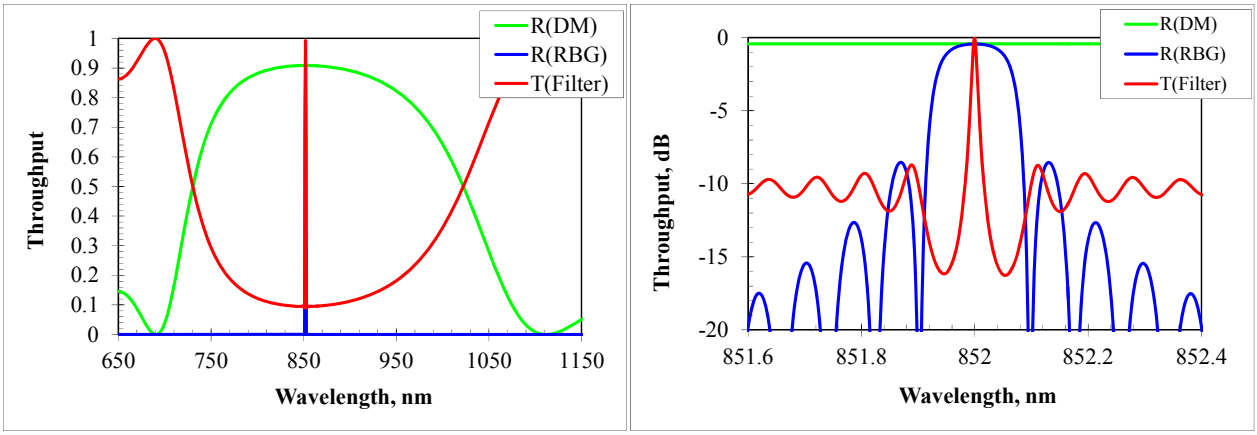

Fig. 4.2-14. Transmission spectrum of a RBG/MDM filter (red), and reflection spectra of a MDM (green) and a RBG (blue). Left – linear scale, right – logarithmic scale.

The technology developed at OptiGrate Corp. also allows fabricating reflecting Bragg mirrors with grating vector tilt in regards to one of the glass surface well below 1 mrad. Therefore, it is possible to fabricate filter by direct deposition of a matching layer (the layer that provides phase matching between RBG and MDM) and a dielectric mirror on one of the facets of a RBG. The fabricated filter will have an ultra-narrow bandwidth and minimum losses resulted from misalignment between mirrors. To fabricate such a filter, a 17 × 17 mm^2 RBG in PTR glass with thickness of 2.89 mm and diffraction efficiency of ~65% was manufactured. Then a matching layer and a quarter-wave alternated dielectric mirror were deposited on a facet of the RBG by electron beam deposition with ion assistance. The high refractive index layers of an MDM were obtained by depositing tantalum pentoxyde layers (Ta_2O_5) while low refractive index layers were obtained by deposition of silica layers (SiO_2). The matching layer was obtained by depositing a

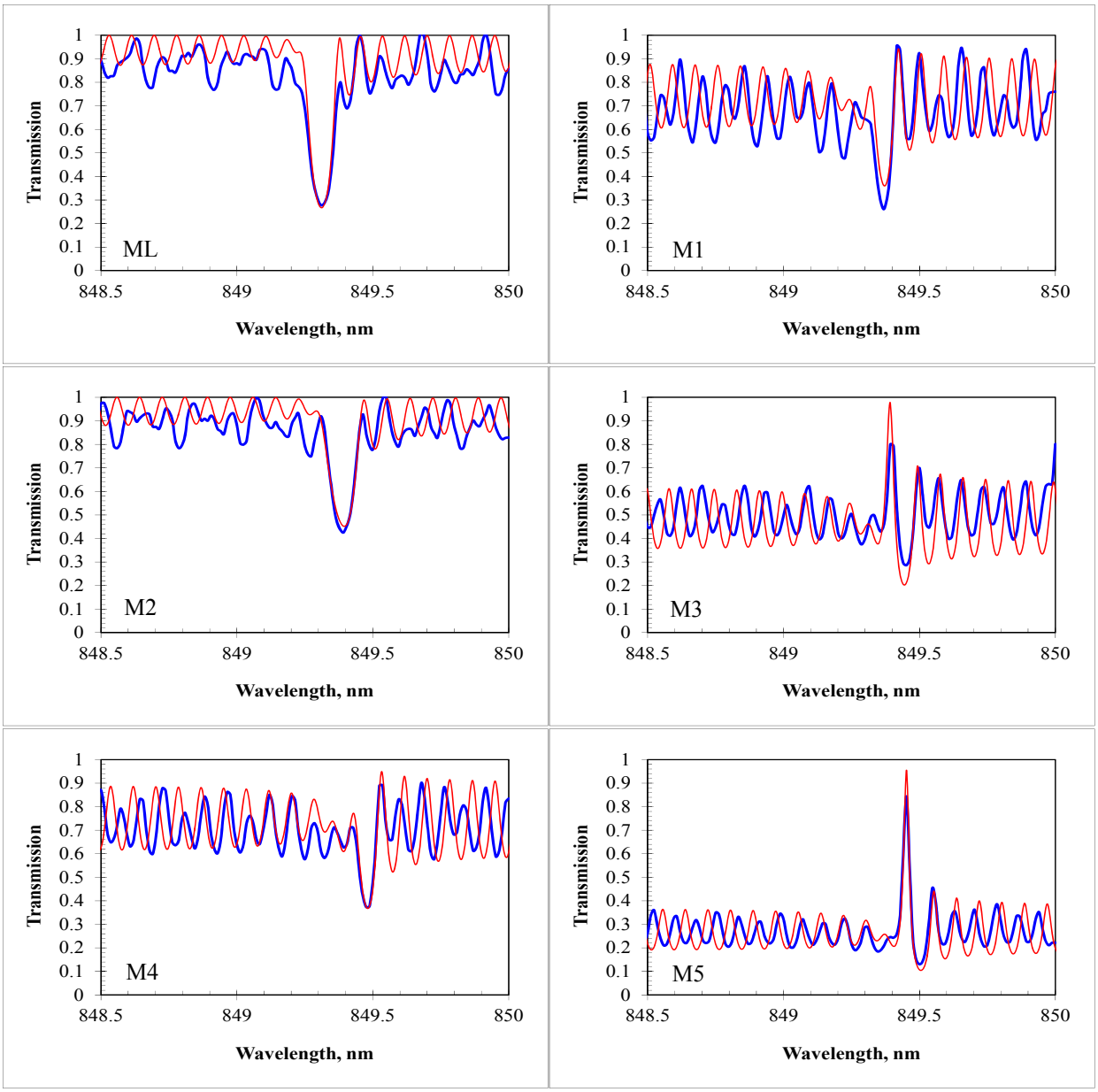

Fig. 4.2-15. Evolution of the transmission spectra of the filter during the process of fabrication, i.e. after deposition of the matching layer (ML) and each of the layers of the dielectric mirror (MX). Blue curve is the measurement and red one is the modeling.

silica layer. Thickness monitoring of each layer was realized by acoustic wave measurement of its weight using a quartz microbalance associated with an in-situ measurement of the transmittance of the assembly with the help of the tunable laser source for 850 nm region and 1 pm spectral resolution, connected to a collimator, and a photodiode associated with a data acquisition card. The control was realized after each layer by scanning the wavelength and measuring the transmitted power. The deposition sequence was the started by depositing a SiO_2 matching layer to correct the end phase of the RBG. Then a 5-layer mirror (Ta_2O_5/SiO_2) was deposited to match as close as possible the reflection coefficient of the RBG. The final reflection coefficient of the dielectric mirror (75%) was however higher than the Bragg mirror (65%). The modeling shows that for such a combination the maximum transmission at resonance is limited

to about 90%. The transmission spectra after the each stage of filter fabrication are shown in Figure 4.2-15. One can see how the filter is forming and how the resonance is appearing while the reflection coefficient of the dielectric mirror is changing. It should be noted that the reflection coefficient of the dielectric mirror increased after deposition of a quarter-wave layer of a high refractive index while it decreased after deposition of a quarter-wave layer of a low refractive index. Therefore, a resonance can only be seen after deposition of the third and fifth layers of the mirror. Also, it can be seen that the measured transmission spectrum and the theoretical one match quite well.

In order to prevent any Fabry-Perot effect with the back face of the filter, we then deposited an AR-coating on the rear facet of the RBG. We used a 2 layer AR-coating with classical formula 0.3H/1.3L centered at 850 nm, with theoretical reflection below 0.1%. Then we re-measured the spectral transmission (Figure 4.2-16). One can see that the filter has very small oscillations outside the resonance. Moreover it transmits 85% and the bandwidth is below 30 pm in 850 nm region. When comparing with theory, one can see that maximum transmission at the resonance is very similar. This limited transmission is due to a mismatch between the reflection coefficients of the Bragg grating (65%) and the dielectric mirror (75%).

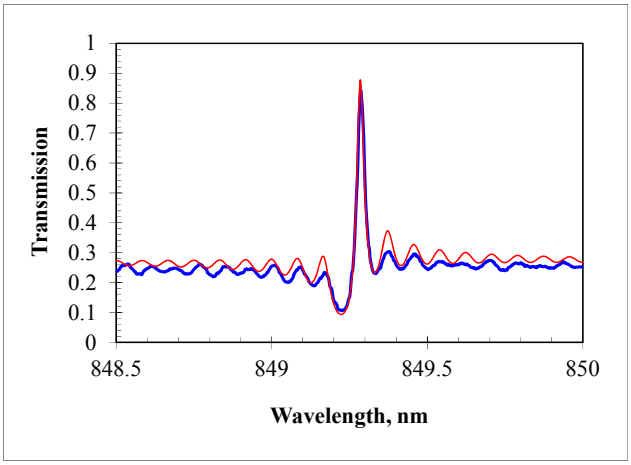

Fig. 4.2-16 Transmission spectrum of the filter in air after AR-coating. Blue – measurement, red - theory.

We have thus demonstrated a new class of spectral filters combining a reflecting Bragg grating recorded in PTR glass with a matched multilayer dielectric mirror. The fabricated filter has a bandwidth of 30 pm and a throughput of 90%. The transmission is limited by the difference of the reflection coefficients of the two mirrors of the cavity. This result paves a way to the fabrication of filters with ultra-narrow bandwidth, high transmission and broadband rejection width.

4.3. Volumetric phase masks based on PTR glasses

4.3.1. Binary phase plates for mode conversion

The use of phase masks which provide a pre-determined profile of phase retardation across the aperture of optical beams is an efficient method for beam control and shaping (see e.g. [93-95]), beam splitting, and coronagraphy [96,97]. It is known that phase can be either controlled by varying the physical thickness or the local refractive index of a plane parallel window. Conventional methods of such optical element fabrication are based on spatially selective etching or deposition [93-97]. However, one of the main drawbacks of such techniques is that these elements are very sensitive to their working condition (dust, humidity, etc.) as the phase profile is controlled by very shallow grooves. Photosensitivity and high optical properties of PTR glass paves a way to the fabrication of volumetric refractive optical elements and preliminary

demonstration of the fabrication of Fresnel lenses using non-linear photosensitivity of PTR glass was performed [98]. Based on this successful demonstration, we then studied how linear photo-sensitivity of PTR glass can be used to the recording of high efficiency two-dimensional binary phase masks for the conversion of a Gaussian beam into higher order Hermite-Gaussian and Laguerre-Gaussian modes.

Let us consider the method for converting a Gaussian beam into the TEM_{11} mode and the LG_{04} mode. Transforming a Gaussian beam into higher order modes can be achieved with 100% conversion efficiency using an interferometric arrangement [99] but this can be time-consuming to align and is sensitive to vibrations. Transformation into the TEM_{11} mode or LG_{04} mode can also be achieved using binary phase masks containing either four or eight sectors in an azimuthal pattern, respectively, with each sector having a phase incursion shifted by π relative to the phase incursion of the adjacent sectors (see Figure 4.3-1) [96,97]. However, this is achieved at the expense of reduced conversion efficiency. While all previous demonstrations of such binary masks have been carried out by local modification of the sample's thickness, we will consider in this paper mode convertors on the basis of volume phase masks (VPMs) where phase incursion is produced by local variations of refractive index.

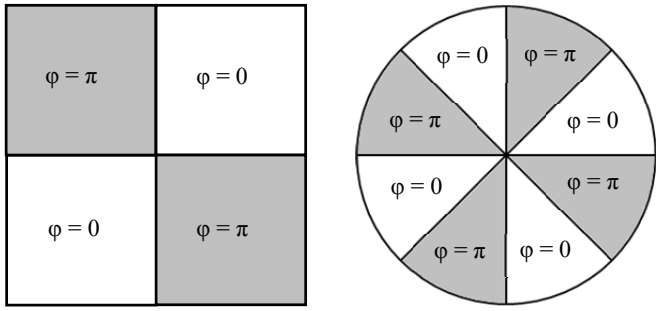

Fig. 4.3-1. Phase profile for a four-sector (a) and eight-sector (b) phase mask.

Before fabricating any prototypes of a VPM, it is important to first understand the function that these masks will perform, and most important to determine the efficiency of mode conversion. Calculation of the efficiency first relies on the fact that the Hermite-Gaussian modes (and Laguerre-Gaussian modes) are orthogonal:

$$\left| \int E^{*}_{n_1 m_1} E_{n_2 m_2} dA \right|^2 = \delta_{n_1 n_2} \delta_{m_1 m_2} \tag{4-4}$$

Here A is area, δ is the Kronecker delta, (*) denotes complex conjugation, and E_{nm} is the electric field of the mode of order n,m. For Hermite-Gaussian modes the field for a given mode is defined as

$$E^{HG}_{nm}(x,y) = E_0 H_n\left(\frac{\sqrt{2}x}{w_0}\right) H_m\left(\frac{\sqrt{2}y}{w_0}\right) e^{-\frac{x^2+y^2}{w_0^2}} \tag{4-5}$$

and for Laguerre-Gaussian modes it is defined as

$$E^{LG}_{nm}(r,\phi) = E_0 \left(\frac{\sqrt{2}r}{w_0}\right)^{|m|} L^{|m|}_n\left(\frac{2r^2}{w_0^2}\right) e^{-\frac{r^2}{w_0^2}} e^{im\phi} \tag{4-6}$$

at the beam waist [100]. Here H_n is the Hermite polynomial of order n and $L_n^{|m|}$ is the associated Laguerre polynomial of order n. Note that the lowest order mode is always a standard Gaussian beam. A Gaussian beam transmitted through a VPM with a given phase distribution will thus no longer be exactly the same as the lowest order mode. Thus the conversion efficiency can be defined as:

$$\eta = \frac{\left|\int E_{nm}^{*} E_{00} T dA\right|^2}{\int |E_{nm}|^2 dA \cdot \int |E_{00} T|^2 dA} \tag{4-7}$$

where T is the transmittance function of the phase mask and the denominator servers as a normalization factor.

Let us now analyze how to design such VPMs. Since the VPMs are binary, the phase profiles may be represented as signum functions, with the four-sector mask and eight-sector mask having a transmittance function of

$$T_4(x,y) = \exp(i\varphi_{avg})\text{sign}(x)\text{sign}(y) \tag{4-8}$$

and

$$T_8(x,y) = \exp(i\varphi_{avg})\text{sign}(x)\text{sign}(y)\cdot\text{sign}(x+y)\text{sign}(x-y) \tag{4-9}$$

respectively. Here φ_{avg} is the phase incursion due to the passage of the beam through the glass which, without loss of generality, we will assume to be zero. A Gaussian beam passing through the centers of such VPMs will have a far field intensity distribution shown in Figure 4.3-2. The distribution of energy, however, may not be similar to the higher order mode of the same width as the Gaussian beam, since the bucket for a higher order mode is much larger than the bucket for a Gaussian beam. Therefore, it is evident that the width w of the mode in question may not be equal to the width u_0 of the incident beam for optimal conversion and thus the efficiency should be defined in terms of the relative widths:

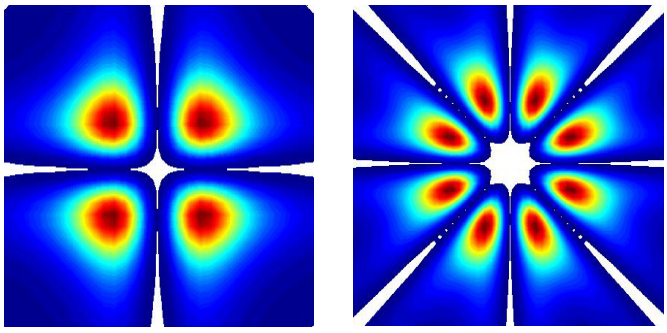

(a) (b)

Fig. 4.3-2. Theoretical far field intensity profile produced by the four-sector (a) and eight-sector (b) VPM.

$$\eta(w,u_0) = \frac{\left|\int E_{nm}^{*}(w) E_{00}(u_0) T dA\right|^2}{\int |E_{nm}(w)|^2 dA \cdot \int |E_{00}(u_0) T|^2 dA} \tag{4-10}$$

For a given incident beam width u_0, calculations indicate that the maximum conversion efficiency of the four sector VPM into the TEM_{11} mode is 68.4% (when $w/u_0 = 0.577$) and the maximum efficiency of the eight sector VPM into the LG_{04} mode is 29% (when $w/u_0 = 0.445$).

In order to validate this model we fabricated two phase masks in 25×25 mm^2 PTR glass plates using the contact copying technique and binary amplitude master masks. A master binary amplitude mask was first recorded lithographically in a fused silica plate for each pattern. This mask permitted selective exposure of the PTR glass with the designed profiles, in order to achieve a lower refractive index only in the UV-exposed regions. The PTR window was then placed in contact with the master having matching fluid in between them and homogeneously exposed to UV radiation from a He-Cd laser at 325 nm with a dosage of 1 J/cm^2. The samples were then developed at a temperature of ~520°C and the refractive index change was then characterized using a liquid-cell shearing interferometer [25]. A refractive index change of 208 ppm and 175 ppm was achieved for the four-sector VPM and eight-sector VPM, respectively. As the total phase incursion is given by

$$\varphi = \frac{2\pi \Delta n L}{\lambda} \tag{4-11}$$

the plates were subsequently polished down to L = 1.52 and 1.81 mm, respectively, with a flatness better than λ/4 at 633 nm in order to secure a π phase shift between the unexposed and the exposed regions at λ = 633 nm. Finally the samples were bleached, resulting in total losses, mostly by scattering, of 2.8×10^{-2} cm^{-1}, i.e. 1.01% in the VPM (ignoring Fresnel reflection).

The phase masks were placed in a collimated single mode beam from a He-Ne laser emitting at 633 nm with a Gaussian intensity distribution, a beam diameter at $1/e^2$ of 6.64 mm, and the intensity distribution of the transmitted beam was characterized in the focal plane of a lens (Figure 4.3-3). Excellent agreement with the theoretical intensity distribution can be observed. In order to quantitatively relate the experimental profile to the theoretical field profile, we first convert the theoretical field profile into an intensity distribution. Rewriting Equation 3-8 to account for this gives

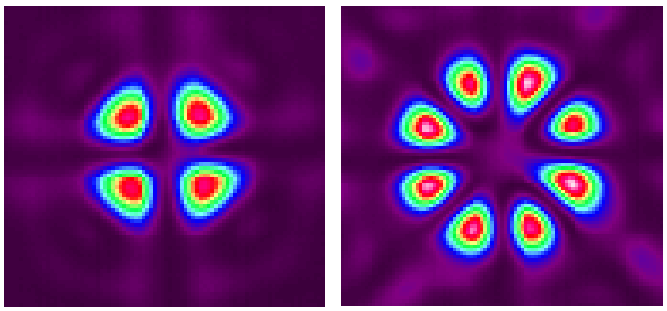

(a) (b)

Fig. 4.3-3. Experimental far field intensity profile produced by the four-sector (a) and eight-sector (b) VPM.

$$\eta(w,u_0) = \frac{\left|\iint \left|E^*_{nm}(w)\right| \sqrt{\left|E_{00}T\right|^2}\, dA\right|^2}{\iint \left|E_{00}T\right|^2 dA \cdot \iint \left|E_{nm}(w)\right|^2 dA} \tag{4-12}$$

Figure 4.3-4 shows the dependence of conversion efficiencies on the ratio of sizes of the original and converted modes for four and eight segment VPMs. One can see good agreement between the theoretical and the experimental conversion efficiencies.

In conclusion we have shown that volume phase masks with plane parallel polished surfaces recorded in PTR glass are new elements for the control of the intensity profile of laser beams. Two prototypes are demonstrated that convert a Gaussian beam to the TEM_{11} mode or the LG_{04} mode with near-theoretical profiles. These phase masks are very robust (the element is written within the volume of the plate and cannot be deleted or altered) and are highly suitable to high power and high energy (CW or pulsed) applications.

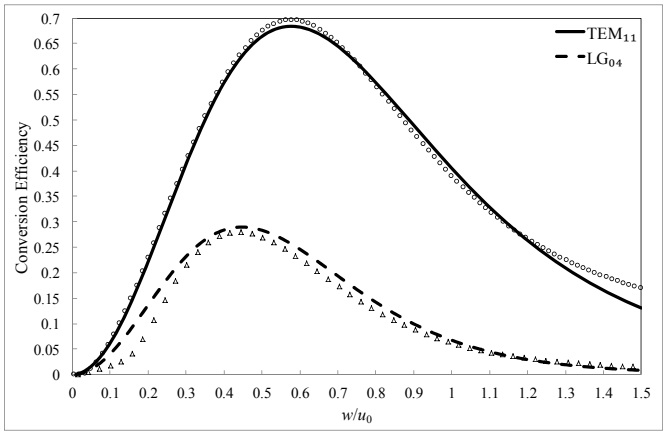

Fig. 4.3-4. Theoretical and experimental conversion efficiency of a beam of width u_0 into the TEM_{11} and LG_{04} modes of width w. Lines – ideal masks, dots – experimental data.

4.3.2. Vortex generation by phase plates

We then studied how PTR glass can be used to fabricate high efficiency phase masks with complex structures. Let us consider typical PTR glass plate with aperture size of couple centimeters and thickness L of few millimeters, e.g. $L = 2$mm. We investigated how to extend the actual technology to the recording of arbitrary change of phase $\Delta\varphi(x,y)$ across the aperture for operating wavelength λ, for example $\lambda = 1.06\mu$m. In order to achieve relative 2π-shift after propagation of laser beam through this phase plate we need relative refractive index change $\Delta n = \lambda/L = 530$ppm which is in range of linear sensitivity of PTR glass. Varying $\Delta\varphi(x,y)$ can be recorded with corresponding varying the dosage of UV-exposure during the recording process. This can be realized with the use of amplitude masks with corresponding varying transmittance across aperture. For recording purposes we proposed to use binary amplitude masks made by lithography with probabilistic distribution of transparant/notransparant micro-areas of small size, for example $a = 2\mu$m. So, for an aperture size of 2 cm we could generate binary map with resolution $10^4 \times 10^4$ on computer. Figure 4.3-5 shows central area of computer-generated amplitude binary mask for the recording of the vortex phase plate.

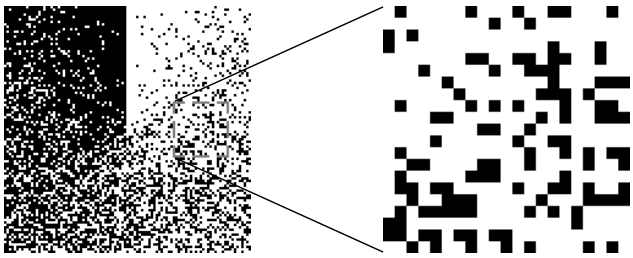

Fig. 4.3-5. Central area of probabilistic amplitude mask for recording of vortex phase plate and local area with filling factor $\nu = 0.25$.

The first method to perform such recording of phase plates in PTR glass is to make a contact copy of the amplitude mask. This method of contact recording is very robust and allows obtaining direct transmission phase elements with almost 100% efficiency. However, it can be shown that severe diffraction that occurs at the edge of each of the micro-squares results in the production of holographic scattering in the final phase mask resulting from the interference between the scattered light and the unperturbed light, dramatically decreasing the efficiency of

the final element. Besides the contact method, imaging systems can also be applied. In this scheme the amplitude mask intensity distribution is imaged on a PTR glass blank and high angular diffraction frequencies connected with the small structural elements are eliminated using a spatial filter. As a result, the PTR glass blank can be illuminated by a cleaned up smooth intensity distribution. To achieve a classical *4f*-system can be used. This system consists of two lenses with identical (or not) focal lengths. These two lenses are separated by a distance equal to the sum of the two focal lengths. A pinhole is added in the beam path between the two lenses (i.e. at the image focal plane of the first lens, or the object focal plane of the second lens, which are overlapped). The amplitude mask is located in the object focal plane of the 1st lens while the recording material is placed in the image focal plane of the 2nd lens. Finally, this optical system is illuminated by a collimated uniform beam. In this setup, the mask is imaged using the two lenses in the PTR glass window and the aperture filters out the high angular diffraction frequencies from small printing "dots" on the amplitude mask.

Method of spatial filtering was applied for recording phase mask with azimuthally increasing phase shift. A probabilistic amplitude mask with size of elementary features (small squares) of 2 μm was placed in object focal plane of the first lens, and its image was recorded in PTR glass. The sample was thermally developed in order to obtain the desired refractive index increment and its properties were characterized. This phase mask has 2π-phase shift for λ = 633 nm at one edge and creates a spiral singular wavefront of optical vortex (Figure 4.3-6). In conclusion, we have shown that PTR glass technology can be extended to the recording of complex phase elements.

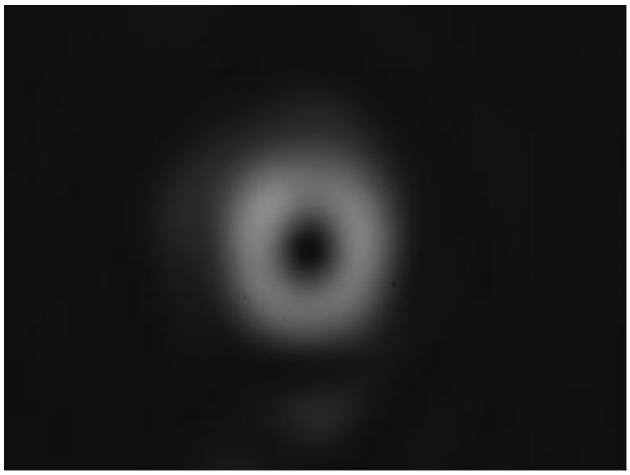

Fig. 4.3-6 Vortex produced after propagation of a Gaussian beam through the phase mask produced from the probabilistic grey scale mask shown in Fig 3.3-5.

4.4. Holographic screens

The ability to have a photosensitive medium with very high optical properties as well as the ability to precisely control the level of crystallization (and therefore scattering) makes PTR glass an ideal material for the fabrication of holographic diffusers [101-103]. Moreover, similarly to volumetric phase plates, these elements are very robust and have very low sensitivity to environmental conditions. Volume holographic screens in PTR glass were fabricated by means of the classical two-step process which includes the exposure to UV radiation at 325 nm using a He-Cd laser and a subsequent thermal development at temperature of ~ 500°C. After the first step, a latent image corresponding to spatial distribution of the intensity of the incident light is created in PTR glass by photoionization of cerium and corresponding photo-reduction of silver. During the second step, NaF nano-crystals are grown inside of PTR glass, predominantly around silver containing nucleation centers. The recording and development procedures were optimized to provide desirable level of scattering in a holographic screen.

Our main approach was focused on the design of a screen with high transmittance and low backscattering for laser beam imaging. The first type of such a screen was made by exposure of PTR glass using a single scanning beam. In this case volumetric diffusers in PTR glass were recorded as a standing wave-field generated by interference of the incident laser beam and the Fresnel reflection from the back side of the PTR glass sample. Such exposed PTR samples were developed with different regimes to induce different crystal sizes and densities and to provide different levels of scattering. A testing setup based on a spectrometer equipped with a diffuse reflectance accessory provided measurement in the spectral range [800-2000] nm with 1 nm resolution. The angular distribution of scattered light was measured by an angular scatterometer. The scattering spectra measured in PTR holographic screens produced with different thermal treatment regimes are presented in Figure 4.4-1. It is seen that the spectral dependence of scattering strongly depends on the average crystal size resulted from conditions of exposure and development. A screen fabricated with small crystals (estimated size of a few tens of nanometer) can be approximated as a Rayleigh diffuser with the scattering spectral dependence proportional to λ^{-a} with a = 4.1. Samples with larger crystals (with diameters of several hundreds of nanometers) have less steep slope of the scattering spectra (a = 3.3). Diffusers with Rayleigh scattering are polarization independent. Diffusers produced with large crystal have a more complicated asymmetric angular diagram. However, the measurement of the angle distribution of scattering shows that this effect is negligible for angles below 20^{o} and that these screens can be accurately be compared with Lambertian surfaces at small angles. In order to further characterize the performances of PTR glass screens, we measured the fluctuations of the reflected power across its aperture and compared to those measured across the aperture of a Spectralon® reflective standard (Figure 4.4-2). It is seen that fluctuations as large as 50% over the aperture are observed on the Spectralon® while only a few percent fluctuations are measured in PTR glass screens. Such high homogeneity of scattered light allows imaging of a laser beam with higher accuracy.

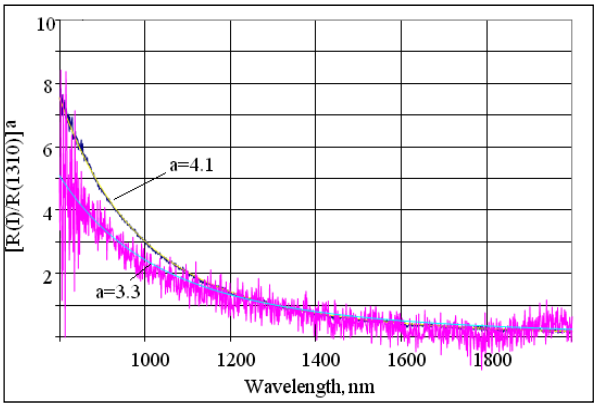

Fig. 4.4-1. Spectral dependence of scattering spectra measured in PTR glass screens that underwent different exposure and thermal developments.

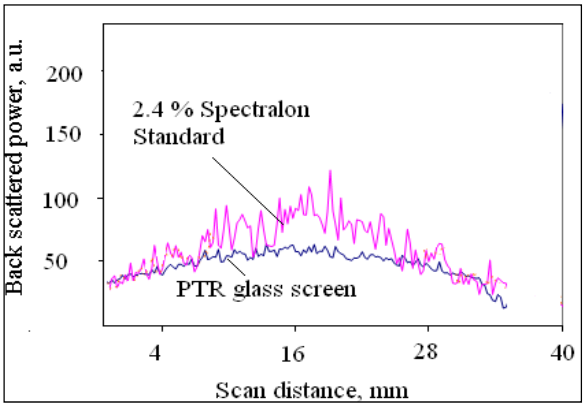

Fig. 4.4-2. Evolution of the back scattering across the aperture of a 2.4 % Spectralon standard and PTR glass holographic screen.

Scaling up the aperture of volumetric screens (up to 100×100 mm^2) was performed not by scanning of a small beam across the aperture of a PTR glass flat but by fixed exposure using an expanded beam from a He-Cd laser (Figure 4.4-3). To provide homogeneous distribution of the

beam intensity across its aperture, laser beam was sent through a glass diffuser with one of surfaces grinded. With such a technique, fluctuations of the intensity of the transmitted intensity of an IR laser beam across the holographic screen aperture were kept below 1%.

In this case, reflection geometry of recording proposed by Yu. N Denisyuk [102,103] was used. The hologram is created by the interference between the incident beam transmitted through PTR sample and the beam being back reflected by a mirror placed behind the PTR glass sample. In this specific case, due to depolarization of the beam through the surface diffuser before entering the PTR glass, the holographic pattern is generated by interference of unpolarized laser beams. The main feature of such holographic screens compared to those obtained previously a narrowing of angular distribution of scattered light. The typical intensity distribution of a He-Ne laser beam transmitted through such a PTR screen is presented in Figure 4.4-4. Such holographic screens do not produce either a halo or a conjugate image. Even though these screens are recorded in UV region, they can be used in visible and IR region. Finally, optimization of the phase modulation during the recording allows suppressing the zero order in the reconstructed image.

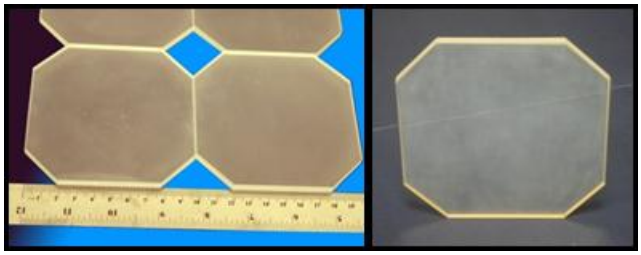

Fig. 4.4-3 Pictures of the glass blanks before recording (left) and of the final 100×100 mm^2 target boards.

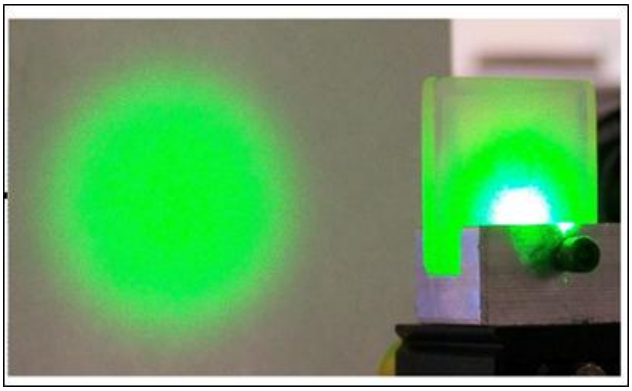

Fig. 4.4-4 Distribution of diffused He-Ne laser beam transmitted through reference-free hologram of ground optical diffuser recorded in PTR glass.

In conclusion, we have shown that the ability to precisely control the volume fraction and size of crystals, and therefore the level of scattering over and broadband spectral range allows fabricating new volumetric diffusers. Moreover, due to the very low level of absorption in PTR glass, these diffusers are ideal target boards for the analysis the intensity distribution of high energy lasers.

4.5. Monolithic solid state laser based on rare-earth doped PTR glass

Development of airborne and spaceborne laser systems dictates a number of extremely challenging requirements for such fine optical devices. One of them is a high tolerance to mechanical and acoustic vibrations. To secure such mechanical stability, the ideal situation would be if all elements of a laser would be incorporated in the volume of a gain medium. The problem preventing a development of such systems is that semiconductor lasers which are naturally all-solid-state cannot accumulate energy and, therefore, cannot produce high energy laser pulses. Deposition of dielectric mirrors to the facets of a solid state gain medium does not

provide any spectral or angular selection and, therefore, does not provide high quality narrow band radiation. We therefore, we studied how we can combine the photosensitive properties of PTR glass with active properties (luminescence), in order to fabricate a monolithic laser (Figure 4.5-1). This design represents a resonator in PTR glass wafer produced by two volume Bragg mirrors. To make such a resonator, a rare earth doped PTR glass wafer is exposed to UV radiation to record a high reflectance mirror and an output coupler. It is important that alignment of the mirrors of the resonator is determined by accuracy of holographic recording and is not sensitive to any mechanical vibrations. Also, by varying the thickness and reflection coefficients of both mirrors; it is possible to produce selection of both transverse and longitudinal modes in such a volume Bragg resonator.

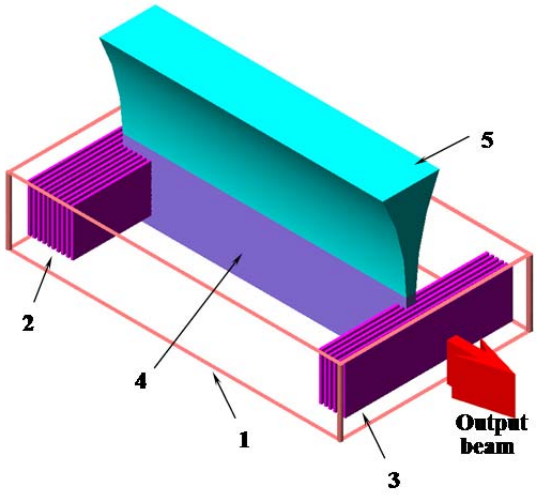

Fig. 4.5-1. Possible geometry of a monolithic solid state laser in PTR glass doped with rare earth ions. 1 - rear-earth doped PTR-glass wafer; 2 – high efficiency VBG as a feedback coupler; 3 – low efficiency VBG as an output coupler; 4 - pumped volume in active PTR-medium; 5 - pumping beam from LD bars.

As previously shown the PTR glass photosensitivity to UV-irradiation is determined by a small concentration of Ce^{3+} introduced in the glass composition which is ionized by near UV radiation and releases free electrons used for photo-reduction of silver which serves as a main component of photo-induced nucleation centers. This feature allows producing a photo-controlled crystallization in the bulk of glass, which results in a refractive index change in UV-exposed areas of a glass volume. This mechanism enables fabrication of phase volume holographic optical elements in PTR glass. The idea of making a monolithic Bragg laser involves doping the PTR glass with luminescence agents, which are rare earth elements Nd, Yb, or Er, in addition to conventional dopants Ce and Ag which are responsible for the photo-sensitivity of PTR glass. It is important to note that concentration of luminescent agents should be about 100 times higher than the concentration of the photosensitive agents. Therefore, the major concern with using additional dopants having similar chemistry in the glass was the opportunity of destroying the photo-induced crystallization, which is a key for recording of volume holograms.

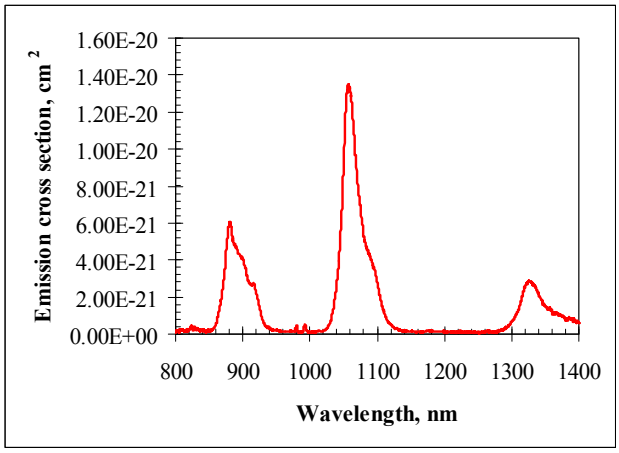

Fig. 4.5-2. Emission cross sections in Nd-doped PTR glasses.

Main efforts were performed towards the development of photosensitive PTR glass doped with Nd-ions. We showed that this glass can be doped with 1 wt.% (or even

more) [104]. The study of Nd-doped PTR glass has shown that it possesses both luminescent and photosensitive properties. Cross section of emission in PTR glass is of 1.4×10^{-20} cm^2 was measured (Figure 4.5-2). This value is typical for silicate laser glasses ranging from 0.9 to 3.6×10^{-20} cm^2 [105]. Absorption coefficient of PTR glass in the region of 1.06 μm is 10^{-4} cm^{-1} which is several times less than that for the best laser glasses. Scattering in pristine PTR glass is comparable to BK7. However, after thermal development it rises to the level of 10^{-3} cm^{-1}. This level of total losses for a laser material with the emission cross section of 1.4×10^{-20} cm^2 is acceptable for the design of both large scale and portable lasers. Photo-thermo-induced refractive index change in Nd-doped PTR glass can achieve several 10^{-4}. This value is enough for recording of 100% diffraction efficiency volume Bragg gratings with thickness exceeding 5 mm that should operate in the range of 1 μm. Several prototypes of such volume Bragg gratings having various efficiency and spectral/angular properties were recorded. It is important to note that the main idea of the use of volume Bragg gratings as components of laser resonators is to produce spectral locking and narrowing of laser emitters. It could be shown [106] that volume Bragg gratings with thickness above 5 mm would provide spectral narrowing of laser below 0.01 nm. Usually such narrow band laser could be produced by a combination of a number of different optical components with high spectral selectivity. The main result of the current research is that Nd-doped PTR glass possesses both spectral and photosensitive properties which provide an opportunity to make portable solid state lasers with extremely narrow spectral lines.

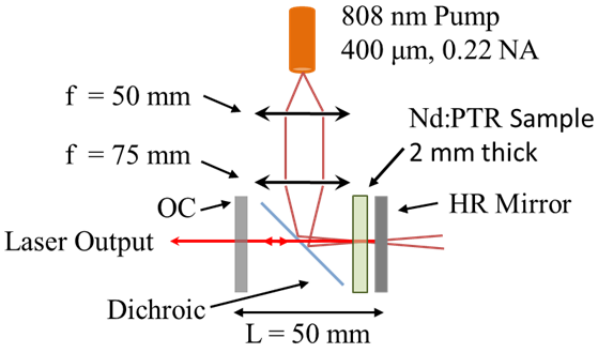

Fig. 4.5-3. Experimental setup for Nd:PTR laser.

To confirm this conclusion, we finally showed that Nd-doped PTR glass can be used as a laser medium. Figure 4.5-3 shows the experimental setup that was designed and assembled. A 2 mm thick Nd-doped PTR glass slab was used as the gain medium. In order to match the Rayleigh length to the sample thickness, a 808 nm pump light should be focused to a diameter of 600 μm. The combination of a 50 mm focal length lens and a 75 mm focal length lens was used to image the output from the 400 μm fiber to a 600 μm spot inside the sample. The Nd-doped PTR glass as gain medium was placed close to the 100% reflective flat mirror. The overlap between the pump and laser beam was achieved using a 45° dichroic mirror. The output coupler at the front end was separated by about 50 mm from the back mirror, completing the laser cavity. The Nd-doped PTR glass sample was not actively cooled in these experiments. The pump source was operated in a quasi-CW regime with a pulse width of 1.5 ms, slightly longer than the measured

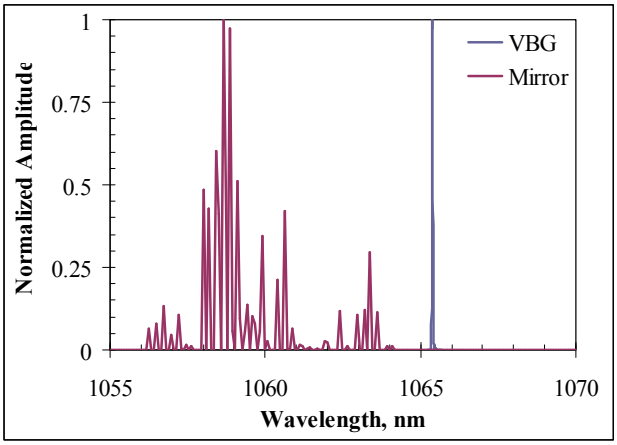

Fig. 4.5-4. Lasing spectra of Nd-doped PTR glass laser with mirror and VBG output couplers

lifetime, and a repetition rate of 100 Hz to keep thermal effects low and maintain low average power.

The transmitted pump power was found to be linearly proportional to the input power with a linear absorption of about 23% which corresponds well to the initially measured absorption coefficient of 1.32 cm^{-1}. Lasing was observed above a threshold of about 4.4 W of incident or ~ 1 W of absorbed power. The lasing spectrum was distributed around 1058 nm and about 10 nm wide. In order to narrow the spectrum we replaced the 99% output coupler by a volume Bragg grating with a diffraction efficiency of ~ 99% and a bandwidth of FWHM linewidth ~230 pm (Bragg wavelength of ~1065.3 nm at normal incidence). Figure 4.5-4 compares the laser output spectra for the mirror and VBG output couplers. A FWHM laser linewidth of 23 pm was measured for the case of VBG output coupler using a 0.01 nm resolution spectrum analyzer.

In summary, rare-earth doped photo-thermo-refractive glasses have shown to be a new and promising laser material. The combination of large optical gain, low loss, and the possibility to write distributed reflectors directly into the active material open a plethora of new possible laser structures that we plan to explore further in the future.

4.6. Chirped volume Bragg gratings

High-power ultrashort laser pulses have found applications in many fields of modern science. Direct optical amplification of low-power ultrashort pulses results in detrimental nonlinear effects and laser-induced damage of amplifying medium due to extremely high peak power of amplified pulses. In order to mitigate these effects, a technique of chirped pulse amplification (CPA) was developed [107]. Using this technique, ultrashort pulses are stretched by certain dispersive optical elements before amplification so that the peak power of the pulses in the amplifier is moderate and does not lead to damage. After amplification the pulses are compressed, resulting in high peak power. Pulse compression is performed with dispersive optical elements that are required to have high damage threshold. Traditionally, pulse stretching and compression in CPA systems is performed with surface diffraction gratings. Conventional technology uses metal-coated gratings. However, the average power of such laser systems is limited by the relatively low damage threshold of metal-coated gratings.

A breakthrough in development of CPA laser systems was done by the use of chirped fiber gratings which replaced pairs of surface gratings in stretchers and compressors [108,109]. This approach has dramatically increased robustness of CPA systems and enables their use in harsher environment but not only in laboratories. However, maximum aperture of fiber chirped gratings did not allow achieving of high power laser systems because of laser induced damage of fibers by a compressed pulse.

Recent invention of volume Bragg gratings with variable period (volume longitudinally Chirped Bragg Gratings, CBGs) in photo-thermo-refractive (PTR) glass has changed dramatically the design of high power femtosecond lasers. Replacing of bulky pairs of conventional surface gratings with compact and robust CBGs for stretching and compression of laser pulses in CPA systems enabled decrease of size and weight of those systems by several times [58,110]. However, conventional CBGs (monolithic, single-pass, retroreflecting) have some limitations

determined by ultimate refractive index modulation and losses (scattering and absorption) in PTR glass, which restrain generation of extremely short high energy pulses with controllable temporal and/or spectral shape. The main goal of the proposed work was to enable substantial increase of stretching time and compression to shorter pulses along with more complex shaping of laser pulses in temporal, spectral, and spatial domains by means of more complex CBGs.

The technical problems to be solved for achieving of the announced goal are increasing of stretching time to decrease power density in amplifier, increasing of spectral width of CBGs to process shorter laser pulses and to utilize broader gain spectra, and for controlling of temporal, spectral, and spatial shapes. To solve the first two problems, it is necessary to increase thickness of CBGs. To solve the third problem one needs to put phase masks which provide phase shift between different spectral components of a laser pulse. However, a considerable increase of thickness and/or bandwidth of CBGs in PTR glass are beyond available technology of glass fabrication and CBG recording. We proposed to create multipass CBGs which increase effective optical path and spectral width, and to create CBGs producing lateral shift of pulse, where all spectral components propagate collinearly while shifted in lateral direction and can be independently controlled by phase and amplitude masks.

A conventional CBG is depicted in Figure 4.6-1. Let us consider a pulse with a spectrum which overlaps with a reflection spectral range of the CBG. For a pulse propagating along axis Z, a blue component is reflected from the front part of a CBG with shorter grating period, while a red component is reflected from the back part of CBG with longer grating period. A delay time between these components (stretching time is $t_{st}=2Ln_{av}/c$, where L is the distance between grating areas resonant for blue and red spectral components of the laser pulse, n_{av} is average refractive index of a CBG, and c – is speed of light. For PTR glass this stretching time is $t_{st}(ps)=100L(cm)$.

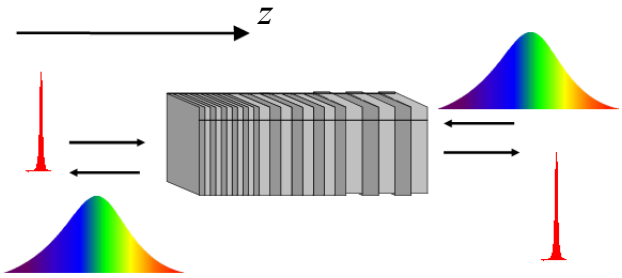

Fig. 4.6-1. Volume Bragg grating with variable period along the beam propagation (z-direction) – volume longitudinal chirped Bragg grating (CBG). Grating period and thickness are not in scale; thickness is usually tens of thousand times larger than the period.

The proposed way to increase stretching time is to provide multipass propagation of a laser pulse in a CBG. It is possible by changing the incident angle. In this case a pulse reflected by a CBG would not overlap with the incident pulse in space. Different spectral components would incur a lateral shift which is not desirable for the further amplification. However, it is important that all these components propagate collinearly. This means that the use of a retroreflecting

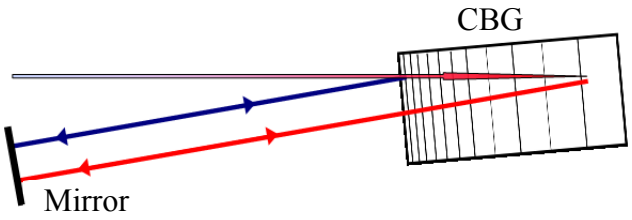

Fig. 4.6-2. A tilted CBG with an external retroreflecting mirror which provides double pass of a laser pulse.

mirror (it can be external as shown in Figure 4.6-2 or deposited on a surface of a CBG) provides doubling of the optical path of a laser pulse in comparison with a conventional CBG working in a retroreflecting mode. It is important that a lateral shift is completely compensated during the third and fourth passages through the CBG after reflection from the mirror. It is clear that this approach can be extended to an arbitrary number of passages to provide an optimal combination between stretching time and losses. A trajectory of a retroreflecting pulse after multiple passes finally would overlap with a trajectory of the incident pulse. Separation of these pulses could be achieved by a polarizing beam splitter. Moreover, we have just showed that tilted CBGs provide lateral shift of different spectral components which propagate collinearly. In this case it is possible to add a mask in such a collimated pulse where each spectral component would be modified independently (Figure 4.6-3). Amplitude mask can provide spectral shaping of pulses while the use of a phase mask can provide temporal shaping of pulses. This method provides not only stretching and compression of laser pulses by complex shaping of pulses in temporal, spectral and spatial domains. Let us now make simple theoretical analysis of this method in case of insertion in the beam path of a simple binary phase element. For a transform limited pulse with spectral intensity S(ν) the temporal intensity after going through a phase mask is:

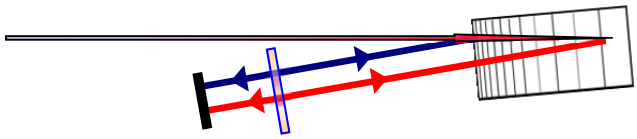

Fig. 4.6-3. A tilted CBG with a mirror at normal incidence and a mask (amplitude or phase) for temporal, spectral or spatial beam shaping or/and GVD correction.

$$I(t) = |F[S(\nu)e^{i*\phi(\nu)}]|^2 \tag{4-13}$$

A simple binary spectral mask divides the spectral intensity S(ν) into S1(ν) and S2(ν). S2(ν) experiences a change in optical path length given as $(n+\varepsilon)\lambda_0$ with n and k being an integer and fraction respectively. The phase function becomes:

$$\phi(\nu) = 2\pi\varepsilon + 2\pi m\lambda_0 \frac{\nu}{c} \tag{4-14}$$

The phase change is only applied to S2(ν) when finding the temporal intensity:

$$I(t) = |F[S_1(\nu) + S_2(\nu)e^{i*\phi(\nu)}]|^2 \tag{4-15}$$

Using E1(t) and E2(t) as the Fourier transform of S1(ν) and S2(ν) respectively the temporal intensity becomes:

$$I(t) = |E_1(t)|^2 + |E_2(t - \frac{n\lambda_0}{c})|^2 + E_1^*(t)E_2(t - \frac{n\lambda_0}{c})e^{i2\pi k} + c.c. \tag{4-16}$$

The first two terms represent temporal effects while the two last terms represent interferences effects. Using this technique, it is then possible to change the temporal shape of a Gaussian pulse for example to a square profile pulse (Figure 4.6-4). This simple calculation can then be extended to a numeric calculation that would calculate the spatial, temporal and spectral profile

of a pulse with a complex temporal and spectral shape after a complex phase and amplitude elements. Similarly, such modeling can then be used for determining the phase and amplitude of the controlling element to achieve a given spatial, temporal and spectral profile.

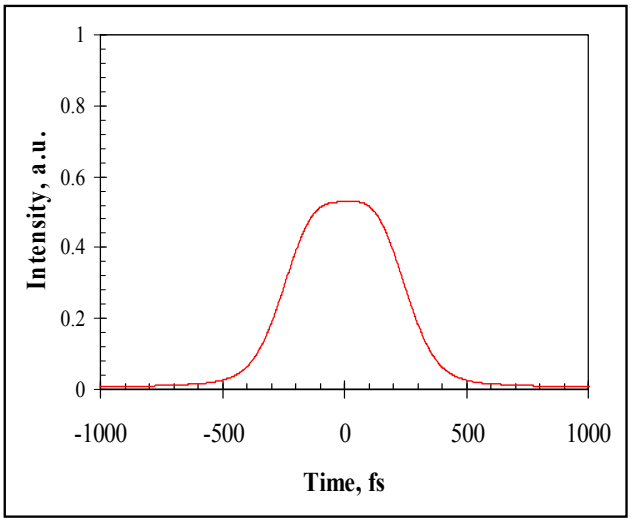

Fig. 4.6-4. Temporal shaping of a Gaussian pulse to a square-like pulse by a binary phase mask.

It is obvious that when it comes to propagating through so large amount of glass, the homogeneity of glass becomes a critical parameter for the quality of the beam diffracted by such a CBG. PTR glass is made by conventional melting in 5-liters crucible, and therefore the homogeneity that can be achieved cannot be as high as the one that main glass manufacturer can obtained. To understand how the glass homogeneity and the beam quality are linked we developed models to predict the M^2 and build a M^2-meter. We first showed that there is a correlation between the measured glass homogeneity as measured using a conventional Fizeau interferometer and the quality of the beam propagating through these glass wafers (Figure 4.6-5).

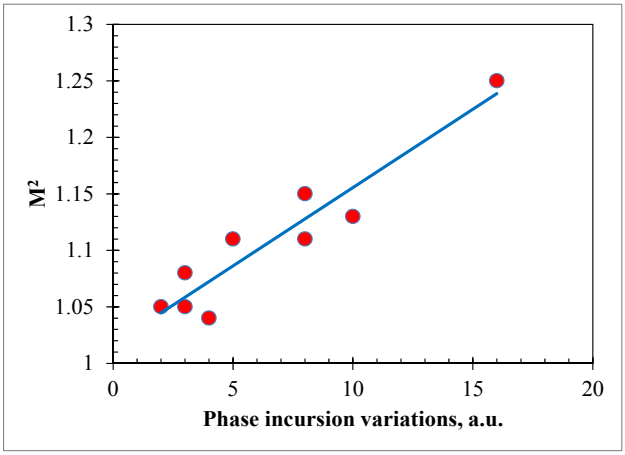

Fig. 4.6-5. Evolution of the beam quality of a Gaussian beam transmitted through an optical window as a function as the phase incursion as measured by Fizeau interferometer.

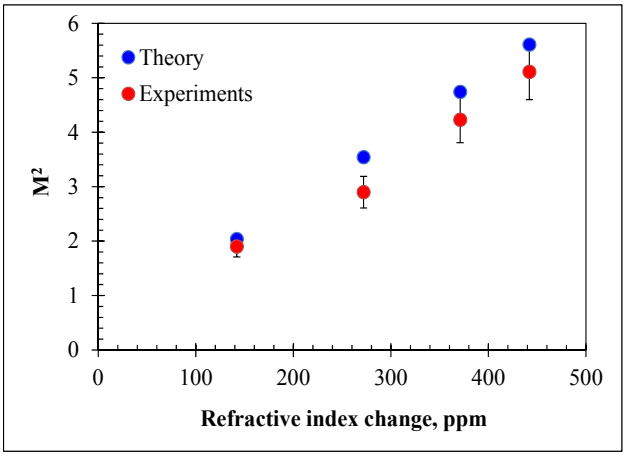

Fig. 4.6-6. Evolution of the beam quality of a Gaussian beam transmitted through Gaussian striae as a function of the maximum refractive index. Blue was obtained by modeling while red show experimental data obtained on PTR glasses with a recorded Gaussian stripe.

But most important is that based on the photosensitivity of PTR glass, we were able to generate artificial striae with predetermined profiles that can be easily added to our simulation program of M^2. That way we were able to generate Gaussian striae by scanning the HeCd laser beam along the glass sample and to control the amplitude of these striae by changing the dosage of UV-exposure. We then characterized these striae and modeled and measured the M^2 after propagation

through these striae (Figure 4.6-6). One can see that there is a very good agreement between these data and that they pave a way towards correlating the glass parameters (homogeneity) with the laser beam parameters (M^2), which becomes critical in case of CBGs.

Chapter 4: Conclusions and Perspectives

4.1. Conclusion on the research activities

My research activities resulted in about 30 peer-reviewed publications and more than 80 presentations in international conferences as well as 5 filed patent applications. These activities are therefore more and more recognized in the scientific community.

My research activities cover a broad range of topics. They include material science (crystallization, mechanical properties, diffusion…), but mostly optics (metrology, laser-matter interaction, optical filtering, thin films, phase plates…). Combining these competences allowed me to solve numerous problems. Actually this multidisciplinary approach permitted for example to reveal the mechanisms of the photosensitivity of photo-thermo-refractive glass, improving its optical properties by understanding its structural properties as well as to fabricate new or optimized optical elements.

In addition, I have developed extra-scientific competences such as the writing of proposals and reports, the management of projects of people and created an international network of active collaborators (both in optics and material science). Finally I have supervised several Master students, Ph.D. students, scientists and postdoctoral fellows.

4.2. Research perspectives

Optical interference filters are involved in many areas of science and industry. With the maturity of the technology that has been gained over the last thirty years, the diversity and complexity of optical functions performed has severely increased (respecting simultaneously the constraints on the intensity and phase, polarization, or achromaticity...). The design of these stacks is now benefiting from the availability of synthesis software that uses the latest optimization procedures (genetic algorithms, method of the needles...). If, in the 2000s, dramatic progress has been made in the field of manufacturing of filters for microelectronics applications (UV photolithography), high-speed optical telecommunications (multiplexers and demultiplexers for DWDM, gain equalizing filters) and biomedical (sharp dichroic filters for fluorescence), the technology has made further progress over the past 5 years, including the field of process automation, and makes possible the deposition of hundreds of layers (a thousand has recently been demonstrated) with a nanometer precision. However, whatever the application, and despite the progress mentioned above, the fabrication of filters with ultimate performances still raises several critical manufacturing issues:

- First, one must be able to control the optical thickness of each layer of the multilayer with nanometer precision, and in some cases, sub-nanometer. Any errors can induce unwanted changes of its optical properties that can sometimes be dramatic.
- Then, during a deposition, due to the shape of the evaporation plume, the optical thickness of each layers of the stack will vary over the substrate surface and thus present non-uniformity. The optical properties of the filter (reflection and transmission) will therefore depend on the area where you carry out the measurement, which, in other words, means that the filter will present only locally the expected properties.
- In the case of filters being spatially structured, the process of fabrication generally induces local losses which strongly decrease the final performance of the filter.

Finally, although the recent technological progress that allow today the deposition of hundreds of layers, these developments were mostly done in visible and near infrared and the fabrication of bandpass filters suitable for mid-infrared region is still a relatively open issue.

The research perspectives are therefore to develop and manufacture new optical filtering functions with optimized performances. To achieve this, it will be necessary to carry out three specific research activities, respectively devoted to:

- the development of processes for photosensitive and/or photo-structures thin film deposition. Potential candidates include: photo-thermo-refractive or photo-etchable materials, chalcogenides…
- the development of procedures for selective excitation of each layer within a complex multilayer
- and finally, the fabrication of new devices taking advantage of the potential of this innovative approach.

In terms of components and filtering functions, this approach can be implemented to create a photo-adjustable Fabry-Perot cavity allowing the fabrication of or ultra-uniform or pixelated bandpass filters. It can also be applied for the fabrication of resonant filters for the near and mid-infrared and or for the fabrication structures with giant optical amplification.

Finally, this new technology would benefit many people and sectors (imaging, space, biology ...) as it would allow the manufacturing of new optical interference filters whose properties could not be achieved until now. In addition, this new technology would strengthen the bridge between the optical thin films and photonic crystals, since it paves a way to the manufacturing of components with spatially structured phase.

Chapter 5: Scientific and administrative activities

5.1. Scientific projects

Over the past 6+ years at CREOL/UCF and OptiGrate Corp., I have participated in numerous US government agencies funded projects on volume holographic optical elements in PTR glasses. Moreover, in addition to be performing the scientific activities of these projects, I have also been a *Principal Investigator*, PI in some of the projects (total budget exceeding $1,000,000). I listed in the next two sections the projects I worked on and included a short description of my duties.

5.1.1. Projects as a co-investigator

[PC1] "*High efficient volume holographic optical elements for high power lasers*" project financed by DARPA, in charge of the study of the optical and structural properties of PTR glasses (2005 – 2006)

[PC2] "*Bragg Selectors of Transverse Modes for High Power Lasers*", project financed by the Missile Defense Agency, in charge of the study of the optical and structural properties of PTR glasses (2005 – 2006)

[PC3] "*Super High Efficiency Diode Sources (SHEDS)*" project financed by DARPA, in charge of the study of the optical and structural properties of PTR glasses (2005 – 2006)

[PC4] "*Architecture for Diode High Energy Laser Systems – ADHELS*" project financed by DARPA (Phase I & II), in charge of the study of low losses in PTR glasses (2005 – 2010)

[PC5] "*High Density Spectral Beam Combining by Volume Bragg Gratings in PTR glass*" project financed by the High Energy Laser service of the Joint Technology Office, (Phase I & II), in charge of the study of low losses in PTR glasses (2005 – 2007)

[PC6] "*Large Format Narrow Band Polarization Insensitive High Throughput Optical Filters for 0.5-2.7 μm Spectral Region*" project financed by NASA (Phase I – SBIR), in charge of the theoretical and experimental study of Fabry-Perot-Bragg filters (2006)

[PC7] "*High power compact single-frequency volume Bragg Er-doped fiber laser*" project financed by NASA (Phase I – SBIR), in charge of the theoretical and experimental study of phase shifted Bragg gratings (2007)

[PC8] "*High resolving power volume diffractive gratings for 400-2700 nm spectral range*" project financed vy NASA (Phase II – SBIR), in charge of the theoretical and experimental study of the properties of volume Bragg gratings (2007 – 2008)

[PC9] "*High Power Diode Pumped Alkali Vapor Lasers and Analog Systems*" project financed by the High Energy Laser service of the Joint Technology Office, in charge of the study of low losses in PTR glasses of the laser diode wavelengths (2008 – 2010)

[PC10] "*Compact stretcher/compressor for high power ultrafast laser based on volume chirped Bragg grating in PTR glass*", Project financed by NAVY (Phase I SBIR project), in charge of the study of scattering losses in PTR glasses (2008 – 2009)

[PC11] "*Development of a tunable volume Bragg laser system for solid state lasers pumping at 1535nm*" project financed by the Army research Laboratory, in charge of the study of small absorption losses in PTR glasses and the development and installation of a calorimetric setup for the measurement of small absorption losses in laser crystals (2009-2010)

[PC12] "*Compact single frequency volume Bragg lasers operating at 1.5 um*" project by NASA (Phase II – SBIR), in charge of the theoretical and experimental study of the properties of moiré Bragg gratings for the selection of longitudinal modes in laser cavities (2009 – 2011)

[PC13] "*Technology and metrology development for fabrication of chirped Bragg gratings with improved characteristics at 1553 nm*" project financed by NAVY (sub-contract from Raydiance, Phase II-a STTR Project), in charge of the study of the quality of the beam diffracted by a chirped Bragg grating (2010-2011)

[PC14] "*Fabrication of chirped Bragg gratings for high power nanosecond-to-femtosecond range pulse compression at 1553 nm*" project financed by NAVY (sub-contract from Raydiance, Phase II.5 STTR Project), in charge of the study of the parameters influencing the quality of the beam diffracted by a chirped Bragg grating (2011)

[PC15] "*Volume Bragg gratings– research, testing and high power applications*" project financed by the High Energy Laser service of the Joint Technology Office (MRI Project), in charge of the study of low losses and the photosensitivity of PTR glasses and volume Bragg gratings (2010-2014)

5.1.2. Projects as a principal investigator

[PI1] "*Photosensitivity of Large-Aperture Homogeneous PTR glass*" project financed by DARPA to Raytheon Network Centric Systems (Project "Large Grating – Phase I), Principal Investigator and in charge of the development of the methods that can be implemented in order to improve the homogeneity of large aperture volume Bragg gratings (2007 – 2008)

[PI2] "*Development of photo-thermo-refractive glasses for mid-IR holographic target boards*", project financed by Naval Air Station to Georgia Tech Institute and entitled "*Holographic Target Board for Ground Target Irradiance/Fluence Measurements*" (Phase II-a & II-b), Principal Investigator and in charge of the study of the dehydration of PTR glasses to increase the transparency range of PTR glasses towards mid-IR (2007 – 2008)

[PI3] "*Large aperture scattering screens with minimal absorption in near IR (Phase III)*", project financed by Naval Air Station to Georgia Tech Institute and entitled "*Holographic Target Board for Ground Target Irradiance/Fluence Measurements*" (Phase III), Principal Investigator and in charge of the study of the homogeneity of large aperture PTR glasses and of the characterization of holographic screens (2008-2009)

[PI4] "*Characterization of Holographic Optical Elements in PTR Glass*" – project financed by DARPA to Raytheon Network Centric Systems (project APPLE – Phase I), Principal Investigator and in charge of the study of scattering losses and the wavefront distortions in the diffracted beam from a transmitting Bragg grating (2008-2009)

[PI5] "*Monolithic rare earth doped PTR glass laser*" project financed by NASA (Phase I – SBIR), Principal Investigator and in charge of the photosensitivity and the luminescence of rare-earth doped PTR glasses (2010)

[PI6] "*Measurements of absorption in thick RBG at 1085nm*" Services for the Army research Laboratory, Principal Investigator and in charge of the characterization of the absorption in thick Bragg gratings and estimating the performances of this Bragg grating in CW 100 W laser beam (2010)

[PI7] *A narrow-band laser source for pumping the Rb D2 transition in the vicinity of 780 nm - Service for absorption measurements*" project LASIR financed by the US Air Force to Boeing LTS Inc (service for OptiGrate Corp.), Principal Investigator and in charge of the characterization of low absorption in reflecting Bragg gratings at 808 nm (2010)

[PI8] "*Demonstration of a compact beam combiner: High power measurements*", project financed by the US Air Force Research Laboratory (Service for OptiGrate Corp.), Principal Investigator and in charge of small absorption losses in multiplexed Bragg gratings for coherent beam combining (2010)

[PI9] "*Monolithic rare earth doped PTR glass laser*" project financed by NASA (Phase II – SBIR), Principal Investigator and in charge of the photosensitivity and the luminescence of rare-earth doped PTR glasses (2011-2012)

[PI10] "*Compact robust stretcher/compressor of ultrashort laser pulses*" project financed by DARPA (BAA Project), Principal Investigator and in charge of properties of the beam stretched and compressed by chirped Bragg gratings (2011-2012)

5.1.3. Table summarizing the projects as a PI

Table 5.1-1 summarizes all the projects I participated as a PI as well as the associated budgets. The main budget is the one that was received from the project funding agency while the additional amount is an additional budget which is provided by the *Florida's High Tech Corridor* (FHTC). These additional funds are obtained after submitting a second proposal related to the main project and aiming to allow further development of the technology developed under the main project.

Tab. 5.1-1. Table summarizing the budgets of the projects I participated as a PI

#	Project Name	Start	End	Budget	FHTC.	Total
1	Photosensitivity of Large-Aperture Homogeneous PTR glass	15/07/2007	15/03/2008	$ 100,000	$ 50,000	$ 150,000
2	Development of photo-thermo-refractive glasses for mid-IR holographic target boards (Phase II)	1/1/2008	30/09/2008	$ 75,000	$ 37,500	$ 112,500
3	Large aperture scattering screens with minimal absorption in near IR (Phase III)	1/1/2008	27/12/2008	$ 65,000	$ 32,500	$ 97,500
4	Characterization of Holographic Optical Elements in PTR Glass (APPLE)	15/01/2008	15/03/2009	$ 115,000	$ 57,500	$ 172,500

5	Monolithic rare earth doped PTR glass laser (Phase I)	15/02/2010	15/07/2010	$ 30,000	$ 10,000	$ 40,000
6	Measurements of absorption in thick RBG at 1085nm	31/3/2010	14/05/2010	$ 2,400	$ 800	$ 3,200
7	A narrow-band laser source for pumping the Rb D2 transition in the vicinity of 780 nm (LASIR)	15/08/2010	15/12/2010	$ 15,000	$ 5,000	$ 20,000
8	Demonstration of a compact beam combiner: High power measurements	15/08/2010	15/12/2010	$ 5,000	$ 1,666	$ 6,666
9	Monolithic rare earth doped PTR glass laser (Phase II)	01/01/2011	31/12/2012	$ 180,000	$ 150,00	$ 330,000
10	Compact robust stretcher/compressor of ultrashort laser pulses	01/01/2011	31/12/2012	$ 79,500	$ 26,500	$ 106,000
		Total Fundings		**$ 666,900**	**$ 371,466**	**$1,038,366**

The overall budget I have been in charged for the past 5 years is about $1,000,000.

5.2. Collaborations

Over the past 7 years, I had the opportunity to develop a network of collaborators that have helped us to perform the research on PTR glass and volume holographic elements. I have summarized our main collaborators as well as the scientific publications and presentations that have resulted from those one.

- **Prof. Dr Edgar D. Zanotto**, LaMaV, Federal University of San Carlos, Brazil – Study of crystallization in PTR glasses – These research activities resulted in 9 publications [1.4, 1.7, 1.11, 1.16, 1.18, 1.19, 1.21, 1.24, 1.25, 1.27] and 18 conference presentations [4.7, 5.2, 5.5, 5.6, 5.7, 5.8, 5.10, 5.11, 5.12, 5.17, 5.18, 5.22, 5.29, 5.32, 5.35, 5.36, 5.41, 5.44].
- **Dr Joachim Deubener**, University of Clausthal, Germany – Study of the mechanical properties of PTR glasses – These research activities resulted in 1 publication [1.13] and 1 conference presentation [5.13].
- **Prof. Michel Lequime**, Institut Fresnel, Université Aix Marseille III, France – Application of volume Bragg gratings to the fabrication of ultra-narrowband filters – These research activities resulted in 1 publication [1.27] and 2 conference presentations [4.6,5-55] (excluding the Ph.D. research activities).

- **Prof. Lionel Canioni**, CPMOH, Université Bordeaux I, France – Study of the interaction of ultrashort pulses with volume Bragg gratings – These research activities resulted in 2 publications [1.14, 1.17] and 3 conference presentations [4.11, 4.13, 4.16].
- **Dr Francisco Serbena**, Federal University of Parana, Brazil – Study of stresses in PTR glasses – These research activities resulted in 1 publication [1.25] and 4 conference presentations [4.7, 5.11, 5.18, 5.32].
- **Prof. Josef Zwanziger**, University of Dalhousie, Canada – Study of PTR glass properties by NMR.
- **Prof. Mauro Baesso**, University of Campinas, Brazil – Study of thermal properties of PTR glasses.
- **Dr Andrey Okhrimchuk**, Aston University, UK – Study of the fabrication of waveguides in PTR glasses.

5.3. Teaching and student supervision

5.3.1. Teaching experience

I have been teaching from 2001 to 2004 at the University Paul Cézanne - Aix-Marseille III. I was a Moniteur at the Centre d'Initiation à l'Enseignement Supérieur (CIES) of the région Provence, Côte d'Azur et Corse. During these three years I have taught general physics to people with either a technical [Sciences et Technologies pour l'Ingénieur (STI)] or a theoretical [Sciences de la Matière (SM) – Mathématiques, Informatique et Applications aux Sciences (MIAS)] background. Table 5.3-1 presents the classes I have taught.

Tab. 5.3-1. Summary of the classes I taught in the 2001-2004 period.

Section	***Year***	***Topics***	***Class***	***Lab***
DEUG STPI	2004	Measurements in electronic		18 H
DEUG STPI & SM	2004	Electronics	10 H	30 H
DEUG STPI & MIAS	2003	Measurements in electricity and thermodynamics		54 H
DEUG STPI & SM	2003	Electronics	10 H	30 H
DEUG STPI & MIAS	2002	Measurements in electricity and thermodynamics		50 H
DEUG STPI & SM	2002	Measurements in electricity and thermodynamics	10 H	
DEUG STPI & MIAS	2001	Electronics		80 H
TOTAL			**30 H**	**262 H**

5.3.2. Student supervision

During the third year of my PhD, I had my first experience of student supervision with a Master student who wanted to have a first experience with academic research. His activities were related to the use of micro-mirror devices for the development of a structured exposure system. During his internship, he made the first spatially controlled exposure of photosensitive materials with

ultimate goal to fabricate a filter with controlled evolution of its spectral response over its aperture.

Since I joined CREOL/UCF, I have been supervising several students, but also scientists and postdoctoral fellows. I provide below a description of all the people I have supervised as well as the activities they were involved in and the resulting scientific papers.

- In 2005, I co-supervised the work of a Visiting Scientist Mr. Aleksander Sinitskii on the study of PTR glass crystallization. These research activities resulted in 2 publications [1.4, 1.16] and 4 conference presentations [5.2, 5.5, 5.6, 5.7].
- In 2005-2008 I supervised a PhD student Mr. Leo Siiman throughout his up to his defense of a PhD dissertation on the study of ultrashort laser pulse interaction with photo-thermo-refractive glass. These research activities resulted in 5 publications [1.10, 1.12, 1.13, 1.14, 1.16], 1 patent application [2.1] and 12 conference presentations [4.8, 4.10, 4.11, 4.13, 4.14, 5.4, 5.16, 5.15, 5.16, 5.20, 5.25, 5.26].
- From 2006 to 2009, I was in charge for a research project conducted at the University of Sao Carlos (Brazil) supervising a Postdoctoral Fellow Dr. Guilherme P. Souza on the study of PTR glass crystallization. These research activities resulted in 6 publications [1.11, 1.19, 1.21, 1.24, 1.25, 1.29], and 10 conference presentations [4.7, 5.11, 5.12, 5.17, 5.18, 5.22, 5.29, 5.35, 5.41, 5.44].
- Since 2009, I am taking part in the supervision of Mr. Marc SeGall (PhD Student), on the fabrication of phase masks in PTR glass. These research activities resulted in 1 patent [2.4] and 2 conference presentations [4.19, 4.22].
- In 2008, I supervised Mr. Apurva Jain (PhD student), on the fabrication of an optical setup for measuring refractive index in glass.
- In 2008-2009, I co-supervised Dr Marie-Laure Anne-Brandily (Postdoctoral Fellow), on the study of PTR glass properties. These research activities resulted in 1 publication [1.23] and 2 conference presentations [5.30, 5.33].
- From 2008 to 2010, I supervised Mr. Dylan Moses (PhD student) on femtosecond pulses stretching and compression by chirped Bragg gratings. These research activities resulted in 2 conference presentations [5.25, 5.43].
- Since 2009, I am supervising Mrs Karima Chamma (Research Scientist) on glass processing and study of crystallization. These research activities resulted in 1 publication [1.22] and 9 conference presentations [3.2, 4.23, 5.34, 5.37, 5.40, 5.47, 5.53, 5.54].
- In 2010-2011, I supervised Mr. Brian Anderson (PhD student) on the study of the photo-ionization of cerium in glasses
- Since 2010, I am co-supervising Mr. Dan Ott (PhD Student) on ultra-narrow optical filtering by moiré Bragg gratings. These research activities resulted in 1 conference presentation [5.52].
- Since mid-2010, I am supervising Mr. Christopher Lantigua (Research Scientist, now accepted to Master Program), on the study of chirped Bragg gratings.

5.4. Publications, patents and presentations

5.4.1. Peer-reviewed publications

[1.1] J. Lumeau, M. Cathelinaud, J. Bittebierre and M. Lequime, "Ultra-narrow bandpass hybrid filter with wide rejection band," Applied Optics **45**(7) 1328– 332 (2006)

[1.2] J. Lumeau and M. Lequime, "Localized measurement of the optical thickness of a transparent window – Application to the study of the photosensitivity of organic polymers," Applied Optics **45**(4), 6099–6105 (2006)

[1.3] J. Lumeau, V. Smirnov and L. B. Glebov, "Tunable narrow-band filter based on a combination of Fabry-Perot etalon and Volume Bragg Grating," Optics Letters **31**(16), 2417–2419 (2006)

[1.4] J. Lumeau, A. Sinitskiy, L. N. Glebova, L. B. Glebov and E. D. Zanotto, "Spontaneous and photo-induced crystallization of PTR glass", Physics and Chemistry of Glasses: European Journal of Glass Science and Technology Part B, **48**(4), 281–284 (2007)

[1.5] M. Lequime and J. Lumeau, "Accurate determination of the optical performances of antireflective coatings by low coherence reflectometry", Applied Optics **46**(23), 5635–5644 (2007)

[1.6] J. Lumeau, L. Glebova and L. B. Glebov, "Influence of UV-exposure on the crystallization and optical properties of photo-thermo-refractive glass", Journal of Non Crystalline Solids, **354**, 425–430 (2008)

[1.7] L. Glebova, J. Lumeau, M. Klimov, E. D. Zanotto and L. B. Glebov, "Role of bromine on the thermal and optical properties of photo-thermo-refractive glass", Journal of Non Crystalline Solids, **354**, 456–461 (2008)

[1.8] L. B. Glebov, J. Lumeau, S. Mokhov, V. Smirnov and B. Ya. Zeldovich, "Reflection of light by composite volume holograms: Fresnel corrections and Fabry-Perot spectral filtering", JOSA A, **25**(3), 751–764 (2008)

[1.9] J. Lumeau, L. Glebova and L. B. Glebov, "Evolution of Absorption Spectra in the Process of Nucleation in Photo-Thermo-Refractive Glass", Advanced Materials Research, **39-40**, 395–398 (2008)

[1.10] L. Siiman, J. Lumeau, and L. B. Glebov, "Nonlinear photosensitivity of photo-thermo-refractive glass by high intensity laser irradiation", Journal of Non Crystalline Solids, **354**, 4070–4074 (2008)

[1.11] J. Lumeau, L. Glebova, G. P. Souza, E. D. Zanotto and L. B. Glebov "Effect of cooling on the optical properties and crystallization of UV-exposed photo-thermo-refractive glass", Journal of Non Crystalline Solids **354**, 4730–4736 (2008)

[1.12] L. Siiman, J. Lumeau, L. B. Glebov, "Phase Fresnel lens recorded in PTR glass by selective exposure to IR ultrashort laser pulses", Optics Letters **34**(1), 40–42 (2009)

[1.13] J. Deubener, H. Bornhöft, S. Reinsch, R. Müller, J. Lumeau, L. N. Glebova, L. B. Glebov, "Viscosity, relaxation and elastic properties of photo-thermo-refractive glass", Journal of Non Crystalline Solids **355**, 126–131 (2009)

[1.14] L. Siiman, J. Lumeau, L. Canioni and L. B. Glebov, "Non-collinear generation of third harmonic of IR ultrashort laser pulses by PTR glass volume Bragg gratings", Optics Express **17**(5) 3564–357 (2009)

[1.15] L. Siiman, J. Lumeau, L. B. Glebov, "Nonlinear photoionization and laser-induced damage in silicate glasses by infrared ultrashort laser pulses", Applied Physics B **96**(1), 127–134 (2009)

[1.16] J. Lumeau, A. Sinitskiy, L. N. Glebova, L. B. Glebov and E. D. Zanotto, "Method to assess the homogeneity of photosensitive glasses: application to photo-thermo-refractive glass", Journal of Non Crystalline Solids **355**, 1760–1768 (2009)

[1.17] L. Siiman, J. Lumeau, L. Canioni and L.B. Glebov, "Ultrashort laser pulse diffraction by volume Bragg gratings in PTR glass", Optics Letters **34**(17), 2572–2574 (2009)

[1.18] J. Lumeau, L. Glebova, L. B. Glebov, V. Golubkov and E. D. Zanotto, "Origin of crystallization-induced refractive index changes in photo-thermo-refractive glass", Optical Materials **32**, 139–146 (2009)

[1.19] G. P. Souza, V. M. Fokin, E. D. Zanotto, J. Lumeau, L. Glebova, L. B. Glebov, "Micro and Nanostructures in Partially Crystallized Photo-Thermo-Refractive Glass", Physics and Chemistry of Glasses: European Journal of Glass Science and Technology Part B **50** (5), 311–320 (2009)

[1.20] V. Smirnov, J. Lumeau, S. Mokhov, B. Ya. Zeldovich and L. B. Glebov, "Ultra-narrow bandwidth Moiré reflecting Bragg gratings recorded in photo-thermo-refractive glass", Optics Letters 35(4), 592–594 (2010)

[1.21] V. M. Fokin, G. P. Souza, E. D. Zanotto, J. Lumeau, L. Glebova, L. B. Glebov, "Sodium Fluoride Solubility in Photo-Thermo-Refractive Glass", Journal of the American Ceramic Society **93**(3), 716–721 (2010)

[1.22] K. Chamma, J. Lumeau, L. Glebova, and L. B. Glebov, "Generation and bleaching of intrinsic color centers in photo-thermo-refractive glass matrix", Journal of Non Crystalline Solids **356** (44-49), 2363–2368 (2010)

[1.23] M. Anne, J. Lumeau, L. Glebova and L.B. Glebov, "Specific absorption spectra of cerium in multicomponent silicate glasses", Journal of Non Crystalline Solids **356** (44-49), 2337–2343 (2010)

[1.24] G. P. Souza, V. M. Fokin, C. F. Rodrigues, A. C. M. Rodrigues, E. D. Zanotto, J. Lumeau, L. Glebova, L. B. Glebov, "Liquid-Liquid Phase Separation in Photo-Thermo-Refractive Glass", Journal of the American Ceramic Society, **94**(1), 145–150 (2011)

[1.25] F. C. Serbena, G. P. Souza, E. D. Zanotto, J. Lumeau, L. Glebova, L. B. Glebov, "Internal Residual Stress in Partially Crystallized Photo-Thermo-Refractive Glass", Journal of the American Ceramic Society, **94**(3) 671–674 (2011)

[1-26] A. V. Mitrofanov, A. J. Verhoef, E. E. Serebryannikov, J. Lumeau, L. Glebov, A. M. Zheltikov, and A. Baltuska, "Optical detection of sub-cycle ionization dynamics in transparent dielectrics", Physical Review Letters **106**, 147401 (2011)

[1-27] J. Lumeau, C. Koc, O. Mokhun, V. Smirnov, M. Lequime and L. B. Glebov, "Single resonance monolithic Fabry-Perot filters formed by volume Bragg gratings and multilayer dielectric mirrors", Optics Letters **36**(10), 1773–1775 (2011)

[1-28] L. Glebova, J. Lumeau and L. B. Glebov, "Photo-thermo-refractive glass co-doped with Nd^{3+} as a new laser medium", Optical Materials **33**, 1970–1974 (2011)

[1-29] G. P. Souza, V. M. Fokin, C. A. Baptista, E. D. Zanotto, J. Lumeau, L. Glebova, L. B. Glebov, "Effect of Bromine on NaF Crystallization in Photo-Thermo-Refractive Glass", Journal of the American Ceramic Society **94**(9), 2906–2911 (2011)

[1-30] J. Lumeau, L. Glebova and L. B. Glebov, "Near-IR absorption in high purity photo-thermo-refractive glass and holographic optical elements: measurement and application for high energy lasers", Applied Optics **50**(30), 5905–5911 (2011)

[1-31] M. SeGall, V. Rotar, J. Lumeau, S. Mokhov, B. Ya. Zeldovich and L. B. Glebov, "Binary Volume Phase Masks in Photo-Thermo-Refractive Glass", Optics Letters, accepted (2011)

5.4.2. Patent applications

[2.1] L. Siiman, J. Lumeau, L. Glebova, V. Smirnov, L.B. Glebov, "Process of production of high efficiency diffractive and refractive optical elements in multi-component silicate glass by nonlinear photo-ionization followed by thermal development", *Patent pending*, Application # **11/799,863**, May 2007

[2.2] L. B. Glebov, J. Lumeau, S. Mokhov, V. Smirnov, B. Ya. Zeldovich, "Volume Moiré Bragg gratings in a photosensitive material", *Patent pending,* Application # **61/178,561**, May 2009

[2.3] O. Andrusyak, L. B. Glebov, J. Lumeau, S. Mokhov, V. Smirnov, B. Ya. Zeldovich, "Laser pulse temporal, spectral and spatial shaping devices on basis of volume diffractive gratings with variable period", *Patent pending*, Application # **61/294,566**, March 2009

[2.4] L. B. Glebov, J. Lumeau, S. Mokhov, O. Mokhun, V. Rotar, M. SeGall, V. Smirnov, B. Ya. Zeldovich, "Fabrication of plane parallel phase plates by means of spatial variations of refractive index in photo-thermo-refractive glass", *Patent pending,* Application # **xx/xxx,xxx**, April 2011

[2.5] A. Jain, L. B. Glebov, L.Glebova, J. Lumeau, V. Smirnov, C. Spiegelberg, " Monolithic solid state lasers", *Filed Patent application*, December 2011

5.4.3. Invited talks

[3.1] M. Lequime and J. Lumeau, "Laser trimming of thin-film filters", Advances in Optical Thin-Films (Jena, Germany), invited talk, paper **5963-08**, September 2005

[3.2] K. Chamma, L. Glebova, J. Lumeau, L. Glebov, "Generation and bleaching of color centers in photo-thermo-refractive glass", XII Conference on the Physics of Non-Crystalline Solids (Iguacu Falls, Brazil), Invited talk, paper **492**, September 2009

[3.3] J. Lumeau, "Optical analyses of the complex crystallization mechanisms of a multicomponent photo-thermo-refractive glass", Crystallization 2009 (Iguacu Falls, Brazil), Invited talk, paper **107**, September 2009

5.4.3. Conference presentations with proceedings

[4.1] J. Lumeau, M. Cathelinaud, J. Bittebierre and M. Lequime, "Narrow bandpass hybrid filter with wide rejection band", Optical Interference Coatings conference (Tucson, Arizona, USA), paper **ThB7**, June 2004

[4.2] M. Demenikov, J. H. Lumeau, V. K. Rotar, A. Sevian, V. I. Smirnov, L. B. Glebov, "Large aperture diffractive elements in PTR glass", Defense and Security Symposium (Orlando, Florida, USA), paper **6216-36**, April 2006

[4.3] J. Lumeau, V. Smirnov, L. B. Glebov, "Tunable ultra-narrow band-pass filters based on Volume Bragg Grating", CLEO/QELS (Long Beach, California, USA), paper **CWK1**, May 2006

[4.4] J. Lumeau, V. Smirnov and L.B. Glebov, "Tunable narrow band-pass filters for laser applications", 19th Solid State and Diode Laser Technology Review (Albuquerque, New Mexico, USA), paper **P-5**, June 2006

[4.5] L. B. Glebov, J. Lumeau, S. V. Mokhov and B. Ya. Zeldovich, "Spectral Transmission of Volume Bragg Gratings: Influence of Uncompensated Fresnel Reflections" Frontiers in Optics (Rochester, New York, USA), paper **JWD58**, October 2006

[4.6] J. Lumeau, V. Smirnov, F. Lemarchand, M. Lequime and L. B. Glebov, "Large aperture tunable ultra-narrow band Fabry-Perot-Bragg filter", Photonics West (San Jose, California, USA), paper **6469-21**, January 2007

[4.7] F. C. Serbena, G. P. Souza, E. D. Zanotto, J. Lumeau, L. Glebova, L. B. Glebov, X. Zhang, "Residual Stress Measurements in Oxyfluoride and Chalcogenide Nano Glass-Ceramics", 17th Annual Users Meeting of the Brazilian Synchrotron Light Laboratory (LNLS campus in Campinas (SP), Brazil), page 128, February 2007

[4.8] L. Siiman, J. Lumeau, and L. B. Glebov, "Sensitivity of photo-thermo-refractive glass to IR femtosecond pulses: application for the recording of phase elements", CLEO Europe (Munich, Germany), paper **CE4-5-TUE**, June 2007

[4.9] J. Lumeau, L. Glebova and L. B. Glebov, "Investigation of the induced absorption and scattering in visible and NIR ranges in photo-thermo-refractive glass", International Congress on Glass (Strasbourg, France), paper **M3**, July 2007

[4.10] L. Siiman, J. Lumeau, and L. B. Glebov, "Photosensitivity of photo-thermo-refractive glass to infrared femtosecond pulses", International Congress on Glass (Strasbourg, France), paper **M18**, July 2007

[4.11] L. Siiman, J. Lumeau, L. Canioni and L. B. Glebov, "Third harmonic generation by volume Bragg grating in photo-thermo refractive glass irradiated by IR femtosecond pulses", Photonics West (San Jose, California, USA), paper **6875-35**, January 2008

[4.12] J. Lumeau, V. Smirnov, and L. B. Glebov, "Phase-shifted volume Bragg gratings in photo-thermo-refractive glass", Photonics West (San Jose, California, USA), paper **6890-10**, January 2008

[4.13] L. Siiman, J. Lumeau, L. Canioni and L. B. Glebov, "Angular selectivity of third harmonic generated in a PTR transmitting Bragg grating by femtosecond pulses", Advanced Solid-State Photonics (Nara, Japan), paper **WB31**, January 2008

[4.14] L. Siiman, J. Lumeau and L. B. Glebov, "Photoionization of wide bandgap silicate glasses by ultrashort IR laser pulses", Boulder Damage Symposium (Boulder, Colorado, USA), paper **7132-6**, September 2008

[4.15] J. Lumeau, S. Mokhov, V. Smirnov, B. Ya. Zeldovich, and L. B. Glebov, "Moiré reflecting Bragg gratings recorded in photo-thermo-refractive glass", CLEO Europe (Munich, Germany), paper **CE4.5**, June 2009

[4.16] J. C. Delagnes, L. Canioni, L. A. Siiman, J. Lumeau, L. B. Glebov, "Direct and Cascaded Third Harmonic generation in Photo-Thermo Refractive glasses and Periodically Poled crystals" UltraFast Optics VII (Arcachon, France), Paper **P1.20**, September 2009

[4.17] S. Mokhov, L. B. Glebov, J. Lumeau V. Smirnov, and B. Ya. Zeldovich, "Moiré filters in volume Bragg gratings", Frontiers in Optics (San Joe, California, USA), paper **FMF2**, October 2009

[4.18] J. Lumeau, V. Smirnov, A. Glebov and L. B. Glebov "Ultra-narrow bandpass filters based on volume Bragg grating technologies", Defense and Security Symposium (Orlando, Florida, USA), paper **7675-15**, April 2010

[4.19] S. Mokhov, M. SeGall, D. Ott, V. Rotar, J. Lumeau, B. Zeldovich, L. Glebov, "Direct Recording of Phase Plates in Holographic Material with Using of Probabilistic Amplitude Masks", Digital Holography and Three-Dimensional Imaging (DH) Topical Meeting (Miami, Florida, USA), paper **JMA11**, April 2010

[4.20] V. Rotar, J. Lumeau, D. Roberts, L. Glebov, "Holographic Screens in Photo-Thermo-Refractive Glass", Digital Holography and Three-Dimensional Imaging (DH) Topical Meeting (Miami, Florida, USA), paper **JMA12**, April 2010

[4.21] A.V. Mitrofanov, A.J. Verhoef, E.E. Serebryannikov, J. Lumeau, L. Glebov, A.M. Zheltikov, and A. Baltuška, "Optical Detection of Attosecond Ionization Dynamics in Transparent Solids", 17th International Conference on Ultrafast Phenomena (Snowmass Village, Colorado, USA), paper **FB2**, July 2010

[4.22] M. SeGall, V. Rotar, J. Lumeau, and Leonid Glebov, "Volume Phase Plates for Optical Beams Control", Frontiers in Optics (Rochester, NY, USA), paper **JWA02**, October 2010

[4.23] L. Glebova, K. Chamma, J. Lumeau and L. Glebov, "Photo-Thermo-Refractive glass – Properties and Applications", *Advances In Optical Materials* (Istanbul, Turkey), paper **AIThC2**, February 2011

[4.24] A. V. Mitrofanov, A. J. Verhoef, E. E. Serebryannikov, J. Lumeau, L. Glebov, A. M. Zheltikov, A. Baltuska, "Attosecond Ionization Dynamics in Transparent Solids", High-Intensity Lasers and High-Field Phenomena (Istanbul, Turkey), paper **HWC2**, February 2011

5.4.3. Conference presentations without proceedings

[5.1] J. Lumeau, "Application of photosensitivity for the realization of optical interference filters", Seminar at the Universität Karlsruhe, Germany, January 2005

[5.2] J. Lumeau, A. Sinitskiy, L. N. Glebova, E. D. Zanotto and L. B. Glebov, "Homogeneity of photosensitivity of PTR glass evaluated by crystallization statistics", First conference on advances in optical materials (Tucson, Arizona, USA), October 2005

[5.3] J. Lumeau and M. Lequime, "Mesure locale de l'épaisseur optique d'une lame transparente : Application à l'étude de la photosensibilité de polymères organiques", Horizon de l'Optique (Chambéry, France), proceedings P. 110 – 111, November 2005

[5.4] L. Siiman, J. Lumeau and L. B. Glebov, "Nonlinear Photoionization of Optical Glass by Femtosecond Pulses", CREOL Industrial Affiliates Day (Orlando, Florida, USA), paper **9**, April 2006

[5.5] V. Smirnov, L. N. Glebova, J. Lumeau, V. Rotar, E. Rotari, A. Sevian, A. Sinitskiy, E. D. Zanotto and L. B. Glebov, "Robust diffractive elements in PTR glass for laser applications", Defense and Security Symposium (Orlando, Florida, USA), paper **6216-35**, April 2006

[5.6] J. Lumeau, A. Sinitskiy, L. N. Glebova, L. B. Glebov and E. D. Zanotto, "Optical and crystallization homogeneity of photo-thermo-refractive glass", Glass and Optical material division, Spring 2006 Meeting (Greenville, South Carolina, USA), paper **GOMD-S5-007-2006**, May 2006

[5.7] J. Lumeau, A. Sinitskiy, L. N. Glebova, L. B. Glebov and E. D. Zanotto, "Spontaneous and photo-induced crystallization of PTR glass", Otto Schott Colloquium (Jena, Germany), paper **P-70**, July 2006

[5.8] A. Tolley, M. O. Prado, J. Lumeau, L. Glebova, L. B. Glebov and E. D. Zanotto, "Nano-crystallization study of photo-thermo-refractive glass by TEM-EDAX and SAXS", 8th International Symposium on Crystallization in Glasses and Liquids (Jackson Hole, Wyoming, USA), paper **CRYSTAL-P15-055-2006**, September 2006

[5.9] J. Lumeau, L. Glebova and L. B. Glebov, "Influence of UV-exposure on the crystallization and optical properties of photo-thermo-refractive glass", XI Conference on the Physics of Non-Crystalline Solids (Rhodes, Greece), paper **P-OP-8-PSII**, November 2006

[5.10] L. Glebova, J. Lumeau, M. Klimov, E. D. Zanotto and L. B. Glebov, "Role of fluorine and bromine concentrations in photo-thermo-refractive glass crystallization", XI Conference on the Physics of Non-Crystalline Solids (Rhodes, Greece), paper **P-NC-5-PSII**, November 2006

[5.11] F. C. Serbena, G. P. Souza, E. D. Zanotto, J. Lumeau, L. Glebova, L. B. Glebov, " Internal residual stresses in a photo-thermo-refractive glass", Latin American workshop on Applications of Powder Diffraction (Campinas (SP), Brazil), paper **67-2374**, April 2007

[5.12] G. P. Souza, V. M. Fokin, E. D. Zanotto, J. Lumeau, L. Glebova and L. B. Glebov, "Microstructural evolution in photo-thermo-refractive (PTR) glass during crystallization", International Congress on Glass (Strasbourg, France), paper **T14**, July 2007

[5.13] H. Bornhoeft, J. Deubener, J. Simon, J. Lumeau, L. Glebova and L. B. Glebov, "Thermo-mechanical properties of PTR (Photo-Thermo-Refractive) glass measured with ultrasonic waves", International Congress on Glass (Strasbourg, France), paper **R20**, July 2007

[5.14] O. Andrusyak, L. Glebova, J. Lumeau, V. Rotar, V. Smirnov, G. Venus, and L. B. Glebov, "Holographic optical elements in photo-thermo-refractive glass", Correlation Optics 2007 (Chernivtsi, Ukraine), Session **3**, September 2007

[5.15] L. Siiman, J. Lumeau and L. B. Glebov, "Short pulse laser interaction with photo-thermo-refractive glass", IMI day (Lehigh, Pennsylvania, USA), October 2007

[5.16]. Lumeau, L. Glebova, L. Siiman and L. B. Glebov, "Investigation of the optical and crystallization properties of photo-thermo-refractive glass", IMI day (Lehigh, Pennsylvania, USA), October 2007

[5.17] G. P. Souza, V. M. Fokin, E. D. Zanotto, J. Lumeau, L. Glebova, L. B. Glebov, "Non-Stoichiometric Crystallization in Photo-Thermo-Refractive (PTR) Glass", ISNCS 2007 (Aracaju, Brazil), paper **P26** , October 2007

[5.18] F. C. Serbena, G. P. Souza, E. D. Zanotto, J. Lumeau, L. Glebova, L. B. Glebov, "Internal Residual Stress Measurements in an Oxyfluoride Nano Glass-Ceramic using Synchrotron Radiation", ISNCS 2007 (Aracaju, Brazil), paper **P24**, October 2007

[5.19] J. Lumeau, L. Glebova and L. B. Glebov, "Effect of Cooling on the Optical and Crystallization Properties of Photo-Thermo-Refractive Glass", ISNCS 2007 (Aracaju, Brazil), paper **P41**, October 2007

[5.20] L. Siiman, J. Lumeau and L. B. Glebov, "Ultrashort laser pulse interaction with photo-thermo-refractive glass", CREOL Industrial Affiliates Day (Orlando, Florida, USA), paper **9**, April 2008

[5.21] J. Lumeau, A. Gusarov, L. Glebova, L. Glebov, "Effect of photoelasticity on the refractive index decrement in photo-thermo-refractive glass", Glass and Optical material division, Spring 2008 Meeting (Tucson, Arizona, USA), paper **GOMD-S5-017-2008**, May 2008

[5.22] G. P. Souza, V. M. Fokin, E. D. Zanotto, J. Lumeau, L. Glebova, L. B. Glebov, "Nucleation Kinetics in Photo-Thermo-Refractive (PTR) Glass", Glass and Optical material division, Spring 2008 Meeting (Tucson, Arizona, USA), paper **GOMD-S1-025-2008**, May 2008

[5.23] J. Lumeau, L. Glebova and L. B. Glebov, "Evolution of Absorption Spectra in the Process of Nucleation in Photo-Thermo-Refractive Glass", European Society of Glass Science and Technology conference (Trencín, Slovakia), paper **30**, June 2008

[5.24] L. Glebova, J. Lumeau, M. Klimov and L. B. Glebov, "Increase of Volume of PTR Glass Caused by Photo-Thermo-Induced Crystallization", European Society of Glass Science and Technology conference (Trencín, Slovakia), paper **46**, June 2008

[5.25] L. Siiman, D. Moses, J. Lumeau and L. B. Glebov, "Ultrashort Laser Pulse Interaction with Photo-Thermo-Refractive Glass", Southeast Ultrafast Conference (Orlando, Florida, USA), poster, January 2009

[5.26] L. Siiman, J. Lumeau and L. B. Glebov, "Interaction of ultrashort IR laser pulses with PTR glass: fundamental mechanisms and applications", Photonics West (San Jose, California, USA), paper **7205-16**, January 2009

[5.27] A. J. Verhoef, A. V. Mitrofanov, D. Kartashov, A. Baltuška, E. E. Serebryannikov, A. M. Zheltikov, J. Lumeau, L. B. Glebov, "Can We Measure Attosecond Tunneling Dynamics in Bulk Solids?", KITP Conference: Concepts and Methods in Quantum Control: Theory and Experiment (UC Santa Barbara, Kavli Institute for Theoretical Physics), May 2009

[5.28] J. Lumeau and L.B. Glebov, "Refractive index measurements in photo-thermo-refractive glass at different stages of hologram fabrication", 8th Pacific Rim Conference on Ceramic and

Glass Technology (PACRIM 8) (Vancouver, British Columbia, Canada), paper **PACRIM8-S25-P205-2009**, June 2009

[5.29] G. P. Souza, V. M. Fokin, E. D. Zanotto, J. Lumeau, L. Glebova, L. B. Glebov, "Diffusion Zone in Crystallized Photo-Thermo-Refractive Glass", 8th Pacific Rim Conference on Ceramic and Glass Technology (PACRIM 8) (Vancouver, British Columbia, Canada), paper **PACRIM8-S25-P176-2009**, June 2009

[5.30] M. Anne, L. Glebova, J. Lumeau and L. B. Glebov, "IR absorption edge of multicomponent silicate glasses", 8th Pacific Rim Conference on Ceramic and Glass Technology (PACRIM 8) (Vancouver, British Columbia, Canada), paper **PACRIM8-S25-005-2009**, June 2009

[5.31] A. Mitrofanov, A. J. Verhoef, A. Baltuška, E. E. Serebryannikov, A. M. Zheltikov, J. Lumeau, and L. B. Glebov, "Mapping of tunneling ionization using an optical two-color pump-probe technique", 18th International Laser Physics Workshop (Barcelona, Spain), paper **2.8.1**, July 2009,

[5.32] J. Lumeau, F. C. Serbena, E. D. Zanotto, L. Glebova, L. Glebov, "Possible mechanisms of crystallization-induced refractive index changes in photo-thermo-refractive glass", XII Conference on the Physics of Non-Crystalline Solids (Iguacu Falls, Brazil), paper **106**, September 2009

[5.33] M. Anne, J. Lumeau, L. Glebova and L. B. Glebov, "Specific absorption spectra of cerium in multicomponent silicate glasses", XII Conference on the Physics of Non-Crystalline Solids (Iguacu Falls, Brazil), paper **323**, September 2009

[5.34] K. Chamma, L. Glebova, J. Lumeau, L. Glebov, "Generation and bleaching of color centers in photo-thermo-refractive glass", XII Conference on the Physics of Non-Crystalline Solids (Iguacu Falls, Brazil), Invited talk, paper **492**, September 2009

[5.35] G. P. Souza, V. M. Fokin, E. D. Zanotto, J. Lumeau, L. Glebova, L. B. Glebov, "Liquid-Phase Separation and Crystallization in Photo-Thermo-Refractive Glass", Crystallization 2009 (Iguacu Falls, Brazil), paper **429**, September 2009

[5.36] C. F. Rodrigues, A. C. M. Rodrigues, E. D. Zanotto, J. Lumeau, L. N. Glebova, L. B. Glebov, "Crystallization of photo-thermo-refractive glasses monitored by electrical conductivity measurements", Crystallization 2009 (Iguacu Falls, Brazil), paper **448**, September 2009

[5.37] J. Lumeau, K. Chamma, L. Glebova and L. B. Glebov, "Ultra-low absorption and laser-induced heating of volume Bragg combiners recorded in photo-thermo-refractive glass", Photonics West (San Francisco, California, USA), paper **7580-103**, January 2010

[5.38] S. Mokhov, J. Lumeau V. Smirnov, B. Ya. Zeldovich, and L. B. Glebov, "High-Aperture Narrow-Band Filter Based on Moiré Principle", Photonics West (San Francisco, California, USA), paper **7598-28**, January 2010

[5.39] S. Mokhov, L. B. Glebov, J. Lumeau, V. Smirnov and B. Ya. Zeldovich, "Optical Resonant Cavities in Volume Bragg Gratings", APS March meeting (Portland, Oregon, USA), paper **X29.00006**, March 2010

[5.40] K. Chamma, J. Lumeau, L. Glebova, L. Glebov, "Study of ionization of cerium in multicomponent silicate glasses", Glass and Optical material division, Spring 2010 Meeting (Corning, New-York, USA), paper **GOMD-SV-031-2010**, May 2010

[5.41] G. P. Souza, V. M. Fokin, C. A. Baptista, E. D. Zanotto, J. Lumeau, L. Glebova, L. B. Glebov, "Effect of Bromine on NaF Crystallization in Photo-Thermo-Refractive Glass", Glass and Optical material division, Spring 2010 Meeting (Corning, New-York, USA), paper **GOMD-SIII-050-2010**, May 2010

[5.42] S. Mokhov, J. Lumeau L. B. Glebov, V. Smirnov and B. Ya. Zeldovich, "High-Aperture Narrow-Band Moiré Filter in Volume Bragg Grating", 41st Annual Meeting of the APS Division of Atomic, Molecular and Optical Physics (Houston, Texas, USA), paper **E1.00159**, May 2010

[5.43] D. Moses, O. Andrusyak, J. Lumeau, V. Smirnov, L. Glebov, "Stretching and compression of ultrashort pulses using chirped volume Bragg gratings in single- and multi-pass configurations", Ultrashort Pulse Laser Workshop for the Directed Energy Professional Society (Broomfield, Colorado, USA), **USPL Workshop Session 3**, June 2010

[5.44] G. P. Souza, V. M. Fokin, E. D. Zanotto, J. Lumeau, L. Glebova, L. B. Glebov, "NaF solubility and Liquid-Liquid Phase Separation in Photo-Thermo-Refractive Glass", International Conference on the Structure of Non-Crystalline Materials (Paris, France), paper **206**, June 2010

[5.45] J. Lumeau and L. B. Glebov, "Correlation between the refractive index change and the crystallization kinetics in photo-thermo-refractive glass", International Congress on Glass (Salvador, Brazil), paper **176**, September 2010

[5.46] J. Lumeau and L. B. Glebov, "Mechanisms of optical bleaching of silver containing particles in photo-thermo-refractive glass", International Congress on Glass (Salvador, Brazil), paper **320**, September 2010

[5.47] K. Chamma, J. Lumeau, L. Glebova and L. B. Glebov, "Effect of dosage and thermal treatment on photo-thermo-refractive glass crystallization properties", International Congress on Glass (Salvador, Brazil), paper **326**, September 2010

[5.48] L. Glebova, J. Lumeau and L. B. Glebov, "Photo-thermo-refractive glass co-doped with Nd^{3+} as a new laser medium", International Congress on Glass (Salvador, Brazil), paper **411**, September 2010

[5.49] L. Glebova, J. Lumeau, V. Smirnov and L. B. Glebov, "Photo-thermo-refractive glass for thick volume holograms", International Congress on Glass (Salvador, Brazil), paper **419**, September 2010

[5.50] J. Lumeau, "Photo-Thermo-Refractive glasses: optical/structural properties and applications", Seminar at the University of Rennes (Laboratoire Verres et Ceramiques), France, November 2010

[5.51] J. Lumeau, "Réseaux de Bragg en volume inscrits dans les verres Photo-Thermo-Réfractifs : propriétés et applications ", Seminar at the University Paul Cezanne Aix Marseille III (Institut Fresnel), France, December 2010

[5.52] D. Ott, S. Mokhov, V. Rotar, J. Lumeau, V. Smirnov, L. Glebov, "Ultrashort laser pulse interaction with photo-thermo-refractive glass", CREOL Industrial Affiliates Day (Orlando, Florida, USA), April 2011

[5.53] K. Chamma, J. Lumeau, L. Glebova, L. Glebov, "Mechanisms of NaF growth in photo-thermo-refractive glass", *Glass and Optical material division, Spring 2011Meeting* (Savannah, Georgia, USA), paper **GOMD - SIII - 014 - 2011**, May 2011

[5.54] J. Lumeau, K. Chamma, L. Glebova, L. Glebov, "Absorption in photo-thermo-refractive glass: metrology, contributions and mitigation", *Glass and Optical material division, Spring 2011Meeting* (Savannah, Georgia, USA), paper **GOMD - SIII - 007 - 2011**, May 2011

[5.55] J. Lumeau, C. Koc, O. Mokhun, V. Smirnov, M. Lequime and L.B. Glebov, "Single resonance monolithic Fabry-Perot filters formed by volume Bragg gratings and multilayer dielectric mirrors", Photonics West (San Francisco, California, USA), paper **8257-24,** January 2012

[5.56] D. Ott, J. Lumeau, S. Mokhov, I. Divliansky, A. Ryasnyanskiy, N. Vorobiev, V. Smirnov, C. Spiegelberg, L. Glebov, "Longitudinal mode selection in laser cavity by moiré volume Bragg grating", Photonics West (San Francisco, California, USA), paper Paper **8236-71** January 2012

[5.57] L. Glebova, V. Smirnov, J. Lumeau, L. Glebov, "Low losses volume Bragg gratings recorded in photo-thermo-refractive glass", submitted to Photonics West (San Francisco, California, USA), paper **8257-44** January 2012

[5.58] A. Jain, L. Glebova , J. Lumeau, V. Smirnov, A. Rappaport, M. Bass, C. Spiegelberg, M. Krainak, L. Glebov, "Rare-Earth Doped Photo-Thermo-Refractive Glass for Monolithic Solid State Lasers", Photonics West (San Francisco, California, USA), paper **8235-51**, January 2012

[5.59] A. Ryasnyanskiy, N. Vorobiev, V. Smirnov, J. Lumeau, L. Glebova, Ch. Spiegelberg, A. Podvyaznyy, and L. Glebov, "Single frequency fiber laser with external volume Bragg resonator", Defense, Security and Sensing (Baltimore, Maryland, USA), April 2012

References

[1] K. O. Hill, Y. Fujii, D. Johnson, and B. Kawasaki, "Photosensitivity in optical fiber waveguides: Application to reflection filter fabrication" Applied Physics Letters **32**, 647 (1978)

[2] Y. Luo, P. Gelsinger, J. Barton, G. Barbastathis, and R. Kostuk, "Optimization of multiplexed holographic gratings in PQ-PMMA for spectral-spatial imaging filters," Optics Letters **33**, 566 (2008)

[3] K. Davis, K. Miura, N. Sugimoto, K. Hirao, "Writing waveguides in glass with a femtosecond laser, " Optics Letters **21**, 1729 (1996)

[4] M. Douay, W. Xie, T. Taunay, P. Bernage, P. Niay, P. Cordier, B. Poumellec, L. Dong, J. Bayon, H. Poignant, and E. Delevaque, "Densification Involved in the UV-Based Photosensitivity of Silica Glasses and Optical Fibers, " J**.** Lightwave Technol. **15**(8), 1328 (1997)

[5] M. Kösters, H. Hsieh, D. Psaltis, and K. Buse, "Holography in commercially available photoetchable glasses," Applied Optics **44**, 3399 (2005)

[6] O. Efimov, L. B. Glebov, V. Smirnov, "High-frequency Bragg gratings in photothermorefractive glass," Optics Letters **23**, 1693 (2000)

[7] K. O. Hill and G. Meltz, "Fiber Bragg Grating Technology Fundamentals and Overview," J**.** Lightwave Technol. **15**(8), 1263 (1997)

[8] G. Town, K. Sugden, J. Williams, I. Bennion, and S. Poole, "Wide-band Fabry–Perot-like filters in optical fiber," IEEE Photon. Technol. Lett. **7**(1), 78 (1995)

[9] S. D. Stookey, "Photosensitive glass (a new photographic medium)," Industrial and Engineering Ghem. **41**, 856 (1949)

[10] S. D. Stookey, G. H. Beall, J.E Pierson, "Full-color photosensitive glass," J. Appl. Phys. **49**, 5114 (1978)

[11] N. F. Borrelli, D. L. Morse, P. A. Sachenik, "Integral photosensitive optical device and method," US Patent **4,541,053** (1985)

[12] V. A. Borgman, L.B. Glebov, N.V. Nikonorov, G.T. Petrovskii, V.V. Savvin, A.D. Tsvetkov," Photothermal refractive effect in silicate glasses," Sov. Phys. Dokl. **34**, 1011 (1989)

[13] L. B. Glebov, N. V. Nikonorov, E. I. Panysheva, G. T. Petrovskii, V. V. Savvin, I. V. Tunimanova, V. A. Tsekhomsky," Polychromatic glasses - a new material for recording volume phase holograms," Sov. Phys. Dokl., **35**, 878 (1990)

[14] O. M. Efimov, L. B. Glebov, L. N. Glebova, K.C. Richardson, and V.I. Smirnov, "High-Efficiency Bragg Gratings in Photo-thermo-refractive Glass," Applied Optics **38**, 619 (1999)

[15] O. M. Efimov, L. B. Glebov, L. N. Glebova, V. I. Smirnov, "Process for production of high efficiency volume diffractive elements in photo-thermo-refractive glass," United States Patent **6,586,141 B1** (2003)

[16] L. Glebov, "Volume Bragg Gratings in PTR Glass--New Optical Elements for Laser Design," 3rd Advanced Solid-State Photonics (ASSP) Topical Meeting. ASSP Technical Digest, Paper Code MD1, Nara, Japan (2008).

[17] L. B. Glebov, "Volume hologram recording in inorganic glasses," Glass Science and Technology **75** C1, 73 (2002)

[18] L. B. Glebov and V. I. Smirnov, "Nonlinear Photosensitivity of Photo-Thermo-Refractive Glass," Optics in the Southeast (2003)

[19] J. Lumeau, L. Glebova and L. B. Glebov, "Evolution of Absorption Spectra in the Process of Nucleation in Photo-Thermo-Refractive Glass," Advanced Materials Research, **39-40**, 395 (2008)

[20] T. Cardinal, O. M. Efimov, H. G. Francois-Saint-Cyr, L. B. Glebov, L. N. Glebova and V. I. Smirnov, "Comparative study of photo-induced variations of X-ray diffraction and refractive index in photo-thermo-refractive glass," Journal of Non-Crystalline Solids **325,** 275 (2003)

[21] J. Lumeau, L. Glebova, L. B. Glebov, V. Golubkov and E. D. Zanotto, "Origin of crystallization-induced refractive index changes in photo-thermo-refractive glass," Optical Materials **32**, 139 (2009)

[22] L. B. Glebov, "Volume Bragg Gratings in PTR Glass--New Optical Elements for Laser Design", 3rd Advanced Solid-State Photonics (ASSP) Topical Meeting, ASSP Technical Digest, Paper Code MD1, Nara, Japan (2008)

[23] J. Lumeau and M. Lequime, "Localized measurement of the optical thickness of a transparent window – Application to the study of the photosensitivity of organic polymers," Applied Optics **45**(4), 6099 (2006)

[24] N. A. Riza, M. Sheikh and F. Perez, "Optical substrate thickness measurement system using hybrid fiber-free space optics and selective wavelength interferometry," Optics Communications **269**(1), 24 (2007)

[25] O. Efimov, L. B. Glebov, H. Andre, "Measurement of the induced refractive index in a photothermorefractive glass by a liquid-cell shearing interferometer**,"** Appl. Opt. **41**, 1864 (2002)

[26] J. Lumeau and L. B. Glebov, "Correlation between the refractive index change and the crystallization kinetics in photo-thermo-refractive glass," International Congress on Glass (Salvador, Brazil), paper **176** (2010)

[27] A. N. Kolmogorov, "A statistical theory for the recrystallisation of metals," Izv. Akad. Nauk USSR, Ser. Mathem. **3**, 355 (1937)

[28] W. A. Johnson, R. F. Mehl, "Reaction kinetics in processes of nucleation and growth," Trans. AIME **135**, 416 (1939)

[29] M. Avrami, "Kinetics of Phase Change. I. General Theory," J. Chem. Phys. **7**, 1103 (1939)

[30] V. Fokin, E. D. Zanotto, N. Yuritsyn, J. W. Schmelzer, "Homogeneous crystal nucleation in silicate glasses: A forty years perspective," Journal of Non Crystalline Solids **352**, 2681 (2006)

[31] K. Chamma, J. Lumeau, L. Glebova and L. B. Glebov, "Effect of dosage and thermal treatment on photo-thermo-refractive glass crystallization properties," International Congress on Glass (Salvador, Brazil), paper **326** (2010)

[32] L. B. Glebov, "Kinetics modeling in photosensitive glass," Optical Materials **25**(4), 413 (2004)

[33] G. P. Souza, V. M. Fokin, E. D. Zanotto, J. Lumeau, L. Glebova, L. B. Glebov, "Micro and Nanostructures in Partially Crystallized Photo-Thermo-Refractive Glass," Physics and Chemistry of Glasses: European Journal of Glass Science and Technology Part B **50** (5), 311 (2009)

[34] L. Glebov, L. Glebova and V. Tsechomskii, and V. Golubkov, "Study of structural transformations in photo-thermo-refractive glass by SAXS and XRD," Proceedings of XX International Congress on Glass, Kyoto, Japan (2004)

[35] L. Glebova, J. Lumeau, M. Klimov, E.D. Zanotto and L.B. Glebov, "Role of bromine on the thermal and optical properties of photo-thermo-refractive glass," Journal of Non Crystalline Solids **354**, 456 (2008)

[36] S. Stević, R. Aleksić and N. Backovi, "Influence of Fluorine on Thermal Properties of Fluorophosphate Glasses," J. Am. Ceram. Soc. **70(**1101), C-264 (1987)

[37] V. Mastelaro and E. Zanotto, "Residual Stresses in a Soda-Lime-Silica Glass-Ceramic," Journal of Non-Crystalline Solids **194**, 297 (1996)

[38] L. B. Glebov and L. Glebova, "Swelling of photo-thermo-refractive glass resulted from thermal development," Glass Science and Technology **75 C2,** 294 (2002)

[39] O. Andrusyak, V. Smirnov, G. Venus, and L. Glebov, "Beam combining of lasers with high spectral density using volume Bragg gratings," Optics Communications Volume **282(**13), 2560 (2009)

[40] O. Andrusyak, D. Drachenberg, V. Smirnov, G. Venus, and L. Glebov, "Fiber laser system with kW-level spectrally-combined output," SSDLTR 2008

[41] A. Sevian, O. Andrusyak, I. Ciapurin, G. Venus, V. Smirnov, and L. Glebov, "Efficient Power Scaling of Laser Radiation by Spectral Beam Combining," Optics Letters **33**, 384 (2008)

[42] K. Chamma, J. Lumeau, L. Glebova, and L. B. Glebov, "Generation and bleaching of intrinsic color centers in photo-thermo-refractive glass matrix," Journal of Non Crystalline Solids **356**(44-49), 2363 (2010)

[43] J. Lumeau, L. Glebova and L. B. Glebov, "Investigation of the induced absorption and scattering in visible and NIR ranges in photo-thermo-refractive glass," International Congress on Glass (Strasbourg, France), paper **M3** (2007)

[44] L. Glebov, E. Boulos, "Absorption spectra of iron and water in silicate glasses," Proc. of International Commission on Glass Conference "Glass in the New Millenium" **S4-2**, Amsterdam (2000)

[45] J. Lumeau, L. Glebova and L. B. Glebov, "Near-IR absorption in high purity photo-thermo-refractive glass and holographic optical elements: measurement and application for high energy lasers," Applied Optics **50**(30), 5905 (2011)

[46] J. Lumeau and L. B. Glebov, "Mechanisms of optical bleaching of silver containing particles in photo-thermo-refractive glass," International Congress on Glass (Salvador, Brazil), paper **320** (2010)

[47] A. Gourevitch, G. Venus, V. Smirnov, D. A. Hostutler, and L. Glebov, "Continuous wave, 30 W laser-diode bar with 10 GHz linewidth for Rb laser pumping," Optics Letters **33**(7), 702 (2008)

[48] N. Vorobiev, L. Glebov, and V. Smirnov, "Single-frequency-mode Q-switched Nd:YAG and Er:glass lasers controlled by volume Bragg gratings," Optics Express **16**(12), 9199 (2008)

[49] L. Glebov, "High brightness laser design based on volume Bragg gratings," Invited Paper, Laser Source and System Technology for Defense and Security II. Proceedings of SPIE **6216**, 621601 (2006)

[50] L. Tsang, J. A. Kong, K. H. Ding, C. On Ao, "Scattering of Electromagnetic Waves – T.2. Numerical Simulations," (Wiley, New York, 2001)

[51] V. S. Vishnu, G. George, V. Divya, M. L. P. Reddy, "Synthesis and characterization of new environmentally benign tantalum-doped $Ce_{0.8}Zr_{0.2}O_2$ yellow pigments: Applications in coloring of plastics," Dyes and Pigments **82**(1), 53 (2009)

[52] S. Y. Marzouk, F. M. Ezz-Eldin, "Optical study of Ce^{3+} ion in gamma-irradiated binary barium-borate glasses," Physica B **430**, 3307 (2008)

[53] L. B. Glebov, E. N. Boulos, "Absorption of iron and water in the Na_2O-CaO-MgO-SiO_2 glasses II," JNCS **424**, 49, (1998)

[54] E. N. Boulos, L. B. Glebov, "Absorption of iron and water in the Na_2O–CaO–MgO–SiO_2 glasses. I. Separation of ferrous and hydroxyl spectra in the near IR region," JNCS **221,** 213 (1997)

[55] L. B. Glebov, Photochromic and photo-thermo-refractive (PTR) glasses," In Encyclopedia of Smart Materials, John Wiley & Sons, NY, 770 (2002)

[56] L. Glebov, V. Dokuchaev, M. Petrov, G. Petrovskii, "Absorption spectra of color centers in alkali silicate glasses," Sov. J. Glass Phys. Chem. **16**, 31 (1990)

[57] O. Andrusyak, V. Smirnov, G. Venus, V. Rotar, and L. Glebov, "Spectral combining and coherent coupling of lasers by volume Bragg gratings," IEEE J. Sel. Top. Quant. **15**, 344 (2009)

[58] K. Liao, M.Cheng, E. Flecher, V.I. Smirnov, L.B. Glebov, and A. Galvanauskas, "Large aperture chirped volume Bragg grating based CPA system," Opt. Express **15**, 4876 (2007)

[59] E. B. Treacy, "Optical pulse compression with diffraction gratings," IEEE. J. Quantum Electron. **5**, 454 (1969)

[60] O. E. Martinez, "Grating and prism compressors in the case of finite beam size," J. Opt. Soc. Am. B **3**, 929 (1986)

[61] H. Kogelnik, "Coupled-wave theory for thick hologram gratings," Bell Syst. Tech. J. **48**, 2909 (1969)

[62] I. V. Ciapurin, L. B. Glebov, V. I. Smirnov, "Modeling of Gaussian beam diffraction on volume Bragg gratings in PTR glass," Proc. of SPIE **5742**, 183 (2005)

[63] Z. Bor, B. Racz, G. Szabo, M. Hilbert, H.A. Hazim, "Femtosecond Pulse Front Tilt Caused by Angular-Dispersion," Opt. Eng. **32**, 2501 (1993)

[64] L. Lepetit, G. Cheriaux, and M. Joffre, "Linear techniques of phase measurement by femtosecond spectral interferometry for applications in spectroscopy," J. Opt. Soc. Am. B **12**, 2467 (1995)

[65] S. Akturk, M. Kimmel, P. O'Shea, R. Trebino, "Measuring pulse-front tilt in ultrashort pulses using GRENOUILLE," Optics Express **11**, 491 (2003)

[66] G. Venus, L. Glebov, V. Rotar, V. Smirnov, P. Crump, and J. Farmer, "Volume Bragg semiconductor lasers with near diffraction limited divergence," Proc. of SPIE **6216**, 621602 (2006)

[67] L. B. Glebov and V. I. Smirnov, "Interaction of photo-thermo-refractive glass with nanosecond pulses at 532 nm," Laser-Induced Damage in Optical Materials. Ed. G.J. Exarhos, A.H. Guenther, N. Kaiser, K.L. Lewis, M.J. Soileau, C.J. Stolz. Proceedings of SPIE **5273,** 396 (2004)

[68] O. M. Efimov, L. B. Glebov, S. Grantham, M. Richardson, "Photoionization of silicate glasses exposed to IR femtosecond pulses," Journal of Non-Crystalline Solids **253**, 58 (1999)

[69] L. B. Glebov, "Optical absorption and ionization of silicate glasses," (invited paper) in "Laser-induced damage in optical materials:2000" Proceedings of SPIE, **4347,** 343 (2001)

[70] A. N. Trukhin, M. N. Tolstoi, L. B. Glebov, V. L. Savel'ev, "Elementary electronic excitations in pure sodium silicate glasses," Physica Status Solidi (b) **99**, 155 (1980)

[71] R. R. Alfano, S. L. Shapiro, "Observation of Self-Phase Modulation and Small-Scale Filaments in Crystals and Glasses," Phys. Rev. Lett. **24**, 592 (1970)

[72] H. J. Fitting, A. N. Trukhin, T. Barfels, B. Schmidt, and A. Von Czarnowsi, "Radiation induced effects in SiO2," Radiation Effects & Defects in Solids **157**, 575 (2002)

[73] R. R. Alfano, S. L. Shapiro, "Observation of self-phase modulation and small-scale filaments in crystals and glasses," Physical Review Letters **24**, 592 (1970)

[74] A. Brodeur and S. L. Chin, "Band-gap dependence of the ultrafast white-light continuum," Physical Review Letters **80**, 4406 (1998)

[75] W. Franz, "Einfluß eines elektrischen feldes auf eine optische absorptionskante," Zeitschrift für Naturforschung **13a**, 484 (1958).

[76] L. V. Keldysh, "Behavior of nonmetallic crystals in strong electric fields," Soviet Physics-JETP **6**, 763 (1958)

[77] L. V. Keldysh, "Ionization in the field of a strong electromagnetic wave," Soviet Physics-JETP **20**, 1307 (1965)

[78] C. B. Schaffer, A. Brodeur, and E. Mazur, "Laser-induced breakdown and damage in bulk transparent materials induced by tightly focused femtosecond laser pulses," Meas. Sci. Technol. **12**, 1784 (2001)

[79] X. Mao, S.S. Mao, and R.E. Russo, "Imaging femtosecond laser-induced electronic excitation in glass," Applied Physics Letters **82**, 697 (2003)

[80] D. G. Papazoglou, I. Zergioti, and S. Tzortzakis, "Plasma strings from ultraviolet laser filaments drive permanent structural modifications in fused silica," Optics Letters **32**, 2055 (2007)

[81] V. I. Smirnov, S. Juodkazis, V. Dubikovsky, J. Hales, B. Ya. Zel'dovich, H. Misawa, and L. B. Glebov, "Resonant third harmonic generation by femtosecond laser pulses on Bragg grating in photosensitive silicate glass," Conference on Lasers and Electro-Optics CLEO-2002, paper **CTuG7** (2002)

[82] S Juodkazis, E Gaizauskas, V Jarutis, J Reif, S Matsuo and H Misawa, "Optical third harmonic generation during femtosecond pulse diffraction in a Bragg grating," J. Phys. D: Appl. Phys. **39**, 50 (2006)

[83] M. Lequime and J. Lumeau, "Laser trimming of thin-film filters," Advances in Optical Thin-Films (Jena, Germany), invited talk, paper **5963-08** (2005)

[84] O. M. Efimov, L. B. Glebov, V. I. Smirnov, "High efficiency volume diffractive elements in photo-thermo-refractive glass", Patent No. **US 6,673,497 B2** (2004)

[85] J. Lumeau, V. Smirnov and L.B. Glebov, "Tunable narrow-band filter based on a combination of Fabry-Perot etalon and Volume Bragg Grating," Optics Letters **31**(16), 2417 (2006)

[86] J. Lumeau, V. Smirnov, F. Lemarchand, M. Lequime and L.B. Glebov, "Large aperture tunable ultra narrow band Fabry-Perot-Bragg filter," Proceeding of SPIE 6469, paper **64690M** (2007)

[87] J. Lumeau, V. Smirnov, and L.B. Glebov, "Phase-shifted volume Bragg gratings in photo-thermo-refractive glass," Proceeding of SPIE 6890, paper **68900A**, (2008)

[88] R. Kashyap, "Fiber Bragg Gratings," Academic Press, 1st edition (1999)

[89] V. Smirnov, J. Lumeau, S. Mokhov, B. Ya. Zeldovich and L. B. Glebov, "Ultra-narrow bandwidth Moiré reflecting Bragg gratings recorded in photo-thermo-refractive glass," Optics Letters **35**(4), 592 (2010)

[90] J. Lumeau, M. Cathelinaud, J. Bittebierre and M. Lequime, "Ultra-narrow bandpass hybrid filter with wide rejection band," Applied Optics **45**(7), 1328 (2006)

[91] H. A. Macleod, "Thin-Film Optical Filters," Third Edition (Institute of Physics Publishing, 2001)

[92] L. B. Glebov, J. Lumeau, S. Mokhov, V. Smirnov and B. Ya. Zeldovich, "Reflection of light by composite volume holograms: Fresnel corrections and Fabry-Perot spectral filtering," JOSA A **25**(3), 751 (2008)

[93] N. Stelmakh, "Harnessing multimode broad-area laser-diode emission into a single-lobe diffraction-limited spot," IEEE Phot. Tech. Lett. **19**, 1392 (2007)

[94] M. Wang, C. Yu, and A. Varela, "Efficient pseudo-nondiffracting beam shaping using a quasicontinuous-phase diffractive element," Opt. Eng. **40**, 517 (2001)

[95] W. Mohammed, M. Pitchumani, A. Mehta, and E. Johnson, "Selective excitation of the LP11 mode in step index fiber using a phase mask," Opt. Eng. **45**, 074602 (2006)

[96] F. Lemarquis, M. Lequime, G. Albrand, L. Escoubas, J. Simon, J. Baudrand, P. Riaud, D. Rouan, A. Boccaletti, P. Baudoz, and D. Mawet, "Manufacturing of 4-quadrant phase mask for nulling interferometry in thermal infrared," Proc. of SPIE **5250** (2004)

[97] A. Carlotti, G. Ricort, C. Aime, "Phase mask coronagraphy using a Mach-Zehnder interferometer," A&A **504**, 663-671 (2009)

[98] L. Siiman, J. Lumeau, L. B. Glebov, "Phase Fresnel lens recorded in PTR glass by selective exposure to IR ultrashort laser pulses", Optics Letters **34**(1), 402 (2009)

[99]G. Machavariani, A. Ishaaya, L. Shimshi, N. Davidson, A. Friesem, and E. Hasman, "Efficient mode transformations of degenerate Laguerre-Gaussian beams," Appl. Opt. **43**, 2561 (2004)

[100]A. Yariv and P. Yeh, "Photonics: Optical Electronics in Modern Communications" (Oxford University Press, 2007)

[101] Wadle and Lakes R. S., "Holographic diffusers with low back-scatter," J. Modern Optics **42**, 1387 (1995)

[102] N. M. Ganzherli, Yu. N. Denisyuk, I. A. Maurer and D. F. Chernykh., "On-Axis Diffuse Screen Based on a Reference-Free Volume Hologram," Technical Physics **50**, 274 (2005)

[103] N. M. Ganzherli, Yu. N. Denisyuk, A. P. Serdobitseva and D. F. Chernykh., "The Phenomenon of Light Concentration by a Speckle Screen Based on a Reference-Free Volume Hologram," Technical Physics Letters **32**(6), 542 (2006)

[104] L. Glebova, J. Lumeau and L. B. Glebov, "Photo-thermo-refractive glass co-doped with Nd^{3+} as a new laser medium," Optical Materials **33**, 1970 (2011)

[105] M. J. Weber (Ed.), "Handbook of Laser Science and Technology – Supplement 2: Optical Materials", CRC Press (1995)

[106] I. V. Ciapurin, L. B. Glebov, V. I. Smirnov, "Modeling of phase volume diffractive gratings - part 1: transmitting sinusoidal uniform gratings" Opt. Eng. **45**, 1 (2006)

[107] D. Strickland and G. Mourou, "Compression of amplified chirped optical pulses," Optics Communications **56**, 219 (1985)

[108] A. Boskovic, M. J. Guy, S. V. Chernikov, J. R. Taylor, and R. Kashyap, "All-fibre diode pumped, femtosecond chirped pulse amplification system," Electron. Lett. **31**, 877 (1995)

[109] A. Galvanauskas, M. E. Fermann, D. Harter, K. Sugden, and I. Bennion, "All-fiber femtosecond pulse amplification circuit using chirped Bragg gratings," Appl. Phys. Lett. **66**, 1053 (1995)

[110] L. B. Glebov, E. Flecher, V. I. Smirnov, A. Galvanauskas, K. Liao, "Stretching and compression of laser pulses by means of high efficiency volume diffractive gratings with variable periods in photo-thermo-refractive glass," United States Patent **7,424,185 B2** (2008)